The processes of melt segregation, magma ascent and pluton emplacement in the continental crust of the Damara Belt, Namibia

by
Duncan James Hall

Dissertation presented for the degree of Doctor of Earth Sciences in the Faculty of Science at Stellenbosch University

Promoter:
Professor Alexander F.M. Kisters
Department of Earth Sciences
Stellenbosch University

March 2016

Declaration

By submitting this dissertation electronically, I declare that the entirety of the work contained herein is my own, original work, that I am the sole author thereof (save to the extent explicitly otherwise stated), that reproduction and publication thereof by Stellenbosch University will not infringe any third party rights and that I have not previously in its entirety or in part submitted it for obtaining any qualification.

Duncan James Hall

Date: March 2016

Abstract

Theoretical models of meso- and macroscale granitic melt/magma transport commonly invoke a prominent role for dilatant fracturing of the wall rocks, but supporting field evidence is in many cases only scantly presented. This dissertation is a compilation of three case studies that integrate some of the theoretical models with field-based aspects from the obliquely exposed south Central Zone magmatic arc of the Damara Belt in Namibia.

Chapter 3 describes interconnected leucogranite networks that accommodate the transport of melt at the outcrop-scale in homogeneous, high-grade near-source gneisses in the western parts of the south Central Zone. The net-structured leucogranite networks include small intrafolial stringers, larger shear-band-hosted veins and still larger fracture-hosted leucogranite sheets, which display a size-based hierarchical distribution that results from the self-organisation of the near-source melt transport pathways. The development of the networks is controlled intrinsically by variations in the rate of melt supply. During periods of elevated melt supply and under conditions of low differential stress, melt-induced extensional fracturing generates hydraulic gradients that result in the formation of melt sheets which represent potential far-field ascent conduits (dykes sensu lato). However, the orientations of the sheets are controlled by wall-rock structures and regional and local stress fields, resulting in this case in the preservation and eventual crystallisation of shallowly-dipping leucogranite sheets that were unfavourably orientated to accommodate buoyancy-driven melt/magma drainage.

Chapter 4 describes the actual drainage of magma along steeply-dipping fracture conduits initiated in well-layered upper amphibolite-facies basement gneisses ~30 km SE of the outcrops presented in chapter 1. Here, the moderately-dipping gneisses contain large-scale leucogranite networks that include deca- to hecto metre-scale subvertical leucogranite lenses interpreted to

document the near-source accumulation of magma necessary for efficient far-field ascent. Field relationships also document the drainage of the subvertical lenses at critical lengths and volumes in excess of 100 m and ~2.4×10^5 m^3 respectively. These values as well as the field relationships are broadly consistent with theoretical models of magma transport along mobilised (self-propagating) hydrofractures. Self-propagating hydrofractures propagate at their tips and close simultaneously along their tails, leaving behind only very subtle and easily overprinted evidence, which may account for the elusiveness of granite conduits in the mid-crust. This work presents the first field evidence of large-scale magma drainage along self-propagating hydrofractures and has important consequences for the subsequent transport of magma through and eventual incremental emplacement within the subsolidus crust.

Chapter 5 examines in more detail the implications of fracture-controlled magma ascent for granite pluton emplacement in lower amphibolite-facies wall rocks ~80 km northeast of the near-source features presented in chapters 3 and 4. Three closely-spaced tabular granitoid plutons that were emplaced roughly contemporaneously at widely-varying structural levels are investigated. Each of the plutons demonstrates the effect of mechanical contrasts in the wall-rock that favour fracture arrest rather than ascent, particularly rigidity and rheological contrasts. However, contrary to the theoretical models, it is shown that rigidity contrasts which cause fracture arrest need not be associated with lithological contacts and the role of increasing differential stress during the fracture-controlled ascent of magma towards the brittle-to-ductile transition is highlighted.

The three chapters outlined above highlight the importance of fracture-controlled magma transport at all scales in the Damara Belt and substantiate some of the theoretical concepts, but also highlight prominent discrepancies between the models and natural systems.

Opsomming

Teoretiese modelle van meso- en makroskaalse granitiese smeltsel/magma vervoer roep oor die algemeen ‘n prominente rol van dilatante breukvorming van die wandgesteentes, maar ondersteunende veldbewyse is in baie gevalle op ‘n onvoldoende wyse voorgestel. Hierdie proefskrif is ‘n samestelling van drie gevallestudies wat teoretiese modelle en veld gebaseerde aspekte vanuit die skuins ontblote suid-Sentrale Sone magmatiese boog van die Damara Belt in Namibië integreer.

Hoofstuk 3 beskryf ‘n onderlinge verbindings netwerk van leukograniet wat die vervoer van smeltsel op dagsoomskaal akkommodeer in hoë-graad naby-bron gneise in die westelike dele van die suid-Sentrale Sone. Die netgestruktureerde leukograniet netwerke sluit in klein intrafoliese smeltselstringe, groter aar-draende skuifskeursones asook groter breukaangedrewe leukograniet plate wat grootte ‘n gebaseerde hiërargiese-verspreiding vertoon as gevolg van die self-georganiseerdheid van die naby-bron smeltsel vervoer bane. Die ontwikkeling van die netwerk is intrinsiek beheer deur variansie in die tempo van smeltsel-toevoer. Smeltsel-geïnduseerde uitstrekkingsbreuking tydens periodes van lae differensiële spanning en verhoogde smeltsel toevoer genereer groot hidroliese gradiënte wat die vorming van groot smeltsel-plate dryf en gevolglik vêr-veld magma dreinerings leikanale kan vorm (gange sensu lato). Egter, die orientasie van die resultante breuke en gange word beheer deur strukture in die wandgesteentes asook regionale en lokale spanningsvelde, wat gevolglik lei tot die ontwikkeling en uiteindelike stolling van die vlak-inklinasie smeltsel plate wat ongunstig georienteer was om druifaangedrewe smeltsel dreinering te akkommodeer.

Hoofstuk 4 adresseer die werklike dreinering van magma deur steil leikanale/gange wat in goed-gelaagde boonste amfiboliet fasies vloergneise sowat ~30 km SO van die dagsome wat

aangebied is in hoofstuk 1. In die geval van die matig-hellende vloergneise met grootskaalse leukograniet netwerke, word deka- tot hektometerskaalse subvertikale leukograniet lense ingesluit en word geïnterpreteer om naby-bron akkumulasie van magma wat noodsaaklik is vir doeltreffende vêr-veld vervoer te dokumenteer. Veld verhoudings dokumenteer onderskeidelik ook die dreinering van die subvertikale lense teen kritiese lengtes en volumes in oormaat van 100 m en ~2.4×10^5 m^3. Hierdie waardes sowel as die veld verhoudings is oor die algemeen in ooreenstemming met teoretiese modelle van magma vervoer deur middel van gemobiliseerde self-propagerende hidrobreuke. Self-propagerende hidrobreuke propageer by hul toppunte en maak terselfdertyd toe by hul sterte en los dus baie subtiele en maklik-oordrukte bewyse agter wat moontlik rekening staan vir die ontwynkendheid van graniet leikanale in die middel-kors. Hierdie verteenwoordig die eerste veld gebaseerde bewyse van grootskaalse magma dreinering deur self-propagerende hidrobreuke en het belangrike gevolge vir die daaropvolgende vervoer van die magma deur en die uieindelike inkrementele inplasing daarvan binne in die subsoliduse kors.

Hoofstuk 5 ondersoek in meer detail die implikasies van breuk-beheerde magma styging vir graniet pluton inplasing in laër-amfiboliet fasies wandgesteentes ~80 km noordoos van die naby-bron strukture wat in hoofstukke 3 en 4 bespreek is. Drie nou-gespasieerde tabletvormige granietiese plutone wat ongeveer gelyktydig ingeplaas was teen wyd uiteenlopende strukturele vlakke in wandgesteentes is ondersoek. Elkeen van die plutone demonstreer die effekte van meganiese kontraste in die wandgesteentes wat breuk propagasie tot stilstand bring eerder as om voorsetting van propagasie te bevoordeel. Meer spesifiek, die drie plutone beklemtoon die rolle wat vertolk word deur vervormingvastheid en reologiese kontraste. Egter, in een geval is dit gewys dat die meganiese kontraste wat breuk propagasie stopsit word nie noodwendig geassosieer met litologiese kontakte nie, soos aanbeveel deur teoretiese modelle van magma

inplasing, deur die belangrikheid van toenemende differensieële spanning te beklemtoon soos wat temperature langs die stygingspad die brosheid-smeebaarheids-oorgang bereik.

Die drie hoofstukke uiteengesit hierbo beklemtoon die belangrkheid van breukbeheerde magma vervoer op alle skale in die middel-kors van die Damara Belt en substansieer sekere van die teoretiese konsepte, maar lig ook uit prominente teenstrydighede tussen die modelle en natuurlike stelsels.

Acknowledgements

If there were to be a single name on this list of those without whom I (probably) would not have embarked upon and (certainly) would not have completed this project, it is that of Alex Kisters. Alex has borne the burden of my supervision with saintly patience and utterly boundless enthusiasm for the work that has occupied my life for the last four years. Alex, I thank you for opportunity you provided and for your priceless contribution towards my development as a young scientist. Your management of my journey through the peaks and troughs of postgraduate research has been exemplary and the privilege of working under your supervision has certainly been underappreciated. The highlights of this project remain those endlessly enlightening discussions held over a cold beer at the end of a hot day in the field. I learnt more on each such occasion than I could by reading a textbook for a month.

To others who have patiently provided constructive criticism on the work contained herein, I thank you for your time and willingness to do so. In this context I would like specifically to thank John Clemens for comments on early versions of some of the work presented here, and also Stefan Jung, who provided thorough peer reviews on two separate occasions. Thanks also to Roberto Weinberg, Mike Brown, Janine Kavanagh, Bob Miller and three anonymous reviewers for their meticulous and constructive peer reviews.

To the postgrad (and post postgrad) gang and clingers-on – Andrea, Andries, Arnie, Gautier, Caps, Carlo, Chris, Cornè, Cynthia, Francesco, Kathryn, Leo, Pieter, (b)Raimund, Shawn, Stephan the red, Stephan the lazy, Theo, Tolene, Valby – some of your comings and goings were erratic, but the friendships formed during days of misery and elation equally shared will, I hope, endure. I have never felt as comfortable amongst any other group of people.

To my parents Trevor and Theresa, I thank you for always allowing me the opportunity to pursue whatsoever took my fancy and also for the patience, understanding and active encouragement of what many would consider a fool's errand. To both of you and to my sister Nicola, your support has been invaluable and I hope you understand what the achievement means to me. Thank you all for only starting to ask, "… so when are you going to finish?" in the final year.

To my late grandmother Sylvia, when I first drafted this acknowledgement your name was in the preceding paragraph. I deeply regret that you did not quite live to see the second of your direct descendants (hopefully!) receive their doctoral degree. It is amazing what can be achieved in a two short generations… humble heritage indeed.

To Loxie Conradie, thank you for smoothing over the administrative and logistical potholes that would certainly have tried my patience to breaking point. Thanks also for providing a sympathetic ear when the road was rough, I am forever in your debt!

Finally, for financial support thanks are again due to Alex Kisters, who, in a bout of temporary insanity, willingly providing funding for a project that ended up taking far longer than either of us would have liked. Thanks in this regard are also due to Ian Buick for assistance with funding through an NRF grant during 2011 and 2012 (no: 69858:2009).

This list is by no means exhaustive, so to anyone not mentioned by name, know that I certainly am grateful for whatever role you have played during my pursuit of this degree.

Contents

List of figures

Chapter 4: Magma accumulation and the onset of far-field ascent

Chapter 5: Controls on the level of pluton emplacement

Chapter 6: Synthesis and conclusions

Chapter 1: Introduction

1.1 Preface

Granite research has traditionally been the domain of petrologists and geochemists investigating the nature of the processes of partial melting and the heat and fluid sources that lead to the generation of granitic magma at depth (e.g. Sederholm, 1907; Bowen and Schairer, 1956; Chappell and White, 1974; Pitcher, 1979; Campbell and Taylor, 1983; Herbert and Sparks, 1988). Today, it is generally agreed that granitoid plutons represent the crystallised products of magmas generated for the most part by partial melting of continental crust (White and Chappell, 1977; Clemens, 1998; Brown, 2013). Inputs from the mantle have also been recognised (Hawkesworth and Kemp, 2006) and, as a result, granitic magmatism is now regarded not only as the primary agent of intracrustal differentiation and recycling, but also of continental crustal growth (Rudnick, 1995; Taylor and McLennan, 2005). During early granite research, the physical processes involved in the movement of large volumes of magma through the crust were considered only peripherally (Petford et al., 2000) and, when discussed, were largely concerned with the so-called "granite space problem," of accommodating the large magma volumes during emplacement, a problem that becomes particularly acute in the brittle upper-crust (Bowen, 1948; Read, 1948; Pitcher, 1979). The space problem has been partly addressed by a growing body of field (e.g. Wiebe and Collins, 1998; Miller and Paterson, 2001; Mahan et al., 2003; Belcher and Kisters, 2006; Miller et al., 2011), geochronological (e.g. Coleman et al., 1995; 2004; Johnson et al., 2003; Glazner et al., 2004; Westraat et al., 2005; Matzel et al., 2006; Michel et al., 2008; Kisters et al., 2012; Leuthold et al., 2012; Barboni et al., 2015) and structural (e.g. McNulty et al., 1996; Cruden et al., 1999; de Saint-Blanquat et al., 2001; Horsman et al., 2005; Morgan et al., 2008) evidence of incremental pluton assembly at much slower time-averaged rates than those necessary to maintain efficient magma ascent (Menand et al., 2015). Thus, our

understanding of the processes that transport magma from source regions in the mid- to deep crust to generally much shallower pluton emplacement levels continues to form the subject of significant debate. Early models combined ascent and emplacement by invoking the concept of magmatic diapirism (Buddington, 1959; Berner et al., 1972; Pitcher, 1979; Coward, 1981; Bateman, 1984; Ramsay, 1989; Paterson and Vernon, 1995), but by the early 1990s purported field evidence of granite diapirs was considered unconvincing (Clemens and Mawer, 1992) and improved modelling of magmatic systems had shown diapirs to be thermally and mechanically unfeasible, particularly in subsolidus crust (Mahon et al., 1988). Channelled fracture-controlled magma ascent is a more viable means of transporting viscous granitic magma through subsolidus crust fast enough to prevent it freezing (Castro, 1987; Clemens and Mawer, 1992; D'lemos et al., 1992; Hutton, 1992; Petford et al., 1993; 1994). The development of ascent models based on the formation of discrete conduits requires the overall process of granitic magma transport to be subdivided into overlapping steps involving (1) the segregation of partial melt from its parent material, (2) the focusing of melt/magma towards discrete ascent conduits, (3) the far-field ascent of magma in the conduits and (4) the arrest of ascent and the emplacement of plutons (Petford et al., 2000; Brown, 2004; Bons et al., 2009). Together these sub-processes must extend over up to 9 orders of magnitude in length-scale and result in volume concentration factors of up to 10^{27} (Bons et al., 2009). This dissertation focuses on the structural controls of the macroscale processes of granitic melt/magma transport (melt segregation and focusing, magma ascent and magma emplacement) in convergent settings and is based on natural examples from the high-grade south Central Zone of the Pan-African Damara Belt in central Namibia.

1.2 Research rationale

Melt/magma transport at the outcrop-scale is usually studied in the field, but any interpretations are based on the static remnants of melt conduits whose mere preservation would indicate failed

melt drainage. The problem then becomes a question as to what extent the granite stringers, sheets or interconnected stockworks that are perceived to represent melt transport networks in the rock-record actually represent efficient segregation and ascent conduits. In order to overcome this problem, and perhaps even more so due to a lack of field evidence, our understanding of the processes of far-field granitic magma transport is largely based on analogue and numerical models which are better suited to describing the transport of more inviscid mafic magmas or hydrothermal fluids. The models are tentatively scaled to be suitably representative of the conditions in the ductile mid-crust during the transport of much more viscous granitic magmas. Likewise, the controls on the depth of pluton emplacement, which are of fundamental importance to subsequent pluton development, have been extensively modelled (numerically and by analogue), but are demonstrated mostly in brittle regimes in the field, whereas granite pluton emplacement occurs at all crustal levels above the anatectic zone. Somewhat strangely, considering the formerly vexing "granite space problem," perhaps the best concurrence between reality and the models is obtained for the processes of wall-rock deformation that accommodate pluton growth, which have been extensively modelled in addition to having been studied in detail in the field (e.g. Benn et al., 1998; Cruden, 1998; Scaillet et al., 1995).

A large part of our understanding of granitic magma transport is based on numerical or analogue models that, due to the dynamic nature of the processes and the apparent lack of field evidence, have not been tested in the field and in nature. The likelihood of recognising field evidence of far-field magma transport increases if extensive sections of the mid- and deep-crust are preserved. The south Central Zone (sCZ) of the northeast-trending Damara Belt in Namibia represents just such a traverse, exposing an oblique section through the magmatic arc of the belt, with its deeper levels (~25 km), containing abundant small-scale leucosome/leucogranite networks, exposed in the west and progressively shallower levels (~12 km), characterised by the

emplacement of voluminous granitoid plutons, exposed along strike towards the east. This obliquity and the outstanding exposure provided by the semi-arid climate represent a superb field laboratory in which to test and evaluate some of the theoretical concepts of magma transport and to integrate them with observations from the field.

By using case studies from the sCZ as an example, this dissertation aims to address the following general questions (see Fig. 1.3):

- To what extent do the leucogranite networks common in high-grade migmatites record relict melt/magma transport pathways and what controls their development and preservation?
- What are the links between these leucogranite networks and far-field magma ascent?
- What are the mechanism(s) of far-field granitic magma ascent and why is so little evidence of the transfer of large volumes of magma preserved in the mid-crust?
- What mechanism(s) arrest ascent and initiate the emplacement of granitoid plutons?

1.3 Structure of the dissertation

By utilising the oblique traverse exposed in the sCZ, this cumulative dissertation presents the results of three separate projects that assess the structural processes of (1) decametre-scale near-source melt/magma transport and focusing, (2) large-scale (~10^5 m^3) near-source magma accumulation and the onset of far-field ascent and (3) the arrest of ascent and initiation of pluton emplacement (Fig. 1.3). This approach is supported throughout by the integration of the field-based data with established theoretical concepts and models.

The dissertation is laid out as follows:

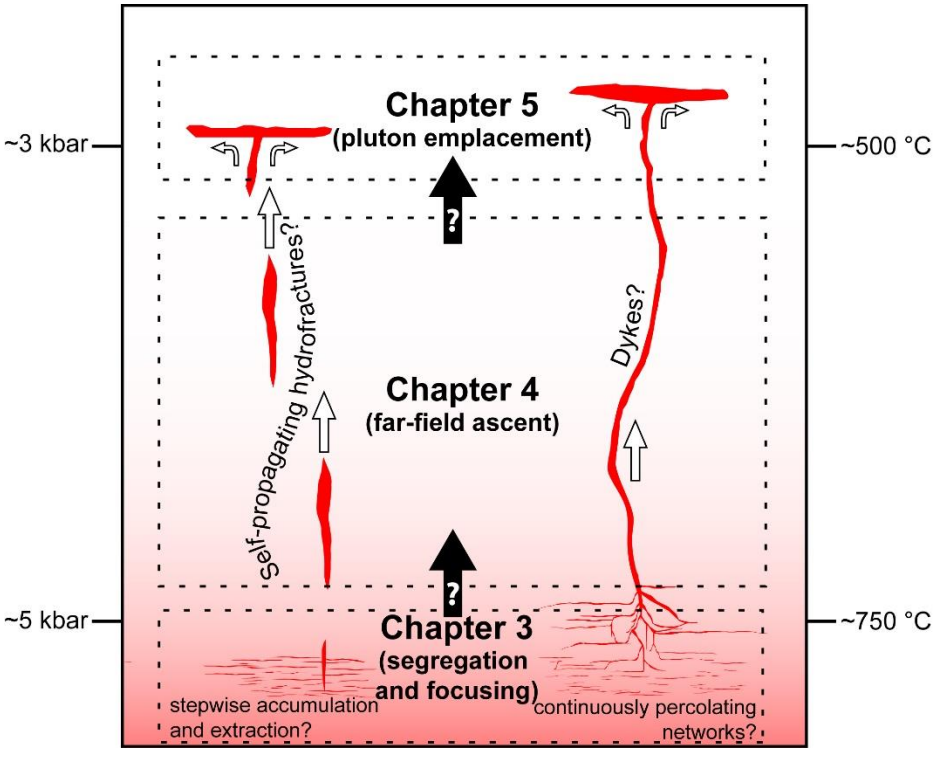

Figure 1.3: *Schematic illustration showing the stages of granitic melt/magma transport discussed in the dissertation with respect to crustal-scale melt/magma transport. Depicted P-T conditions reflect those of the wall rocks in the south Central Zone of the Damara Belt.*

Chapter 2 provides the relevant background as well as a brief description of the pertinent aspects of the geology and setting of the sCZ.

Chapter 3 describes mechanisms of near-source melt segregation and transport in granulite-facies gneisses through the formation of interconnected leucogranite networks that show characteristics of self-organised behaviour (Fig. 1.3).

Chapter 4 describes the episodic accumulation and drainage of large volumes of magma outside the zone of partial melting, but within suprasolidus crust, interpreted to represent the initiation of far-field ascent of the magma batches that later accumulate at emplacement sites higher up in the crust (Fig. 1.3).

Chapter 5 compares the structural and/or lithological and/or stress controls on the level of emplacement of three closely-spaced syntectonic plutons situated at different structural levels in the lower amphibolite-facies central parts of the sCZ (Fig. 1.3).

Chapter 6 is the conclusion chapter and aims to summarise and synthesise the broader implications of the research and highlight the issues that remain unresolved by suggesting potential avenues for future research.

Chapters 3 and 5 of this cumulative dissertation represent published works that have appeared in Earth and Planetary Science Letters and the Journal of African Earth Sciences respectively. Full references for these and other research outputs from this project are presented in Appendix A.

Chapter 4 has been submitted to the Journal of Metamorphic Geology and is, at the time of writing, undergoing peer review.

REFERENCES

Barboni, M., Annen, C. & Schoene, B., 2015. Evaluating the construction and evolution of upper crustal magma reservoirs with coupled U/Pb zircon geochronology and thermal modeling: A case study from the Mt. Capanne pluton (Elba, Italy). *Earth and Planetary Science Letters*, 432, 436-448.

Bateman, R., 1984. On the role of diapirism in the, segregation, ascent and final emplacement of granitoid magmas. *Tectonophysics*, 110(3), 211-231.

Belcher, R. W. & Kisters, A. F., 2006. Progressive adjustments of ascent and emplacement controls during incremental construction of the 3.1 Ga Heerenveen batholith, South Africa. *Journal of Structural Geology*, 28(8), 1406-1421.

Benn, K., Odonne, F. & de Saint Blanquat, M., 1998. Pluton emplacement during transpression in brittle crust: new views from analogue experiments. *Geology*, 26(12), 1079-1082.

Berner, H., Ramberg, H. & Stephansson, O., 1972. Diapirism theory and experiment. *Tectonophysics*, 15(3), 197-218.

Bons, P. D., Becker, J. K., Elburg, M. A. & Urtson, K., 2009. Granite formation: Stepwise accumulation of melt or connected networks?. Earth and Environmental Science *Transactions of the Royal Society of Edinburgh*, 100(1-2), 105-115.

Bowen, N. L., 1948. The granite problem and the method of multiple prejudices. *Geological Society of America Memoirs*, 28, 79-90.

Bowen, N. L. & Schairer, J. F., 1956. *The evolution of the igneous rocks*. New York: Dover Publications, 259 p.

Brown, M., 2004. The mechanism of melt extraction from lower continental crust of orogens. *Geological Society of America Special Papers*, 389, 35-48.

Brown, M., 2013. Granite: From genesis to emplacement. *Geological Society of America Bulletin*, 125(7-8), 1079-1113.

Buddington, A. F., 1959. Granite emplacement with special reference to North America. *Geological Society of America Bulletin*, 70, 671.

Campbell, I. H. & Taylor, S. R., 1983. No water, no granites-No oceans, no continents. *Geophysical Research Letters*, 10(11), 1061-1064.

Castro, A., 1987. On granitoid emplacement and related structures. A review. *Geologische Rundschau*, 76(1), 101-124.

Chappell, B. & White, A., 1974. Two contrasting granite types. *Pacific geology*, 8(2), 173-174.

Clemens, J. D., 1998. Observations on the origins and ascent mechanisms of granitic magmas. *Journal of the Geological Society*, 155(5), 843-851.

Clemens, J. D. & Mawer, C. K., 1992. Granitic magma transport by fracture propagation. *Tectonophysics*, 204(3), 339-360.

Coleman, D. S., Glazner, A. F., Miller, J. S., Bradford, K. J., Frost, T. P., Joye, J. L. & Bachl, C. A., 1995. Exposure of a Late Cretaceous layered mafic-felsic magma system in the

central Sierra Nevada batholith, California. *Contributions to Mineralogy and Petrology*, 120(2), 129-136.

Coleman, D. S., Gray, W. & Glazner, A. F., 2004. Rethinking the emplacement and evolution of zoned plutons: Geochronologic evidence for incremental assembly of the Tuolumne Intrusive Suite, California. *Geology*, 32(5), 433-436.

Coward, M. P., 1981. Diapirism and gravity tectonics: report of a Tectonic Studies Group conference held at Leeds University, 25–26 March 1980. *Journal of Structural Geology*, 3(1), 89-95.

Cruden, A. R., 1998. On the emplacement of tabular granites. *Journal of the Geological Society*, 155(5), 853-862.

Cruden, A. R., Tobisch, O. T. & Launeau, P., 1999. Magnetic fabric evidence for conduit-fed emplacement of a tabular intrusion: Dinkey Creek Pluton, central Sierra Nevada batholith, California. *Journal of Geophysical Research: Solid Earth* (1978–2012), 104(B5), 10511-10530.

D'lemos, R. S., Brown, M. & Strachan, R. A., 1992. Granite magma generation, ascent and emplacement within a transpressional orogen. *Journal of the Geological Society*, 149(4), 487-490.

de Saint-Blanquat, M., Law, R. D., Bouchez, J. L. & Morgan, S. S., 2001. Internal structure and emplacement of the Papoose Flat pluton: An integrated structural, petrographic, and magnetic susceptibility study. *Geological Society of America Bulletin*, 113(8), 976-995.

Glazner, A. F., Bartley, J.M., Coleman, D.S. & Gray, W., Taylor, R.Z., 2004. Are plutons assembled over millions of years by amalgamation from small magma chambers? *GSA Today*, 14, 4-12.

Hawkesworth, C. J. & Kemp, A. I. S., 2006. Evolution of the continental crust. *Nature*, 443(7113), 811-817.

Herbert, E. H. & Sparks, R. S. J., 1988. The generation of granitic magmas by intrusion of basalt into continental crust. *Journal of Petrology*, 29, 599-624.

Horsman, E., Tikoff, B. & Morgan, S., 2005. Emplacement-related fabric and multiple sheets in the Maiden Creek sill, Henry Mountains, Utah, USA. *Journal of Structural Geology*, 27(8), 1426-1444.

Hutton, D. H., 1992. Granite sheeted complexes: evidence for the dyking ascent mechanism. *Geological Society of America Special Papers*, 272, 377-382.

Johnson, S. E., Fletcher, J. M., Fanning, C. M., Vernon, R. H., Paterson, S. R. & Tate, M. C., 2003. Structure, emplacement and lateral expansion of the San José tonalite pluton, Peninsular Ranges batholith, Baja California, México. *Journal of Structural Geology*, 25(11), 1933-1957.

Kisters, A. F. M., Vietze, M. E. & Buick, I., 2012. Deformation and age of the Stinkbank pluton and implications for the correlation of tectonometamorphic episodes in the Pan-African Damara Belt. *South African Journal of Geology*, 115(3), 309-326.

Leuthold, J., Müntener, O., Baumgartner, L. P., Putlitz, B., Ovtcharova, M. & Schaltegger, U., 2012. Time resolved construction of a bimodal laccolith (Torres del Paine, Patagonia). *Earth and Planetary Science Letters*, 325, 85-92.

Mahan, K. H., Bartley, J. M., Coleman, D. S., Glazner, A. F. & Carl, B. S., 2003. Sheeted intrusion of the synkinematic McDoogle pluton, Sierra Nevada, California. *Geological Society of America Bulletin*, 115(12), 1570-1582.

Mahon, K. I., Harrison, T. M. & Drew, D. A., 1988. Ascent of a granitoid diapir in a temperature varying medium. *Journal of Geophysical Research: Solid Earth* (1978–2012), 93(B2), 1174-1188.

Matzel, J. E., Bowring, S. A. & Miller, R. B., 2006. Time scales of pluton construction at differing crustal levels: Examples from the Mount Stuart and Tenpeak intrusions, North Cascades, Washington. *Geological Society of America Bulletin*, 118(11-12), 1412-1430.

McNulty, B. A., Tong, W. & Tobisch, O. T., 1996. Assembly of a dike-fed magma chamber: The Jackass Lakes pluton, central Sierra Nevada, California. *Geological Society of America Bulletin*, 108(8), 926-940.

Menand, T., Annen, C. & de Saint Blanquat, M., 2015. Rates of magma transfer in the crust: Insights into magma reservoir recharge and pluton growth. *Geology*, 43, 199-202.

Michel, J., Baumgartner, L., Putlitz, B., Schaltegger, U. & Ovtcharova, M., 2008. Incremental growth of the Patagonian Torres del Paine laccolith over 90 ky. *Geology*, 36(6), 459-462.

Miller, C. F., Furbish, D. J., Walker, B. A., Claiborne, L. L., Koteas, G. C., Bleick, H. A. & Miller, J. S., 2011. Growth of plutons by incremental emplacement of sheets in crystal-rich host: evidence from Miocene intrusions of the Colorado River region, Nevada, USA. *Tectonophysics*, 500(1), 65-77.

Miller, R. B. & Paterson, S. R., 2001. Construction of mid-crustal sheeted plutons: Examples from the North Cascades, Washington. *Geological Society of America Bulletin*, 113(11), 1423-1442.

Morgan, S., Stanik, A., Horsman, E., Tikoff, B., de Saint Blanquat, M. & Habert, G., 2008. Emplacement of multiple magma sheets and wall rock deformation: Trachyte Mesa intrusion, Henry Mountains, Utah. *Journal of Structural Geology*, 30(4), 491-512.

Paterson, S. R., & Vernon, R. H., 1995. Bursting the bubble of ballooning plutons: a return to nested diapirs emplaced by multiple processes. *Geological Society of America Bulletin*, 107(11), 1356-1380.

Petford, N., Kerr, R. C. & Lister, J. R., 1993. Dike transport of granitoid magmas. *Geology*, 21(9), 845-848.

Petford, N., Lister, J. R. & Kerr, R. C., 1994. The ascent of felsic magmas in dykes. *Lithos*, 32(1), 161-168.

Petford, N., Cruden, A. R., McCaffrey, K. J. W. & Vigneresse, J. L., 2000. Granite magma formation, transport and emplacement in the Earth's crust. *Nature*, 408(6813), 669-673.

Pitcher, W. S., 1979. The nature, ascent and emplacement of granitic magmas. *Journal of the Geological Society*, 136(6), 627-662.

Ramsay, J. G., 1989. Emplacement kinematics of a granite diapir: the Chindamora batholith, Zimbabwe. *Journal of Structural Geology*, 11(1), 191-209.

Read, H. H., 1948. Granites and granites. *Geological Society of America Memoirs*, 28, 1-20.

Rudnick, R. L., 1995. Making continental crust. *Nature*, 378(6557), 571-577.

Scaillet, B., Pêcher, A., Rochette, P. & Champenois, M., 1995. The Gangotri granite (Garhwal Himalaya): laccolithic emplacement in an extending collisional belt. *Journal of Geophysical Research: Solid Earth* (1978–2012), 100(B1), 585-607.

Sederholm, J.J., 1907. On Granite and Gneiss: Their Origin, Relations and Occurrence in the Pre-Cambrian Complex of Fennoscandia. *Bulletin, Community of Geology, Finland*, 23, 110p.

Taylor, S. R., & McLennan, S. M., 1995. The geochemical evolution of the continental crust. *Reviews of Geophysics*, 33(2), 241-265.

Westraat, J., Kisters, A. M., Poujol, M. & Stevens, G., 2005. Transcurrent shearing, granite sheeting and the incremental construction of the tabular 3.1 Ga Mpuluzi batholith, Barberton granite–greenstone terrane, South Africa. *Journal of the Geological Society*, 162(2), 373-388.

White, A. J. & Chappell, B. W., 1977. Ultrametamorphism and granitoid genesis. *Tectonophysics*, 43(1), 7-22.

Wiebe, R. A. & Collins, W. J., 1998. Depositional features and stratigraphic sections in granitic plutons: implications for the emplacement and crystallization of granitic magma. *Journal of Structural Geology*, 20(9), 1273-1289.

Chapter 2: Background

2.1 Microscale melt transport and small-scale segregation

Large-scale magma transport requires that melt first become separated from its protolith, within which melting occurs at temperatures >~650 ºC along the triple-point junctions and contacts between reacting mineral grains (Jurewicz and Watson, 1984; Sawyer, 2001; Holness and Sawyer, 2008). Broadly speaking, prograde partial melting may follow one of two reaction pathways depending on the availability of hydrous fluids, either within the protolith or introduced from elsewhere along deformation-controlled pathways (e.g. Ward et al., 2008; Sawyer, 2010). Fluid-present partial melting occurs readily at relatively lower temperatures, but is usually considered of secondary importance since only a small amount of hydrous fluid remains in crustal rocks as temperatures near the wet solidus (Kriegsman, 2001; Brown, 2013). Moreover, fluid-present partial melting reactions are associated with negative dP/dT slopes (negative volume change) that concentrate rather than diffuse melt during initial partial melting (Clemens and Droop, 1998). Fluid-absent partial melting usually occurs by the breakdown of hydrous micas or amphiboles and is associated with a positive dP/dT slope (Clemens and Droop, Op. cit.; Petford and Koenders, 1998; Rushmer, 2001; Droop and Brodie, 2012). This increase in volume is crucial in the early stages of melt segregation in generating the pressure gradients that, along with the interfacial tension between the melt and the matrix grains of the protolith (Brown et al., 2011), result in the development of locally pervasive microscale melt networks that eventually fill the porosity created during partial melting when melt concentrations reach the melt connectivity transition at ~7-8 vol.% melt (Vigneresse et al., 1996; Rosenberg and Handy, 2005). Below this threshold, melt remains trapped within the grain framework of the protolith unless deviatoric stresses create gradients in magmastatic head down which the melt may be

mobilised into larger contiguous melt-bearing structures or networks (Holness and Sawyer, 2008; Sawyer, 2008; 2014).

At melt concentrations above ~7-8 %, the melt pockets connect, the wall-rocks weaken significantly (Arzi, 1978) and melt begins to flow through, and thereby segregate from, its residuum under the influence of by gravity-, stress- or deformation-induced pressure gradients. The precise mechanisms by which segregation occurs are controversially discussed (Sawyer, 2014), but melt movement at the grain scale must be limited by the viscosity and distribution of the melt. This causes melt pressure to increase with continued melting, promoting melt-induced shearing of the wall-rock matrix during compaction, locally enhancing the permeability of the protolith and the efficiency of melt segregation (Rutter and Mecklenburgh, 2006). The presence/strength of pre-existing anisotropies and fabrics in the protolith also plays an important role in controlling the development of the locally pervasive networks of anisotropy-parallel melt veins (Sawyer, 2014) and melt-filled oblique shear-bands that are preserved as outcrop-scale deformation band- or net-structured leucosome networks in most migmatite terrains (Sawyer, 2008). These leucosomes usually preserve cumulate compositions (residue + some melt; Solar and Brown, 2001; Johnson et al., 2003; Sawyer, 2008; Brown et al., 2014) and the networks are commonly interpreted as recording former melt transport pathways that accommodate the transport of melt within and eventually out of source layers (e.g. Brown, 1994, 2013; Tanner, 1999; Marchildon and Brown, 2003; White et al., 2004; Morfin et al., 2013; Weinberg et al., 2013; 2015).

2.2 Macroscale magma transport

2.2.1 Melt segregation and focusing

Outcrop-scale leucosome networks accommodate the transport of magma away from sites of partial melting within the confines of the source layer and typically coarsen with increasing distance from the source (Sawyer, 2014). Eventually, relatively coarse leucosome networks accomplish mesoscale magma transport out of the source layers down buoyancy- or deformation-induced pressure gradients. Pressure gradients resulting from buoyancy are initially only small (Rutter and Mecklenburgh, 2006) and the largest driving force of melt extraction at this scale is believed to be the dilation associated with dilatant shearing and extensional fracturing promoted by the reduced mean and differential stresses in partially molten/high-grade wall rocks (Davidson et al., 1994). These conditions result in the development of the magma-filled fracture networks represented by leucogranite fracture networks in migmatite terrains (Vanderhaeghe, 1999; Kisters et al., 2009; Weinberg and Regenauer-Lieb, 2010; Reichardt and Weinberg, 2012). In addition to acting as magma transport conduits themselves, the intersections between these fracture geometries result in the development of permeable corridors along which the magmas may be pervasively transported in response to buoyancy and deformation-induced gradients towards extraction points near the top of the anatectic zone from where far-field melt ascent can be initiated (Weinberg, 1999).

2.2.2 Far-field magma ascent

Far-field magma ascent through subsolidus crust remains the most controversial stage in the transport of granitic magmas from deep sources to shallow sinks, due in part to the perceived lack of physical field evidence in exposed mid-crustal terrains. The formation of near-pervasive magma-filled fracture networks described above accommodates the ascent of magma in the suprasolidus anatectic zone, but the networks are not sustainable under subsolidus conditions (Weinberg, 1999). Thus, mechanisms of discrete, focused magma ascent are generally considered more viable for the transport of the magma across and beyond the anatectic front into

cooler overlying rocks. Fracture-controlled models of magma ascent along dykes or self-propagating hydrofractures are the most prominent discrete far-field ascent mechanisms in the literature (Fig. 1. 3; e.g. Lister and Kerr, 1991; Clemens and Mawer, 1992; D'lemos et al., 1992; Hutton, 1992; Petford et al., 1993; 1994; 2000; Bons et al., 2001; 2009; Reichardt and Weinberg, 2012). Fracture-controlled conduits are thought to form as brittle-elastic mode I fractures that open against the least compressive principal stress (Anderson, 1951), generating large pressure gradients that strongly focus magma from the wall rocks. Magma transport is achieved by the propagation of the fractures at their tips in response to tensile stresses generated by the buoyancy of the magma they contain (Cook et al., 1964; Pollard, 1973; Clemens and Mawer, 1992; Nakashima, 1993; Gudmundsson and Brenner, 2001). The fractures may also utilise pre-existing anisotropies, allowing the ascent of magma along fractures that form parallel to steep anisotropies in convergent settings (Lucas and St-Onge, 1995; Brown and Solar, 1998). Nevertheless, the problem of the lack of field evidence persists and our understanding of fracture-controlled granitic magma ascent is based largely on conceptual, analogue and two-dimensional analytic/numerical modelling (see Rivalta et al., 2015). Both of the models of fracture-controlled of magma ascent (dykes and self-propagating hydrofractures) require the accumulation of magma within- or near the suprasolidus source rocks for ascent to be efficient (Diener et al., 2014), and the question as to whether pervasive near-source magma fracture networks accumulate sufficient hydraulically connected melt to feed the ascent conduits remains controversial (Bons et al., 2009).

2.3 Pluton emplacement levels

The contrast between steeply-orientated buoyancy-driven ascent conduits and the commonly subhorizontal granitoid plutons implies that emplacement is initiated where subvertical magma transport switches to subhorizontal (Menand, 2011). Furthermore, many plutons are now

recognised as laterally extensive bodies with broadly tabular aspect ratios (McCaffrey and Petford, 1997; Cruden, 1998) that are assembled by the repeated accretion of sills (Annen et al., 2006; 2015; de Saint-Blanquat, 2006; Menand, 2008; Annen, 2011; Leuthold et al., 2012). The process by which emplacement is initiated has accordingly become known as the dyke-to-sill transition. A primary control for some level of neutral buoyancy on the dyke-to-sill transition has been largely disregarded due both to field evidence and analogue modelling (Menand, 2011). Since dykes propagate ideally at high-angles to the least compressive principal stress, stress rotation has also been suggested as a potential control on the level of emplacement, but the propagation of fractures along anisotropies at high angles to the least compressive stress (Rosenberg, 2004) as well as analogue models (Menand et al., 2010) suggest that stress rotation on its own is unlikely to initiate sill formation and pluton emplacement.

Instead, a mechanical control on the dyke-to-sill transition is suggested by the so-called level of preferred emplacement around the brittle-to-ductile transition in the upper-crust (Vigneresse, 1995; Brown and Solar, 1999; Burov et al., 2003). The role for the mechanical properties of the wall rocks is consistent with the propagation of fractures through heterogeneous crust (Brenner and Gudmundsson, 2004; Taisne and Jaupart, 2009; Gudmundsson et al., 2010). Mechanical anisotropies that may arrest ascending dykes include fractures and slipping bedding contacts (Cooke and Underwood, 2001) and contacts between wall rocks of contrasting stiffness (Youngs moduli) or rheology (e.g. Gudmundsson, 2011; Wiebe and Collins, 1998). Kavanagh et al. (2006) found that the mere presence of these anisotropies may arrest fracture ascent, but is insufficient to initiate sill development and, thus, pluton emplacement where the strength of the arresting interface is high.

2.4 Geology of the south Central Zone

2.4.1 Tectonic framework

The NE-trending Damara Belt in central Namibia represents the suture formed during convergence, subduction and eventual soft collision between the Kalahari and Congo Cratons as part of Gondwana assembly in the Pan-African (*c*. 550-500 Ma; Fig. 2.4.1; Miller, 1983; Gray et al., 2008; Meneghini et al., 2014). The belt has been divided into several NE-trending tectonostratigraphic zones that reflect the bivergent symmetry typical of collisional belts worldwide (Miller, 1983; 2008). The high-grade Central Zone magmatic arc of the belt is divided into the relatively lower grade north Central Zone (nCZ) and the higher grade south Central Zone (sCZ), the latter of which contains the three case studies presented in chapters 3, 4 and 5.

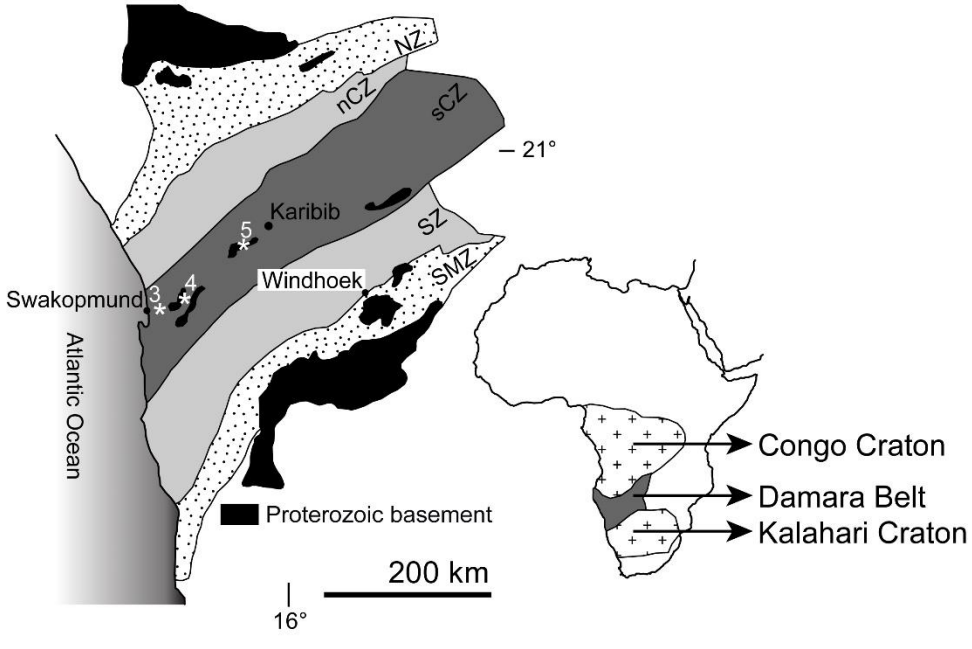

Figure 2.4.1: *The Damara Belt records the Pan-African (c. 550-500 Ma) suturing of the Kalahari and Congo Cratons. The tectonostratigraphic subdivision (zones labelled) of the belt after Miller (1983; 2008) subdivides the Central Zone magmatic arc into a lower grade north- and a higher grade south Central Zone (nCZ and sCZ). The locations of the three case studies from the sCZ presented in chapters 3, 4 and 5 are indicated by asterisks. NZ = Northern Zone; OLZ = Okahandja Lineament Zone; SZ = Southern Zone; SMZ = Southern Marginal Zone. Modified after Miller (1983) and Kisters et al. (2009).*

2.4.2 Lithostratigraphy

The sCZ provides the deepest levels of exposure in the Damara Belt and includes isolated dome-like inliers of Palaeoproterozoic (*c.* 2.0-1.7 Ga; Kröner et al., 1991; Tack et al., 2002) basement gneisses that trace the leading edge of the Congo Craton. The basement inliers are largely undifferentiated and are comprised mostly of quartzofeldspathic gneisses and metavolcanics that are intruded in many cases by much younger Pan-African granites (Miller, 2008). A pronounced unconformity marks the contact between the basement rocks and the overlying Proterozoic Damara Supergroup. The Damara Supergroup comprises a highly heterogeneous mixed siliciclastic/carbonate succession that documents the evolution of the Damara Belt from initial rifting through final convergence. Correspondingly, the Damara Supergroup is strongly mechanically layered from the level of the basement cover contact, which represents a major crustal-scale discontinuity that can be traced long the length of the sCZ, through to contacts in its upper parts that juxtapose rheologically distinct siliciclastic and carbonate metasediments. This mechanical heterogeneity exerts a marked control on the level of granite emplacement throughout the sCZ (Miller, 2008; Kisters et al., 2012), although the reasons for this have not been discussed in any detail.

2.4.3 Structural geology

The structure of the sCZ is the result of two or three deformational events (Jacob, 1974; Miller, 1983). D1/D2 are similar, low-angle events characterised by the development of bedding-parallel fabrics and recumbent folds that are refolded and commonly overprinted by D2/3 folding. Upright and slightly NE-SW verging, ENE-trending folding during D2/3 produced the prominent NE-trending grain of the sCZ. The folds are associated with ENE-trending axial planar foliations (S2/S3) that commonly contain shallowly NE-plunging hinge-parallel stretching lineations (L3). D3 also record top-to-the-NW thrusting, which is localised in the high-grade west into the

pervasively recrystallised marble units of the Damara Supergroup. The same region is characterised by pervasive orogen-parallel constrictional strains, such as SW-closing sheath folds (Coward, 1983) and shallowly SW/NE-plunging mineral stretching lineations (L2/3), that formed in response to orogen-parallel extrusion of the lower parts of the belt (Downing and Coward, 1981; Oliver, 1994). Overall, D2/3 deformation in the sCZ records the rheologically-controlled response of wall rocks at various structural levels to high-angle NW-SE directed shortening during convergence and NW-directed subduction of the Kalahari beneath the Congo craton (Gray et al., 2008).

2.4.4 Metamorphism and partial melting

The CZ Damara Belt is a typical high-T, low-P terrain with its highest grades recorded in the far west of the sCZ, along the Atlantic seaboard around the town of Swakopmund (Fig. 2.4.4). Metamorphic conditions recorded in garnet- and cordierite-bearing metapelites in this area and some 30 km inland indicate peak conditions of 7±0.5 kbar at 750±50 ºC (Masberg, 2000) and 5±1 kbar at 750 ºC respectively (Jung and Mezger, 2003). These conditions resulted in both the fluid-present and fluid-absent partial melting of fertile lithologies of the Damara Supergroup in the western sCZ (Masberg, 2000; Jung and Mezger, 2003; Ward et al., 2008). Further east, around the town of Karibib in the central sCZ, mid- to lower amphibolite-facies conditions of 3±1 kbar and 550-600 ºC are documented by dolomite-calcite thermometry and confirmed by isotopic fractionation during the hydrothermal alteration of a calcite-, garnet- and clinopyroxene-bearing assemblage by a peak-metamorphic mineralising fluid at the Navachab Gold Mine (Puhan, 1983; Dziggel et al., 2009; Wulff et al., 2010). This progression documents a gradual decrease in metamorphic grade from west to east along the strike of the sCZ (Fig. 2.4.4) that is interpreted as recording the oblique exposure of the belt from mid- to lower-crustal levels (20-25

km) in the west to progressively shallower levels towards the east, reaching ~8-12 km around Karibib.

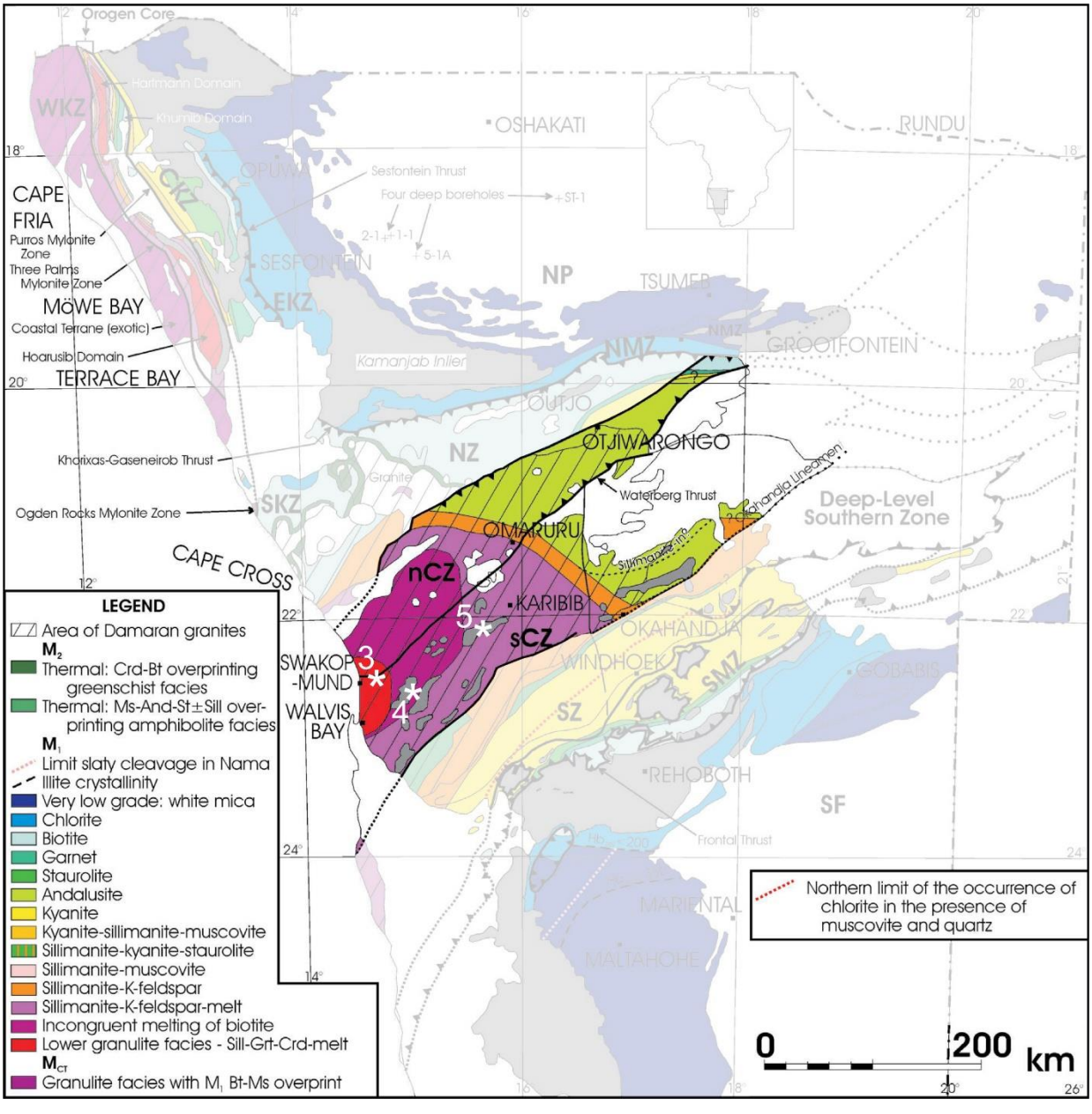

Figure 2.4.4: *Metamorphic zonation for pelitic rocks in the north (nCZ) and south Central Zones (sCZ). Locations of the case studies discussed in chapters 3, 4 and 5 are indicated by the white asterisks. Adapted from Miller (2008).*

The timing and heat sources for metamorphism in the sCZ remain contentious, with various authors suggesting between one and three episodic thermal peaks that span *c.* 540 and 470 Ma. Masberg (2000) argues for a single prolonged metamorphic event from *c*. 540-500 Ma, which records a clockwise P-T path that documents prograde heating and compression during crustal thickening, through isothermal decompression to later isobaric cooling. Nex et al. (2001) suggest a multi-stage evolution with the first peak being characterised by medium-P (4±1 kbar), medium-T (550-600 ºC) metamorphism during collision and orogenic thickening at *c*. 540-530 Ma. A broadly contemporaneous thermal event was attributed by Meneghini et al. (2014) to ridge subduction in the late Neoproterozoic and early Cambrian. Most authors agree that this early episode was followed by a pronounced high temperature (>700 ºC), medium pressure (5±1 kbar) event between 530 and 510 Ma (Jung and Mezger, 2003). This later event has been suggested to be a result of crustal thickening by some authors (e.g. Jung and Mezger, Op. cit.) and slab detachment and mantle upwelling by others (e.g. Meneghini et al., 2014). A third, post-tectonic metamorphic peak, is commonly related to heat advection associated with emplacement of the voluminous late- to post tectonic S-type granitoids into the sCZ (Gray et al., 2006). However, this association is somewhat ambiguous as all three of the peaks are broadly coeval with an equally prolonged period of episodic magmatism in the sCZ, suggesting that the effects of "regional" metamorphism and the advection of heat associated with voluminous granitic magmatism are closely related and not easily distinguished in the region.

2.4.5 Granitic magmatism

The prolonged metamorphism in the sCZ is reflected by a similarly long-lived period of granitic magmatic activity (Fig. 2.4.5). Although extensive evidence of in situ partial melting is preserved in the western sCZ, granitoid plutons in the sCZ generally preserve Nd, Sr, and Pb isotopic signatures related to the high-T, high-P (P up to ~10 kbar, T up to ~1000 °C) partial

melting of both the felsic mid- and mafic lower-crust of the belt (Jung et al., 2002; 2015; Ostendorf et al., 2014; Osterhus et al., 2014; Stammeier et al., 2015). An input from the lithospheric mantle is also recognised in some cases (Jung et al., 2015).

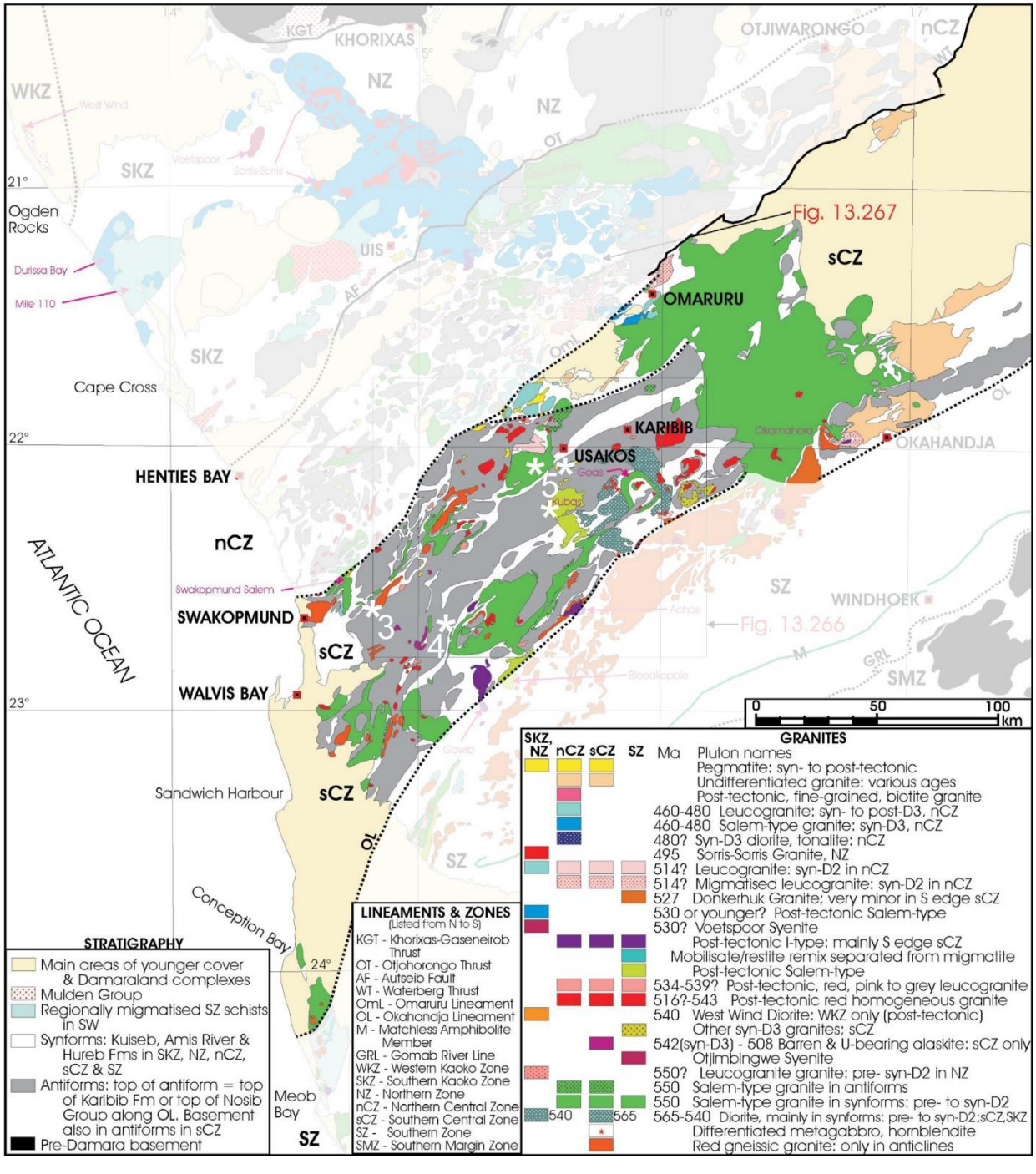

Figure 2.4.5: *Map of the granitic intrusive rocks in the south Central Zone (sCZ). Locations of the case studies discussed in chapters 3, 4 and 5 are indicated by the white asterisks. Adapted from Miller (2008).*

The oldest granitoid suite, known as the Goas Diorite Suite comprises gabbroic- to granodioritic plutons that record U-Pb zircon ages between *c.* 570 and *c.* 545 Ma that are consistent with emplacement during crustal convergence (De Kock et al., 2000; Jacob et al., 2000; Jung et al., 2002; Milani et al., 2014). The intrusion of the Goas Suite is confined to the area southwest of Karibib in the central sCZ, where they form numerous roundish plutons developed around the locally-exposed basement-cover interface (Fig. 2.4.5). The slightly younger Salem Granite Suite is far more widespread and commonly forms extensive (up to 1000s of km^2) sheet- or lopolith-like, texturally distinctive biotite granite plutons whose emplacement is lithologically controlled within the upper parts of the Damara Supergroup (Miller, 2008). Salem-type granites are commonly folded parallel to the regional trends, suggesting an early timing that is reflected by U-Pb zircon ages of between 555 and 545 Ma (Johnson et al., 2006; Kisters et al., 2012; Ostendorf et al., 2014). The youngest widespread granites in the sCZ are post-tectonic, peraluminous S-type granites that were emplaced through region between *c.* 525 and 510 Ma, at the same time as the basement gneisses and Damara Supergroup were undergoing partial melting in the far-west of the sCZ (Jung and Mezger, 2003).

REFERENCES

Anderson, E. M., 1951. The dynamics of faulting and dyke formation with applications to Britain. Oliver and Boyd, Edinburgh, 206 p.

Annen, C., 2011. Implications of incremental emplacement of magma bodies for magma differentiation, thermal aureole dimensions and plutonism–volcanism relationships. Tectonophysics, 500(1), 3-10.

Annen, C., Blundy, J. D. & Sparks, R. S. J., 2006. The genesis of intermediate and silicic magmas in deep crustal hot zones. Journal of Petrology, 47(3), 505-539.

Annen, C., Blundy, J. D., Leuthold, J. & Sparks, R. S. J., 2015. Construction and evolution of igneous bodies: Towards an integrated perspective of crustal magmatism. *Lithos*, 230(1), 206-221.

Arzi, A. A., 1978. Critical phenomena in the rheology of partially melted rocks. *Tectonophysics*, 44(1), 173-184.

Bons, P. D., Dougherty-Page, J. & Elburg, M. A., 2001. Stepwise accumulation and ascent of magmas. *Journal of Metamorphic Geology*, 19(5), 627-633.

Bons, P. D., Becker, J. K., Elburg, M. A. & Urtson, K., 2009. Granite formation: Stepwise accumulation of melt or connected networks?. *Earth and Environmental Science Transactions of the Royal Society of Edinburgh*, 100(1-2), 105-115.

Brenner, S. L. & Gudmundsson, A., 2004. Arrest and aperture variation of hydrofractures in layered reservoirs. *Geological Society, London, Special Publications*, 231(1), 117-128.

Brown, C. R., Yakymchuk, C., Brown, M., Fanning, C. M., Korhonen, F. J., Piccoli, P. M. & Siddoway, C. S., 2014, May. Are cumulate granites characteristic of migmatitic gneiss domes? An example from the Fosdick Mountains of Marie Byrd Land, West Antarctica. In *EGU General Assembly Conference Abstracts*, 16, 4580.

Brown, M., 1994. The generation, segregation, ascent and emplacement of granite magma: the migmatite-to-crustally-derived granite connection in thickened orogens. *Earth-Science Reviews*, 36(1), 83-130.

Brown, M., 2013. Granite: From genesis to emplacement. *Geological Society of America Bulletin*, 125(7-8), 1079-1113.

Brown, M. & Solar, G. S. 1998. Granite ascent and emplacement during contractional deformation in convergent orogens. *Journal of Structural Geology*, 20(9), 1365-1393.

Brown, M. & Solar, G. S., 1999. The mechanism of ascent and emplacement of granite magma during transpression: a syntectonic granite paradigm. *Tectonophysics*, 312(1), 1-33.

Brown, M., Korhonen, F. J. & Siddoway, C. S., 2011. Organizing melt flow through the crust. *Elements*, 7(4), 261-266.

Burov, E., Jaupart, C. & Guillou-Frottier, L., 2003. Ascent and emplacement of buoyant magma bodies in brittle-ductile upper crust. *Journal of Geophysical Research: Solid Earth* (1978–2012), 108(B4).

Clemens, J. D. & Droop, G. T. R., 1998. Fluids, P–T paths and the fates of anatectic melts in the Earth's crust. *Lithos*, 44(1), 21-36.

Clemens, J. D. & Mawer, C. K., 1992. Granitic magma transport by fracture propagation. *Tectonophysics*, 204(3), 339-360.

Cook, J., Gordon, J. E., Evans, C. C. & Marsh, D. M., 1964. A mechanism for the control of crack propagation in all-brittle systems. In *Proceedings of the Royal Society of London A: Mathematical, Physical and Engineering Sciences*, 282(1391), 508-520.

Cooke, M. L. & Underwood, C. A., 2001. Fracture termination and step-over at bedding interfaces due to frictional slip and interface opening. *Journal of Structural Geology*, 23(2), 223-238.

Coward, M. P., 1983. The tectonic history of the Damara belt. Evolution of the Damara Orogen. *Special Publication of the Geological Society of South Africa*, 11, 409-421.

Cruden, A. R., 1998. On the emplacement of tabular granites. *Journal of the Geological Society*, 155(5), 853-862.

D'lemos, R. S., Brown, M. & Strachan, R. A., 1992. Granite magma generation, ascent and emplacement within a transpressional orogen. *Journal of the Geological Society*, 149(4), 487-490.

Davidson, C., Schmid, S. M. & Hollister, L. S., 1994. Role of melt during deformation in the deep crust. *Terra Nova*, 6(2), 133-142.

De Kock, G. S., Eglington, B., Armstrong, R. A., Harmer, R. E. & Walraven, F., 2000. U-Pb and Pb-Pb ages of the Naauwpoort rhyolite, Kawakeup leptite and Okongava Diorite: implications for the onset of rifting and of orogenesis in the Damara belt, Namibia. *Communications of the Geological Survey of Namibia*, 12, 81-88.

de Saint-Blanquat, M., Habert, G., Horsman, E., Morgan, S. S., Tikoff, B., Launeau, P. & Gleizes, G., 2006. Mechanisms and duration of non-tectonically assisted magma emplacement in the upper crust: the Black Mesa pluton, Henry Mountains, Utah. *Tectonophysics*, 428(1), 1-31.

Diener, J. F., White, R. W. & Hudson, T. J., 2014. Melt production, redistribution and accumulation in mid-crustal source rocks, with implications for crustal-scale melt transfer. *Lithos*, 200, 212-225.

Downing, K. N. & Coward, M. P., 1981. The Okahandja Lineament and its significance for Damaran tectonics in Namibia. *Geologische Rundschau*, 70(3), 972-1000.

Droop, G. T. R. & Brodie, K. H., 2012. Anatectic melt volumes in the thermal aureole of the Etive Complex, Scotland: the roles of fluid-present and fluid-absent melting. *Journal of Metamorphic Geology*, 30(8), 843-864.

Dziggel, A., Wulff, K., Kolb, J. & Meyer, F. M., 2009. Processes of high-T fluid–rock interaction during gold mineralization in carbonate-bearing metasediments: the Navachab gold deposit, Namibia. *Mineralium Deposita*, 44(6), 665-687.

Gray, D. R., Foster, D. A., Goscombe, B., Passchier, C. W. & Trouw, R. A., 2006. 40 Ar/39 Ar thermochronology of the Pan-African Damara Orogen, Namibia, with implications for tectonothermal and geodynamic evolution. *Precambrian Research*, 150(1), 49-72.

Gray, D. R., Foster, D. A., Meert, J. G., Goscombe, B. D., Armstrong, R., Trouw, R. A. J. & Passchier, C. W., 2008. A Damara orogen perspective on the assembly of southwestern Gondwana. *Geological Society, London, Special Publications*, 294(1), 257-278.

Gudmundsson, A., 2011. Deflection of dykes into sills at discontinuities and magma-chamber formation. *Tectonophysics*, 500(1), 50-64.

Gudmundsson, A. & Brenner, S. L., 2001. How hydrofractures become arrested. *Terra Nova*, 13(6), 456-462.

Gudmundsson, A., Simmenes, T. H., Larsen, B. & Philipp, S. L., 2010. Effects of internal structure and local stresses on fracture propagation, deflection, and arrest in fault zones. *Journal of Structural Geology*, 32(11), 1643-1655.

Holness, M. B. & Sawyer, E. W., 2008. On the pseudomorphing of melt-filled pores during the crystallization of migmatites. *Journal of Petrology*, 49(7), 1343-1363.

Hutton, D. H., 1992. Granite sheeted complexes: evidence for the dyking ascent mechanism. *Geological Society of America Special Papers*, 272, 377-382.

Jacob, R.E., 1974. Geology and metamorphic petrology of part of the Damara Orogen along the lower Swakop River, South West Africa. *Precambrian Res. Unit Bull*. 17, 201.

Jacob, R. E., Moore, J. M. & Armstrong, R. A., 2000. Zircon and titanite age determinations from igneous rocks in the Karibib District, Namibia: implications for Navachab vein-style gold mineralization. *Communications of the Geological Survey of Namibia*, 12, 157-166.

Johnson, T. E., Hudson, N. F. C. & Droop, G. T. R., 2003. Evidence for a genetic granite–migmatite link in the Dalradian of NE Scotland. *Journal of the Geological Society*, 160(3), 447-457.

Johnson, S. D., Poujol, M. & Kisters, A. F.M., 2006. Constraining the timing and migration of collisional tectonics in the Damara Belt, Namibia: U-Pb zircon ages for the syntectonic Salem-type Stinkbank granite. *South African Journal of Geology*, 109(4), 611-624.

Jung, S., Hoernes, S. & Mezger, K., 2002. Synorogenic melting of mafic lower crust: constraints from geochronology, petrology and Sr, Nd, Pb and O isotope geochemistry of quartz diorites (Damara orogen, Namibia). *Contributions to Mineralogy and Petrology*, 143(5), 551-566.

Jung, S. & Mezger, K, 2003. Petrology of basement-dominated terranes: I. Regional metamorphic T–t path from U–Pb monazite and Sm–Nd garnet geochronology (Central Damara orogen, Namibia). *Chemical Geology*, 198(3), 223-247.

Jung, S., Kröner, A., Hauff, F. & Masberg, P., 2015. Petrogenesis of synorogenic diorite–granodiorite–granite complexes in the Damara Belt, Namibia: Constraints from U–Pb zircon ages and Sr–Nd–Pb isotopes. *Journal of African Earth Sciences*, 101, 253-265.

Jurewicz, S. R. & Watson, E. B., 1984. Distribution of partial melt in a felsic system: the importance of surface energy. *Contributions to Mineralogy and Petrology*, 85(1), 25-29.

Kavanagh, J. L., Menand, T. & Sparks, R. S. J., 2006. An experimental investigation of sill formation and propagation in layered elastic media. *Earth and Planetary Science Letters*, 245(3), 799-813.

Kisters, A. F. M., Ward, R. A., Anthonissen, C. J. & Vietze, M. E., 2009. Melt segregation and far-field melt transfer in the mid-crust. *Journal of the Geological Society*, 166(5), 905-918.

Kisters, A. F. M., Vietze, M. E. & Buick, I., 2012. Deformation and age of the Stinkbank pluton and implications for the correlation of tectonometamorphic episodes in the Pan-African Damara Belt. *South African Journal of Geology*, 115(3), 309-326.

Kriegsman, L. M., 2001. Partial melting, partial melt extraction and partial back reaction in anatectic migmatites. *Lithos*, 56(1), 75-96.

Kröner, A., Retief, E. A., Compston, W., Jacob, R. E. & Burger, A. J., 1991. Single-grain and conventional zircon dating of remobilized basement gneisses in the central Damara belt in Namibia. *South African Journal of Geology*, 94(5-6), 379-387.

Leuthold, J., Müntener, O., Baumgartner, L. P., Putlitz, B., Ovtcharova, M. & Schaltegger, U., 2012. Time resolved construction of a bimodal laccolith (Torres del Paine, Patagonia*). Earth and Planetary Science Letters*, 325, 85-92.

Lister, J. R. & Kerr, R. C., 1991. Fluid-mechanical models of crack propagation and their application to magma transport in dykes. *Journal of Geophysical Research: Solid Earth* (1978–2012), 96(B6), 10049-10077.

Lucas, S. B. & St-Onge, M. R., 1995. Syn-tectonic magmatism and the development of compositional layering, Ungava Orogen (northern Quebec, Canada). *Journal of Structural Geology*, 17(4), 475-491.

McCaffrey, K. J. W. & Petford, N., 1997. Are granitic intrusions scale invariant?. *Journal of the Geological Society*, 154(1), 1-4.

Marchildon, N. & Brown, M., 2003. Spatial distribution of melt-bearing structures in anatectic rocks from Southern Brittany, France: implications for melt transfer at grain-to orogen-scale. *Tectonophysics*, 364(3), 215-235.

Masberg, P., 2000. Garnet growth in medium pressure granulite-facies metapelites from the central Damara Orogen: igneous versus metamorphic history. *Communications of the Geological Survey. Namibia*, 12, 115-124.

Menand, T., 2008. The mechanics and dynamics of sills in layered elastic rocks and their implications for the growth of laccoliths and other igneous complexes. *Earth and Planetary Science Letters*, 267(1), 93-99.

Menand, T., 2011. Physical controls and depth of emplacement of igneous bodies: A review. *Tectonophysics*, 500(1), 11-19.

Menand, T., Daniels, K. A. & Benghiat, P., 2010. Dyke propagation and sill formation in a compressive tectonic environment. *Journal of Geophysical Research: Solid Earth* (1978–2012), 115(B8).

Meneghini, F., Kisters, A., Buick, I. & Fagereng, Å., 2014. Fingerprints of late Neoproterozoic ridge subduction in the Pan-African Damara belt, Namibia. *Geology*, 42(10), 903-906.

Milani, L., Kinnaird, J. A., Lehmann, J., Naydenov, K. V., Saalmann, K., Frei, D. & Gerdes, A., 2014. Role of crustal contribution in the early stage of the Damara Orogen, Namibia: New constraints from combined U–Pb and Lu–Hf isotopes from the Goas Magmatic Complex. *Gondwana Research*, 28(3), 961-986.

Miller, R. M., 1983. The Pan-African Damara Orogen of South West Africa/Namibia. In: Miller, R.M. (ed), Evolution of the Damara Orogen of South West Africa/Namibia. *Special publication of the geological society of South Africa*, 11, 431-515.

Miller, R.M., 2008. *The Geology of Namibia volume 2: Neoproterozoic to Lower Paleozoic*. Geological Survey of Namibia, Windhoek, Namibia.

Morfin, S., Sawyer, E. W. & Bandyayera, D., 2013. Large volumes of anatectic melt retained in granulite facies migmatites: An injection complex in northern Quebec. *Lithos*, 168, 200-218.

Nakashima, Y., 1993. Static Stability and Propagation of a Fluid-Filled Edge Crack in Rock: Implication for Fluid Transport in Magmatism and Metamorphism. *Journal of Physics of the Earth*, 41(3), 189-202.

Nex, P. A. M., Oliver, G. J. H. & Kinnaird, J. A., 2001. Spinel-bearing assemblages and PT-t evolution of the Central Zone of the Damara Orogen, Namibia. *Journal of African Earth Sciences*, 32(3), 471-489.

Oliver, G. J., 1994. Mid-crustal detachment and domes in the central zone of the Damaran orogen, Namibia. *Journal of African Earth Sciences*, 19(4), 331-344.

Ostendorf, J., Jung, S., Berndt-Gerdes, J. & Hauff, F., 2014. Syn-orogenic high-temperature crustal melting: Geochronological and Nd–Sr–Pb isotope constraints from basement-derived granites (Central Damara Orogen, Namibia). *Lithos*, 192, 21-38.

Osterhus, L., Jung, S., Berndt, J. & Hauff, F., 2014. Geochronology, geochemistry and Nd, Sr and Pb isotopes of syn-orogenic granodiorites and granites (Damara orogen, Namibia)—Arc-related plutonism or melting of mafic crustal sources?. *Lithos*, 200, 386-401.

Petford, N. & Koenders, M. A., 1998. Self-organisation and fracture connectivity in rapidly heated continental crust. *Journal of Structural Geology*, 20(9), 1425-1434.

Petford, N., Kerr, R. C. & Lister, J. R., 1993. Dike transport of granitoid magmas. *Geology*, 21(9), 845-848.

Petford, N., Lister, J. R. & Kerr, R. C., 1994. The ascent of felsic magmas in dykes. *Lithos*, 32(1), 161-168.

Petford, N., Cruden, A. R., McCaffrey, K. J. W. & Vigneresse, J. L., 2000. Granite magma formation, transport and emplacement in the Earth's crust. *Nature*, 408(6813), 669-673.

Pollard, D. D., 1973. Derivation and evaluation of a mechanical model for sheet intrusions. *Tectonophysics*, 19(3), 233-269.

Puhan, D., 1983. Temperature and pressure of metamorphism in the Central Damara orogen. In: Miller, R.McG. (Ed.), Evolution of the Damara Orogen of South West Africa/Namibia, *Geological Society of South Africa Special Publication*, 11, 219-223.

Reichardt, H. & Weinberg, R. F., 2012. The dike swarm of the Karakoram shear zone, Ladakh, NW India: Linking granite source to batholith. *Geological Society of America Bulletin*, 124(1-2), 89-103.

Rivalta, E., Taisne, B., Bunger, A. P. & Katz, R. F., 2015. A review of mechanical models of dike propagation: Schools of thought, results and future directions. *Tectonophysics*, 638, 1-42.

Rosenberg, C. L., 2004. Shear zones and magma ascent: a model based on a review of the Tertiary magmatism in the Alps. *Tectonics*, 23(3).

Rosenberg, C. L. & Handy, M. R., 2005. Experimental deformation of partially melted granite revisited: implications for the continental crust. *Journal of Metamorphic Geology*, 23(1), 19-28.

Rushmer, T., 2001. Volume change during partial melting reactions: implications for melt extraction, melt geochemistry and crustal rheology. *Tectonophysics*, 342(3), 389-405.

Rutter, E. H. & Mecklenburgh, J., 2006. The extraction of melt from crustal protoliths and the flow behaviour of partially molten crustal rocks: An experimental perspective. In: Brown, M., & Rushmer, T. (eds), *Evolution and differentiation of the continental crust*. Cambridge University press, Cambridge, 386-429.

Sawyer, E. W., 2001. Melt segregation in the continental crust: distribution and movement of melt in anatectic rocks. *Journal of Metamorphic Geology*, 19(3), 291-309.

Sawyer, E.W., 2008. *Atlas of Migmatites*. The Canadian Mineralogist, Special Publication 9. NRC Research Press, Ottawa, Ontario, Canada. 371 p.

Sawyer, E. W., 2010. Migmatites formed by water-fluxed partial melting of a leucogranodiorite protolith: microstructures in the residual rocks and source of the fluid. *Lithos*, 116(3), 273-286.

Sawyer, E. W., 2014. The inception and growth of leucosomes: microstructure at the start of melt segregation in migmatites. *Journal of Metamorphic Geology*, 32(7), 695-712.

Solar, G. S. & Brown, M., 2001. Petrogenesis of migmatites in Maine, USA: possible source of peraluminous leucogranite in plutons?. *Journal of Petrology*, 42(4), 789-823.

Stammeier, J., Jung, S., Romer, R. L., Berndt, J. & Garbe-Schönberg, D., 2015. Petrology of ferroan alkali-calcic granites: Synorogenic high-temperature melting of undepleted felsic lower crust (Damara orogen, Namibia). *Lithos*, 224, 114-125.

Tack, L., Williams, I., & Bowden, P. (2002). SHRIMP constraints on early post-collisional granitoids of the Ida Dome, central Damara (Pan-African) Belt, western Namibia. In *11th IAGOD Quadrennial Symposium and Geocongress. Windhoek, Namibia*: Geol. Survey Nambia, 1-5.

Taisne, B. & Jaupart, C., 2009. Dike propagation through layered rocks. *Journal of Geophysical Research: Solid Earth* (1978–2012), 114(B9).

Tanner, D. C., 1999. The scale-invariant nature of migmatite from the Oberpfalz, NE Bavaria and its significance for melt transport. *Tectonophysics*, 302(3), 297-305.

Vanderhaeghe, O., 1999. Pervasive melt migration from migmatites to leucogranite in the Shuswap metamorphic core complex, Canada: control of regional deformation. *Tectonophysics*, 312(1), 35-55.

Vigneresse, J. L., 1995. Control of granite emplacement by regional deformation. *Tectonophysics*, 249(3), 173-186.

Vigneresse, J. L., Barbey, P. & Cuney, M, 1996. Rheological transitions during partial melting and crystallization with application to felsic magma segregation and transfer. *Journal of Petrology*, 37(6), 1579-1600.

Ward, R., Stevens, G. & Kisters, A., 2008. Fluid and deformation induced partial melting and melt volumes in low-temperature granulite-facies metasediments, Damara Belt, Namibia. *Lithos*, 105(3), 253-271.

Weinberg, R. F., 1999. Mesoscale pervasive felsic magma migration: alternatives to dyking. *Lithos*, 46(3), 393-410.

Weinberg, R. F. & Regenauer-Lieb, K., 2010. Ductile fractures and magma migration from source. *Geology*, 38(4), 363-366.

Weinberg, R., Hasalova, P., Ward, L. & Fanning, C., 2013. Interaction between deformation and magma extraction in migmatites: Examples from Kangaroo Island, South Australia. *Geological Society of America Bulletin*, 125, 1282-1300.

Weinberg, R. F., Veveakis, E. & Regenauer-Lieb, K., 2015. Compaction-driven melt segregation in migmatites. *Geology*, 43(6), 471-474.

White, R. W., Powell, R. & Halpin, J. A., 2004. Spatially-focussed melt formation in aluminous metapelites from Broken Hill, Australia. *Journal of Metamorphic Geology*, 22(9), 825-845.

Wiebe, R. A. & Collins, W. J., 1998. Depositional features and stratigraphic sections in granitic plutons: implications for the emplacement and crystallization of granitic magma. *Journal of Structural Geology*, 20(9), 1273-1289.

Wulff, K., Dziggel, A., Kolb, J., Vennemann, T., Böttcher, M. E. & Meyer, F. M., 2010. Origin of mineralizing fluids of the sediment-hosted Navachab Gold Mine, Namibia: Constraints from stable (O, H, C, S) isotopes. *Economic Geology*, 105(2), 285-302.

Chapter 3: Melt segregation and near-source transport

This chapter constitutes a presentation of the published research paper: ***The stabilization of self-organised leucogranite networks– implications for melt segregation and far-field melt transfer in the continental crust***[1] by Hall and Kisters.

This paper was first authored by Duncan Hall with standard supervision entailing academic guidance and editorial support from Alex Kisters. The following aspects were carried out independently by Duncan Hall: (1) field work and data collection, (2) processing and interpretation of the data, (3) box-counting image analyses and interpretation, (4) preparation and submission of the manuscript and (5) manuscript revision and successful resubmission.

[1]Hall, D. J. & Kisters, A. F. M, 2012. ***The stabilization of self-organised leucogranite networks-Implications for melt segregation and far-field melt transfer in the continental crust***. *Earth and Planetary Science Letters*, 355, 1-12.

Earth and Planetary Science Letters 355–356 (2012) 1–12

Contents lists available at SciVerse ScienceDirect

Earth and Planetary Science Letters

journal homepage: www.elsevier.com/locate/epsl

The stabilization of self-organised leucogranite networks—Implications for melt segregation and far-field melt transfer in the continental crust

Duncan Hall, Alexander Kisters*

Department of Earth Sciences, University of Stellenbosch, Matieland 7602, South Africa

ARTICLE INFO

Article history:
Received 20 April 2012
Received in revised form
26 August 2012
Accepted 27 August 2012
Editor: T.M. Harrison

Keywords:
magma migration
self-organization
granite emplacement

ABSTRACT

Net-structured leucocratic vein systems are ubiquitous in high-grade and migmatite terrains and are interpreted to represent interconnected former magma-bearing structures that accommodated the migration of granitic magmas out of their anatectic source regions. Net-structured leucogranite vein systems in high-grade gneisses from the Damara Belt in Namibia describe a size-based hierarchy and spatial distribution that indicates self-organisation of the magma transfer system. The internal geometry and connectivity of the net-structured leucogranites are controlled by variations in melt pressure, whereas regional strains control the orientation of the leucogranites. Foliation-parallel (stromatic) and shear-band-hosted granite veins accommodate transport at relatively low melt volumes and account for the metre-scale segregation of melt close to the anatectic source. During times of higher melt supply, the formation of extensional fractures that cross-cut stromatic and shear-band-hosted melt sheets at high angles is promoted. Extensional fracturing and associated dilatancy create gradients in magmastatic head that cause melt to be drained from pervasive stromatic and shear-band-hosted vein networks into spaced dilatant fractures. This has the potential to initiate buoyancy-driven far-field melt transfer along suitably orientated extensional fractures as vertical dykes or self-propagating hydrofractures. Our results suggest that melt transfer systems are able to adjust to variations in melt supply by forming conduits that accommodate varying melt volumes and will tend to develop towards a state of self-organisation.

1. Introduction

The ascent of granitic magmas from anatectic regions in the mid- and lower-crust to form large plutonic complexes in the upper crust is commonly conceptualised into two end-member models that either describe focused or pervasive magma transfer through the continental crust (Fig. 1). Pervasive flow is interpreted to occur along networks of granite conduits, such as interconnected fracture systems or sheets along layer anisotropies (Bons et al., 2004; Weinberg, 1999), or through flow along structurally controlled interconnected dilational sites near the anatectic region (Collins and Sawyer, 1996). Focused flow describes magma transfer through distinct fracture conduits, either by the establishment and maintenance of conventional dykes (e.g. Brown, 1994; Clemens, 2005; Petford et al., 1994; Weinberg, 1996), the initiation of self-propagating fractures (e.g. Bons and Arnold, 2003; Bons and van Milligen, 2001; Clemens and Mawer, 1992; Weinberg and Regenauer-Lieb, 2010) or by channelised flow associated with crustal scale shear-zones (Brown and Solar, 1998a). Focused transport invokes a focusing of the magma from more pervasive melt segregation structures close to the anatectic source into spaced and fewer transport structures that accommodate the far-field transport through the crust (throughout the paper the term melt is used to describe a melt phase with or without crystallization products).

High-grade, migmatitic terrains commonly display morphologically and geometrically complex interconnected networks of former magma-bearing conduits (Brown, 2007). These can take the form of pervasive leucogranite networks, bedding- or foliation-parallel leucogranite sheets (e.g. Collins and Sawyer, 1996; Weinberg, 1999) or leucogranite networks made up of intersecting foliation-parallel and low- and high-angle morphologies (Bons et al., 2009; Brown, 2007; Sawyer, 2008; Weinberg and Mark, 2008). The migration of granitic magmas in such networks is commonly regarded to be determined mainly by external factors, such as wall-rock anisotropies and/or pressure gradients induced during deformation of rheologically anisotropic rock (e.g. Bons et al., 2009; Brown, 2007; Brown and Solar, 1999; Brown et al., 1995; Guernina and Sawyer, 2003; Marchildon and Brown, 2003; Vanderhaeghe, 1999). The mechanisms that focus melt flow and account for the transition from local-scale segregation near the source to far field magma transport through mostly subsolidus crust are less well understood.

A more active role of the melt in the creation of its own transfer pathways is indicated by a number of studies that suggest that leucosome distributions in high-grade terrains display certain characteristics of self-organised critical behaviour, such as scale-invariance, hierarchical arrangements and power-law size/frequency

* Corresponding author.
E-mail address: akisters@sun.ac.za (A. Kisters).

0012-821X/$ - see front matter © 2012 Elsevier B.V. All rights reserved.
http://dx.doi.org/10.1016/j.epsl.2012.08.033

distributions (Bonamici and Duebendorfer, 2010; Bons et al., 2004; Brown, 2010; Soesoo et al., 2004; Tanner, 1999). In the absence of external factors, self-organisation predicts the development and stabilization of a hierarchical pattern of magma conduits, the morphology of which is determined by factors intrinsic to the magma system itself, i.e. the "… *the system adjusts to accommodate the flux*," rather than the converse (Bons and Arnold, 2003, p. 670).

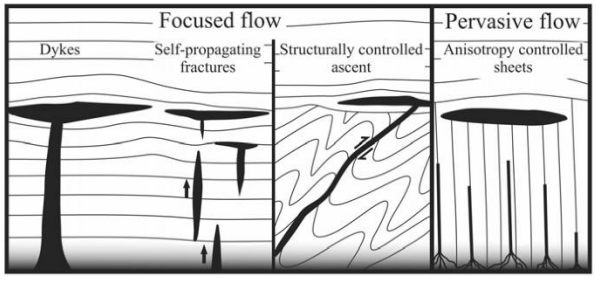

Fig. 1. Schematic sketch of the main current models for the transfer of granitic magmas across the continental crust (after Bons et al., 2004). Focused flow may occur in conventional dykes (e.g. Petford et al., 1994), self-propagating hydrofractures (e.g. Bons et al., 2004; Clemens and Mawer, 1992; Kisters et al., 2009) or along crustal-scale shear zones (e.g. Brown and Solar, 1998a). Pervasive flow may occur, for example, in interconnected fracture networks (e.g. Petford and Koenders, 1998), along tributary networks to multiple anisotropy controlled granite sheets (e.g. Weinberg, 1999), or by porous flow in the anatectic region (e.g. Collins and Sawyer, 1996).

This paper describes the spatial arrangement, geometry and connectivity of a leucogranite network that is inferred to represent former magma ascent pathways from well-exposed high-grade rocks of the Pan-African (550–500 Ma) Damara Belt in Namibia. The study aims to provide a field-based data set documenting the structural controls, spatial relationships and distribution of former magma-bearing structures that accommodated magma transfer in this mid-crustal section. We also discuss implications of the above results for our understanding of the formation and stabilization of granitic magma conduits in the continental crust.

2. Geological setting

The Damara Belt in central Namibia forms the suture between the Kalahari and the Congo Cratons that collided during the assembly of Gondwana in the latest Neoproterozoic and early

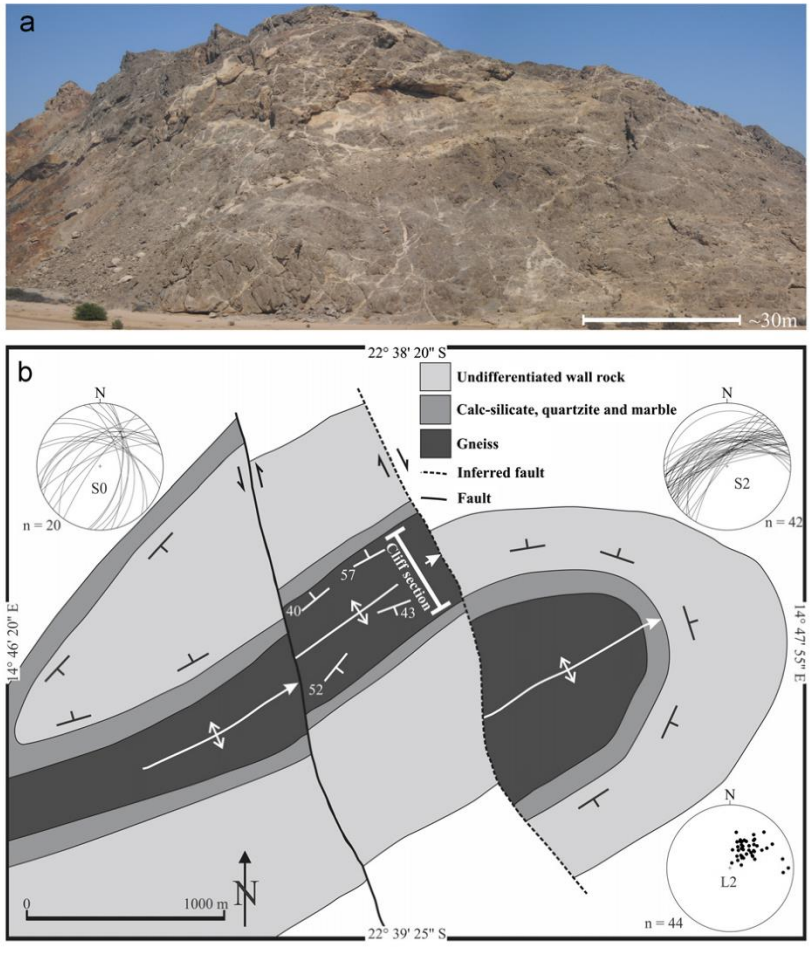

Fig. 2. (a) Photographic panel of the NE-facing slope of the main cliff section containing variable amounts of leucogranite stringers or sheets. Leucogranites are concentrated towards the top of the hill, in the crest of an antiformal structure (see part b of this figure). (b) Simplified geological map of the area, the location of the cliff section is indicated. The leucogranites are hosted in the gneisses that form the core of the F2 antiform. Equal area stereographic projections into the lower hemisphere (used throughout this paper) of S0, S2 and L2 are shown. The folded bedding (S0) defines the steep NE plunge of the F2 antiform and the axial planar foliation (S2) defines a slight SE vergence of the fold. The projection of the L2 stretching lineation (X axis of the finite strain ellipsoid with $X \geq Y \geq Z$) shows it to be parallel to the plunge of the fold.

Phanerozoic (Miller, 1983). The deeply eroded SW parts of the Central Zone (CZ; after Miller, 1983) record peak *P–T* conditions of ~5–6 kbar and ~750–800 °C, with associated syntectonic partial melting and voluminous granite plutonism (Jung and Mezger, 2001; Masberg, 2000; Tack and Bowden, 1999; Ward et al., 2008). Anatectic features are recorded in both the basement gneisses and the supracrustal rocks of the overlying Neoproterozoic Damara Supergroup (Miller, 1983; Jung and Mezger, 2001) and are particularly well exposed in the deeply incised riverbeds of the Khan and Swakop rivers in the SW parts of the CZ, along the northern margin of the Namib Desert. This study focuses on cliff sections and pavements exposed along the Swakop River that are composed of upper-amphibolite facies, largely metasedimentary rocks of the upper Khan Formation of the Damara Supergroup. The upper Khan Formation reaches a thickness of > 1000 m in this section and comprises mainly quartzo-feldspathic biotite-gneisses, amphibole and biotite schist, feldspathic as well as pure quartzite with interspersed conglomerates, calc-silicate rocks and marble horizons (Miller, 2008).

Structures in this part of the CZ are dominated by an early generation (D1) of km-scale recumbent nappes that have been refolded by NE-trending, near-upright folds (F2 after Jacob (1974); F3 after Miller (1983)). The first-order, regional-scale F2 folds are doubly-plunging and often take the form of SW-closing sheath folds (Coward, 1983). A prominent NE-plunging stretching lineation (L2) is parallel to the hinges of the F2 sheath folds. The constrictional strains and pronounced NE-SW stretch are interpreted to have formed in response to the lateral, orogen-parallel extrusion of the rocks of the CZ during NW–SE directed D2 shortening (Kisters et al., 2004; Poli and Oliver, 2001).

The study area covers ~0.5 km^2 and is centred on a steep-sided hill (22° 38′ 46″S, 14° 47′ 04″E) that offers excellent 3D exposure of steep cliff sections and subhorizontal pavements (Fig. 2a). Medium- to coarse-grained quartzo-feldspathic biotite gneisses form the core of a NE-trending, moderate- to steep NE-plunging, close- to tight third-order F2 antiform with a half wavelength of approximately 200 m and an amplitude of > 100 m. An intercalated succession of calc-silicate felses, marble and quartzite horizons delineate the limbs of the F2 fold, but are eroded near the top of the hill, in the crest of the fold (Fig. 2b).

The gneisses in the core of the fold show a spaced and streaky, steep NW-dipping foliation (S2; Fig. 2b), defined by biotite and the grain-shape preferred orientation of quartz and feldspar grains and accentuated by sheet-like, foliation-parallel leucogranite stringers. The gneissosity is axial planar to the F2 antiform, indicating the slight SE vergence of the fold. Stretched quartz–feldspar aggregates and rodded leucogranites define a prominent, steep NE plunging stretching lineation (L2; Fig. 2b) that is parallel to the plunge of the F2 fold.

3. Leucocratic features

Leucogranite stringers and pods are compositionally and texturally distinct from the gneisses and comprise alkali-feldspar (~50%), quartz (~25%), plagioclase (~20%), biotite (~2%) and muscovite (~2%) with accessory hornblende and zircon. The leucogranites range from sub-mm, foliation-parallel stringers and veinlets to > 5 m wide pods and > 3 m wide sheets that can be followed for > 100 m along strike. In situ partial melting in this part of the low-T granulite-facies terrain of the south CZ is widespread, particularly in metapelitic units (Jung and Mezger, 2003; Kisters et al., 2009; Ward et al., 2008). However, peritectic phases that would indicate in situ partial melting in the quartzo-feldspathic gneisses are absent and contacts between the leucogranites and the host gneisses are generally sharp. This suggests that the leucogranites in the outcrops are the crystallization products of anatectic magmas, or the parts thereof that have migrated out of their source and have been injected as leucocratic veins into the gneisses. The morphology and spatial pattern of leucogranite stringers, veins and sheets, however, closely resemble net-structured migmatites described by Sawyer (2008) in which distinct sets of leucogranite morphologies exhibit a net-like structure within the darker host gneisses (see below). Based on these similarities, we follow the nomenclature devised by Sawyer (2008) and refer to the leucocratic rocks as leucogranite stringers, veins or sheets. Though the spatial arrangement of the leucogranites and wall rocks closely resembles that of net-structured migmatites (*sensu lato*), we emphasize that the leucogranites have not formed in situ through partial melting of the host gneisses.

3.1. Leucogranite geometries

Based on orientation, morphology and their relationship with the wall-rock gneissosity (S2), the following three types of leucocratic stringers, veins and sheets can be distinguished (Fig. 3).

3.1.1. Intrafolial leucogranites

Intrafolial leucocratic stringers, veinlets and pods are contained in the S2 foliation. These are the smallest, but most abundant leucogranites in the gneisses. They generally form thin, up to 1 cm wide and > 50 cm long, fine-grained (0.1–1 mm) stringers pervasively developed within the wall-rock gneissosity. The veins are commonly parallel-sided and are generally spaced at intervals of between 1 and 25 cm. The veins may also describe anastomosing patterns and less regular morphologies such as pinch-and-swell and boudinage within the S2 foliation. The long axis of the boudins plunges moderately to the SW, perpendicular to L2 (*Y* axis of the strain ellipsoid). In places, the coalescence of closely-spaced, anastomosing stringers results in thicker (10–20 cm) leucocratic bands, which envelope thin slivers of wall-rock.

3.1.2. Shear-band-hosted leucogranites

Shear-band-hosted leucocratic veins form at low to intermediate angles (10°–60°) to the S2 foliation. Thinner examples are more common and typically exhibit lengths of between 0.5 and

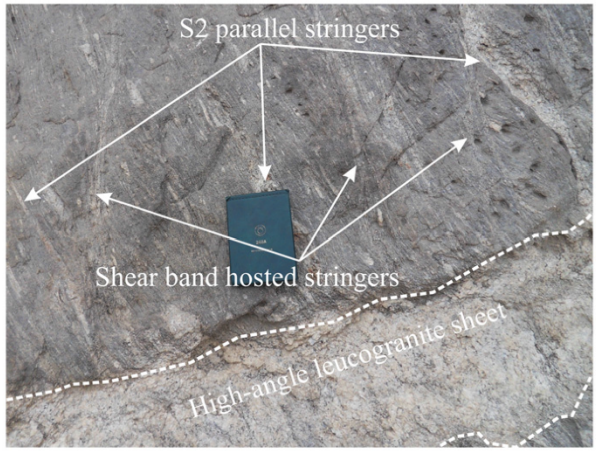

Fig. 3. Leucogranite stringers, veins and sheets can be grouped by morphology, orientation and their relationship with the enveloping S2 gneissosity into (1) S2-parallel (intrafolial) stringers, (2) S2-oblique shear-band-hosted veins, and (3) leucogranite sheets that cut across the foliation at high angles (see text for further discussion).

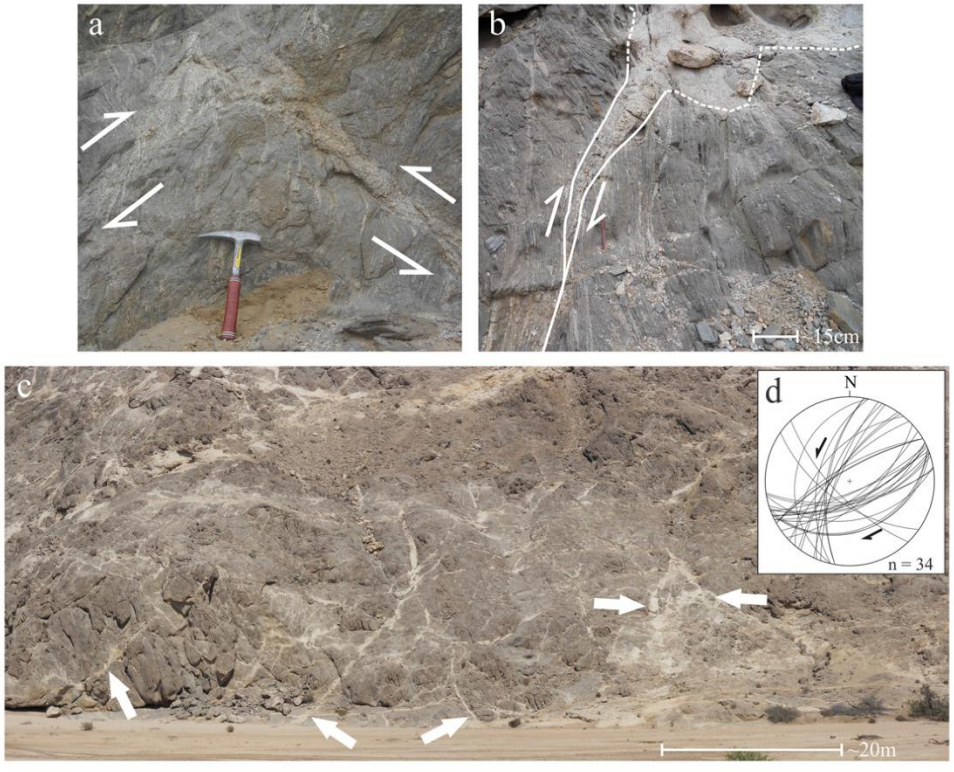

Fig. 4. (a) Intersection between conjugate leucogranite-bearing shear bands showing foliation drag and inflation near the intersection; arrows indicate shear sense along the shear bands. (b) Intersection between a leucogranite-bearing SSE-dipping shear band (solid line) and a high-angle sheet (boundaries indicated by dashed lines). The widening of the shear band and textural continuity between the two morphologies is interpreted to indicate connectivity between the two vein geometries. (c) Large, intersecting and/or cross-cutting conjugate shear-band-hosted leucogranite sheets (annotated by arrows) form a network in the lower parts of the cliff section along the Swakop River. (d) Stereographic projection of shear bands with sense of shear indicated. The shear band orientations describe a conjugate set that intersect along a moderately SW plunging axis which defines the intermediate (Y) axis of the finite strain ellipsoid. The acute angle between the conjugate (2θ) set is, on average ~70°, but individual conjugates may show angles of between ~30° and 90°.

2–3 m along strike whereas thicker examples (> 20 cm thick) are less abundant, but are significantly larger with strike extents of > 20 m. The leucocratic material is commonly concentrated in the centre of the shear bands, but the volume of material in shear bands of comparable size is highly variable. As a result, shear bands may contain large, up to tens of centimetre wide leucogranite sheets or only mm-wide stringers. The wider sheets show a fairly regular distribution with spacings of between 15 and 20 m. In places, foliation trajectories around shear bands define pucker structures suggesting that magma was originally contained, but subsequently extracted from the shear bands (Kriegsman, 2001).

The orientations of the shear bands describe a conjugate set in which a moderate to steeply SE dipping set can be distinguished from a moderate to steeply ~NW dipping set (Fig. 4). Foliation drag indicates an apparent oblique dextral, top-to-the-north sense of shear for the southerly dipping set and a sinistral shear sense for the more northerly dipping set. The latter does not show any consistent sense of dip-slip displacement. Contacts between the leucocratic veins and sheets in shear bands and the wall rocks may be sharp or diffuse where the leucogranite stringers interfinger on a millimetre-scale with the surrounding wall-rock foliation.

3.1.3. *High-angle leucogranite sheets*

Tabular, shallow to moderate SW-dipping granite sheets that cross-cut the S2 foliation at high angles represent the largest geometrically distinct leucogranite bodies in the outcrops (Fig. 5). Smaller examples are commonly between 10 and 20 m in strike length and up to 40 cm wide, whereas larger sheets are laterally extensive and can be traced throughout the entire outcrop for distances > 150 m with widths of 2 m and, locally, up to 5 m. Spacing between individual high-angle sheets of similar size is fairly regular and varies between 3 and 10 m in the lower and central parts of the outcrops. Towards the top parts of the cliff, in the crest of the F2 antiform (see Fig. 5d), spacing between high-angle sheets decreases to 1–3 m. There is no or only very little lateral displacement of foliation planes or other marker features across the high-angle sheets.

3.2. *Connectivity between leucogranites*

Both sharply cross-cutting contacts, as well as gradual contacts between the various leucogranite geometries are common. In the latter case, mineralogical and textural continuity at outcrop scale are maintained and leucogranites commonly progressively widen where they grade into one another. This results in irregular and undulating contacts, particularly where high-angle granite sheets join with foliation-parallel or shear-band-hosted veins (e.g. Fig. 5a). Along the intersections of continuous leucogranites, blocks of wall-rock are commonly separated and rotated with respect to surrounding wall-rock structures, suggesting rotation in the presence of an interconnected magma phase (Fig. 6a). In cases where veins display sharply truncating contacts,

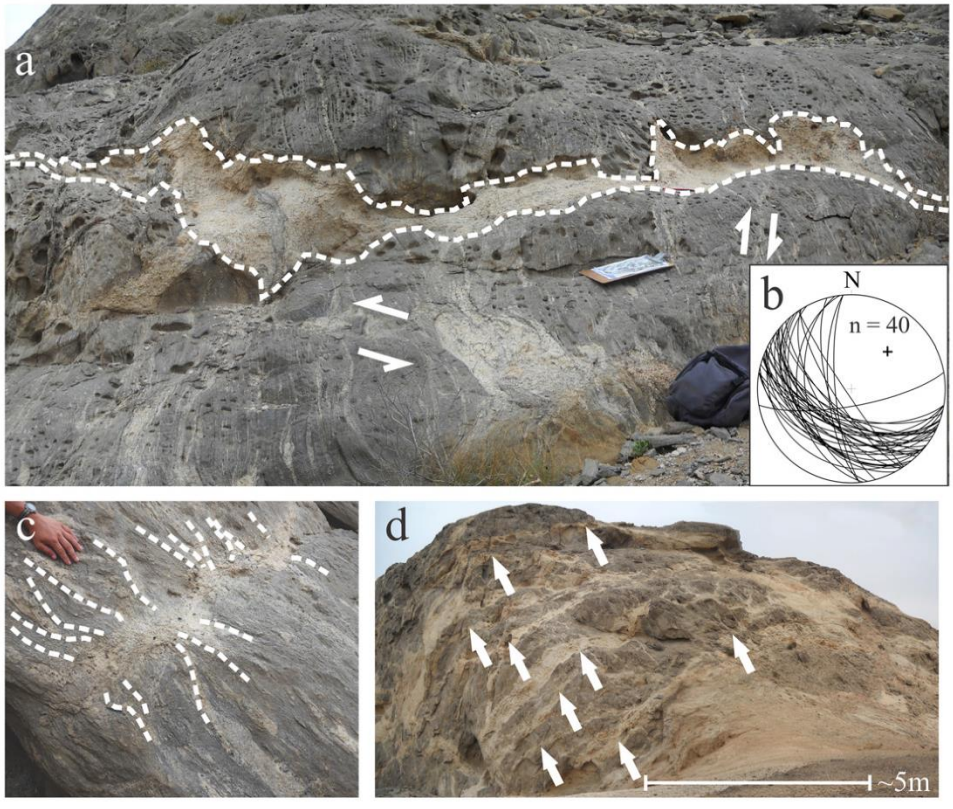

Fig. 5. (a) Oblique section through a gently undulating leucogranite sheet with highly irregular boundaries (annotated by dashed line; clipboard is approximately 30 cm long) orientated at high-angles to S2. S2 runs from top to bottom and is accentuated by numerous intrafolial leucogranite stringers. Textural and compositional continuity between the high-angle leucogranite sheet and the intrafolial and shear-band-hosted leucocratic veins (shear sense indicated by half-arrows) indicate connectivity between the different vein geometries. (b) Stereographic projection showing the orientation of the high-angle leucosome sheets, normal to L2 (average orientation indicated by the cross), suggesting that the high-angle sheets occupy extensional fractures. (c) Collapse of the S2 foliation, annotated by the dashed lines, delineates a pucker structure (centre of image) in a high-angle leucogranite sheet. This suggests magma extraction from an initially inflated leucogranite sheet (Kriegsman, 2001). (d) The spacing between high-angle leucogranite sheets decreases to ~1–3 m and size increases significantly towards the top of the outcrop (arrows indicate high-angle leucosomes). Cross-cutting relationships between leucogranite sheets indicate multiple episodes of granite sheeting.

consistent relationships can be recorded only at individual outcrop scale where, in general, high-angle leucogranite sheets truncate both shear-band-hosted and intrafolial veins and stringers. Shear-band-hosted veins, in turn, commonly truncate the intrafolial stringers. These consistent cross-cutting relationships are, however, not the general case through the cliff section. Cross-cutting intrusive phases within high-angle granite sheets are common and up to three phases of texturally and/or compositionally distinct granites can be recorded in individual sheets (Fig. 6b). The coexistence of both continuous and cross-cutting relationships suggests that the three granite geometries formed part of multiple and temporally disparate leucogranite networks injected into the gneisses.

3.3. *Structural controls of leucogranite occurrence*

Boudinage of the foliation-parallel leucocratic veins corresponds to their emplacement and progressive deformation along the axial planar foliation (S2), which approximates the *XY* plane of the finite strain ellipsoid during the D2 deformation ($X \geq Y \geq Z$). The emplacement of the large, mainly SW dipping high-angle granite sheets normal to the steep NE plunging regional L2 stretch axis (X axis of the finite strain ellipsoid) indicates that they occupy mode I (extensional) fractures (see Fig. 5b). The orientation of and displacement along the conjugate set of granite-bearing shear bands also point to their formation during subhorizontal NW–SE directed shortening and NE–SW extension. The common intersection between the shear band and high-angle granite sheets along a moderately SW plunging axis also suggests a structural control on the orientations of the leucogranites.

While some of the leucogranites appear folded, boudinaged or rodded, they are commonly devoid of pervasive solid-state fabrics except for a weakly developed grain-shape preferred orientation of quartz discs. The boudinage of the intrafolial stringers within the S2 foliation indicates that most of the strain that was not accommodated by the migration/loss of magma was partitioned into the biotite-rich wall rocks (Bonamici and Duebendorfer, 2010). Taken together, the orientation, intersection and progressive deformation of the leucocratic veins reflects their control by the regional D2 strains that are also recorded elsewhere in the CZ (e.g. Kisters et al., 2009; Poli and Oliver, 2001).

4. Spatial distribution of leucogranites

The leucogranite networks in this section of the Swakop River comprise sheets, veins and stringers that extend over five orders of magnitude in length scale (mm to > 100 m). At first glance, the veins display a clear hierarchy in their sizes and spatial distributions, particularly with respect to their locations within the F2

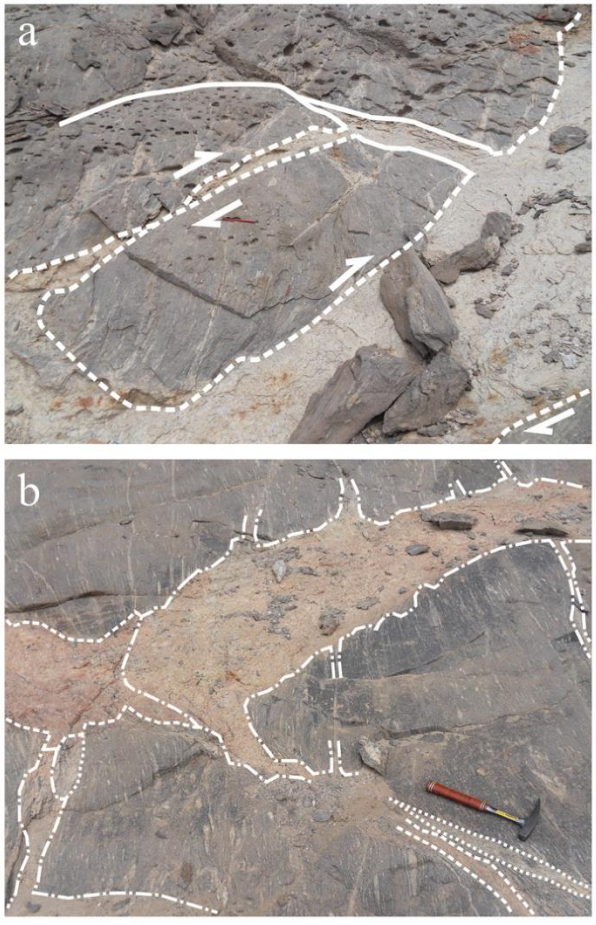

Fig. 6. (a) Segregation of magma into shear bands results in the dismemberment of the wall rocks into blocks bound by leucogranite. The block in the centre of the photograph (see pencil on block for scale) is separated from the surrounding wall rock by shear-band-hosted granite sheets (dashed lines) and a high-angle granite sheet (solid line). (b) Outcrop showing cross-cutting relationships between compositionally distinct intrusive phases as depicted by the line styles. Continuity between the leucogranites hosted in the wall rock and the large granite concentrations are indicated where the lines open into the wall rock.

antiform. Small intrafolial stringers dominate at the base of the outcrop near the Swakop River, whereas larger shear band and high-angle leucogranite sheets become progressively more dominant towards the crest of the antiform where multiple, cross-cutting high-angle leucogranite sheets represent the volumetrically most significant granite bodies. Throughout the gneiss pavements, the foliation-parallel leucocratic stringers and veins are volumetrically small, closely spaced and the most abundant leucogranite morphology. In contrast, high-angle leucogranite sheets are up to three orders of magnitude larger, but far less common, with a spacing of several metres. Oblique shear band leucogranites are intermediate, both in terms of size as well as relative abundance, with respect to the two end-members and have lengths of up to tens of metres.

Power-law distributions and scale-invariant relationships between leucosome size and frequency have been indicated by a number of studies of in situ natural migmatites (e.g. Bonamici and Duebendorfer, 2010; Bons et al., 2009), the image analysis of migmatite outcrops (e.g. Bonamici and Duebendorfer, 2010; Tanner, 1999), the analysis of leucosomes from drill core (Soesoo et al., 2004) and numerical as well as analogue modelling (e.g. Bons et al., 2004; Bons and Arnold, 2003; Bons and van Milligen, 2001; Urtson and Soesoo, 2009). Such distributions can be the result of fractal-type models, such as the Menger Sponge analogue proposed by Tanner (1999) as well as of models that suggest stepwise accumulation and extraction of melts from the source of melting (Bons et al., 2009). Both power-law distributions and scale-invariance of leucosomes in migmatites and granite veins in high-grade gneisses can be taken as indications of self-organisation (Bonamici and Duebendorfer, 2010; Tanner, 1999), although this interpretation is not without problems (Marchildon and Brown, 2003).

In order to describe possible spatial and size/frequency relationships between different leucogranite geometries, detailed photographic panels and line-drawings of selected outcrops and of the cliff section as a whole were analysed. Selected panels were analysed by (1) a simple counting of leucogranite features based on the line drawings, and (2) by a box-counting image analysis of binarised versions of subsets of a number of photographic panels.

4.1. Count of leucogranites by morphology

The present analysis represents a first and semi-quantitative approach aimed at highlighting the hierarchy of leucogranite geometries in the outcrops, i.e. a system where numerous small stringers and veins converge to form progressively larger and less numerous leucogranite sheets. To avoid the problem of counting leucogranite stringers, veins and sheets from several overprinting networks, two m-scale images showing continuous granites were selected. In addition, an outcrop-scale image of the central parts of the cliff section was used to give an indication of the relative abundance of the larger leucogranite sheets ($> \sim 10$ cm thick shear band and high-angle leucogranites) in the system as a whole. The lack of complete 3D exposure means that the total volume of individual structures cannot be accurately determined in the outcrops. However, a power-law distribution of vein widths is likely to be indicative of an underlying power-law size (volume) distribution (Bons et al., 2009). As there is a general increase in width from intrafolial through shear-band-hosted to high angle leucogranites, they were counted according to morphology.

The steep outcrops in images (a) and (b) (Fig. 7) represent a view of a surface oblique to the *YZ* plane and are thus orientated at high angles to the L2 lineation representing an oblique section through the S2 foliation. Image (c) shows a subhorizontal pavement along the base of the outcrop that is at a high angle to the *YZ* plane and, thus, slightly oblique to the *XZ* plane. The original resolution of image B did not allow for the counting of the small-scale intrafolial leucocratic stringers. However, this image was instead used to analyse the relative abundance of the larger high-angle and shear-band-hosted leucogranites over an area that samples these leucogranites more completely.

4.1.1. Results and interpretation

The results of the simple counts are shown in Fig. 7. The abundance of shear-band-hosted and high-angle leucogranite sheets in images (a) and (c) differs by factors of 12 and 2.5 respectively and, in both cases, the intrafolial leucogranite stringers are around an order of magnitude more common than high-angle leucogranite sheets. In image (b), the abundance of the shear band and high-angle leucogranites differs by a factor of ~ 2, similar to image (c).

Although these results show variation, the larger leucogranite morphologies are, in all of the images, less common than the smaller foliation parallel or shear-band-hosted types. The variation in the results for the various images may reflect the sampling of (1) different sections of the outcrop exposed at different angles with respect

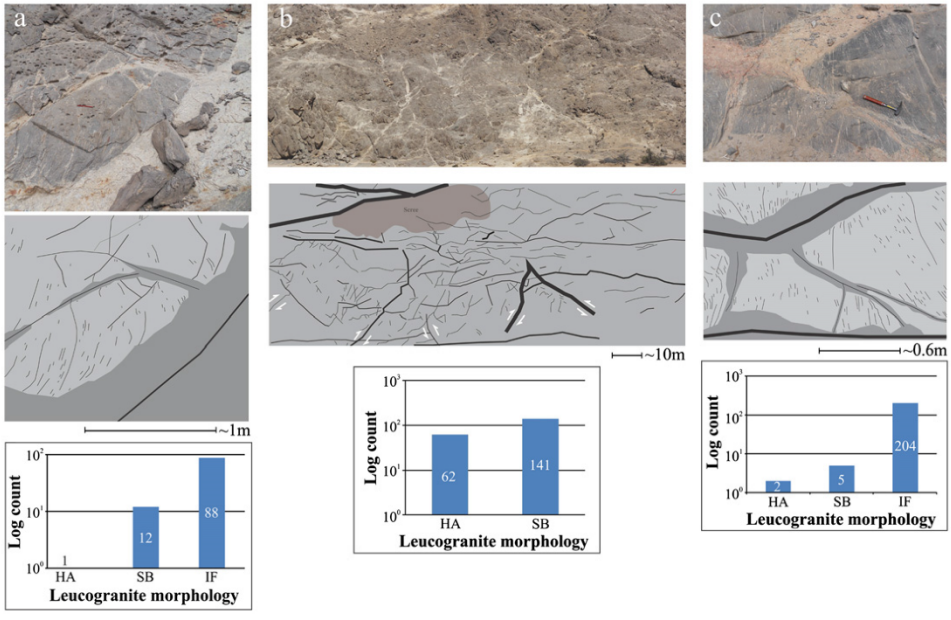

Fig. 7. Leucogranites were counted by morphology on the line drawings above each plot. Features of ~1 mm were resolvable in images (a) and (c) and features of ~10 cm in image (b). The counts of the leucogranites are displayed on logarithmic axes below each of the images (IF=intrafolial leucogranites, SB=shear-band-hosted leucogranites and HA=high-angle leucogranites).

to the rock fabrics and planar leucogranites, (2) spatially separate systems that record different magma transfer episodes, or (3) incompletely exposed leucocratic vein networks. For a leucogranite network to be described as scale-invariant, a power-law relationship between leucogranite size and frequency is required. By using leucogranite type as a proxy for size, this basic count of the leucogranite veins and sheets highlights a hierarchy amongst the different geometries.

4.2. Box-counting image analysis

Previous studies have used 1D line counts and 2D box-counting image analysis of binary images of migmatite outcrops to analyse and identify a possible power-law frequency–size relationship in the distribution of leucogranites (e.g. Bonamici and Duebendorfer, 2010; Marchildon and Brown, 2003; Tanner, 1999). The box-counting method "*…measures the frequency of a phenomenon at a given scale of observation…*," (Bonamici and Duebendorfer, 2010, p. 1121) thus giving an indication of the frequency of a phenomenon at successively increasing box-sizes. The procedure used here follows that described by Turcotte (1997) and Marchildon and Brown (2003) and was performed using ImageJ, an open source image analysis software (Rasband, 1997–2012) and the Fraclac plugin (Karperien, 1999–2012). The images are divided into grids of incrementally increasing cell (box) sizes and the number of cells that contain leucocratic material for each cell size are counted, effectively measuring the number of cells of a given size necessary to cover the feature being measured (Marchildon and Brown, 2003). Where a power-law distribution exists, the count (Nd) and the scale (box size; n) can be related by the power law

$$N_d = kn^{-D}$$

where k is a constant and D is the fractal dimension, often calculated by determining the slope of the power-law curve (Bonamici and Duebendorfer, 2010; Tanner, 1999; Turcotte, 1997). In such cases, the data can be said to be scale-invariant/fractal with fractal dimension equal to D (Bonamici and Duebendorfer, 2010).

Seven detailed images (a–g; Fig. 8) that cover areas in the range of ~0.3 m^2 to ~2 m^2 and an eighth, smaller scale image (h) that covers ~1800 m^2 of the central portion of the main cliff face were analysed. The detailed images show only the smaller leucogranite geometries, namely, intrafolial and smaller shear-band-hosted leucogranite veins, in continuous networks. Image (h) is an image of the main face and is thus a composite of numerous different leucogranite vein networks and generally shows only the larger features, i.e. the medium to large shear-band-hosted and the high-angle leucogranite sheets (≥ 10 cm wide). The abundance of leucocratic material in the images varies between ~6 and ~30 per cent.

4.2.1. Results and interpretation

The data derived from the box counting image analysis shown in Fig. 8 produce approximately straight lines on the log–log plots between box sizes of ~10 and >100 pixels. To determine the linearity of these plots, a least squares linear regression was used. The correlation coefficients of the least squares regressions (r^2) shown on the figure represent the degree of fit of the log–log data to a straight line, over the entire range of box sizes. The relatively high r^2 values indicate scale-invariance in the morphology, and possibly the distribution of the leucogranites over the straight-line segments of the graphs, i.e. over two orders of magnitude of box size (Marchildon and Brown, 2003). Beyond box sizes of ~100 pixels, the linear trend breaks down and the data become jagged, likely due to the sequential increase in box size used in the analysis. Fractal dimensions (D) of similar datasets are commonly modelled by determining the slopes of the least-squares linear regressions which, in this case, fall between 1.86 and 1.92. These values are similar to those obtained for leucogranites in Bavarian migmatites analysed by Tanner (1999). Image H shows a slightly elevated D-value of 1.92. Since fractal dimension can be related to complexity or "roughness" (Marchildon and Brown, 2003), it is possible that this higher value indicates the temporal superposition of leucogranite networks

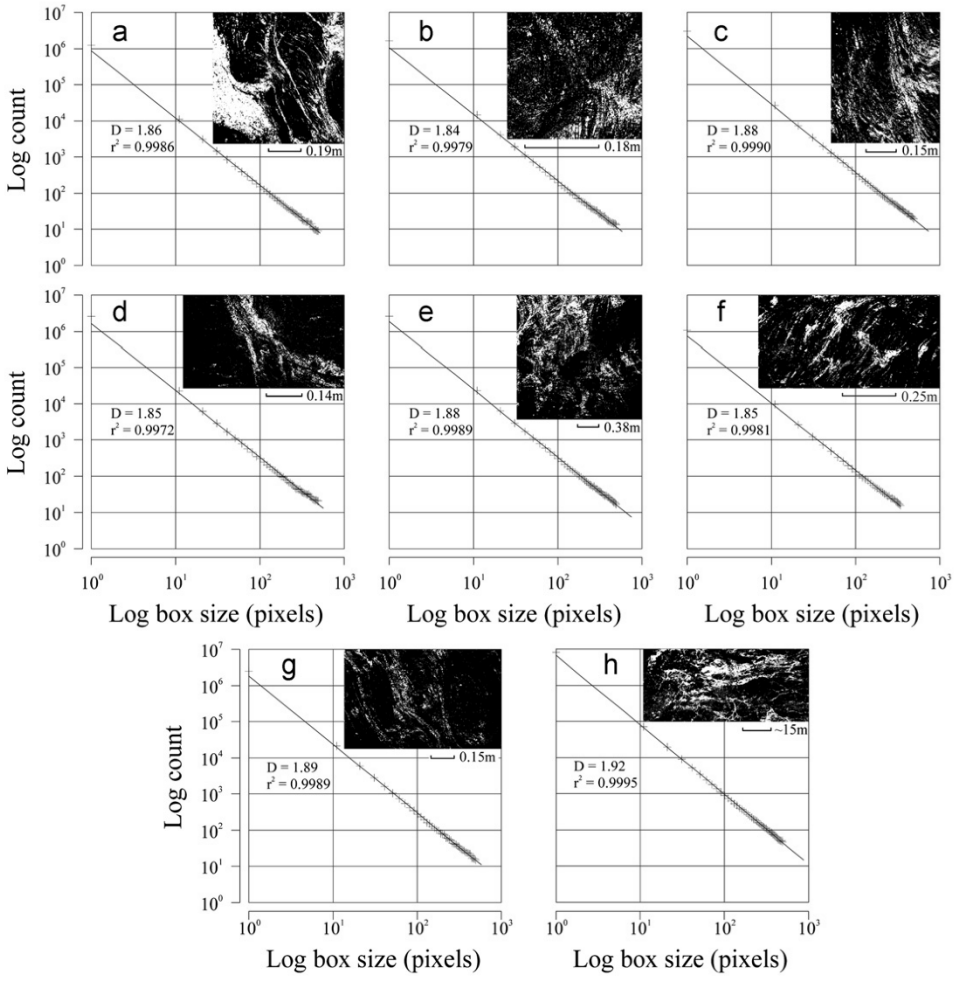

Fig. 8. Log–log plots of the count of the number of boxes containing leucocratic material (Y axis) vs. box size in pixels (x axis). Insert images are binary versions of the contoured images used in the analysis. Fractal dimensions (D) and correlation coefficients (r^2) of the least squares linear regression used to determine $-D$ are shown for each analysis.

(Bonamici and Duebendorfer, 2010), which is clearly indicated by the cross-cutting relationships of leucogranites in the outcrops. The individual image analyses display invariance over only limited scales, but the fact that the leucogranites show scale-invariance over a range of outcrop-scales (from tens of centimeters in images (a)–(g) to hundreds of metres scale in image (h)) suggests that the scale-invariance would probably extend between and beyond the scales of the individual analyses (Bons et al., 2009).

4.2.2. Discussion of the box-counting image analysis

Numerous studies suggest the straight line segments on log–log plots of frequency versus scale and the high r^2 values of the linear regressions used to model the fractal dimension represent power-law distributions (Clauset et al., 2009 and examples therein). However, high correlation coefficients of the least-squares linear regressions are not reliable indicators of whether the data truly follow a power-law distribution (Clauset et al., 2009; Gonzato et al., 1998). Moreover, potential errors and uncertainties in the analysis of natural magma transfer networks may be introduced by factors both intrinsic to the actual physical processes of magma flow as well as to the analytical method. The most obvious complication is the sampling of multiple and successive magma flow events that may each have resulted in distinct and overprinting leucogranite networks in the same outcrop. The image analysis only captures the finite pattern of cross-cutting and overprinting networks that likely formed under different boundary conditions, thereby obscuring any clear statistical relationship. Moreover, leucogranite networks represent highly transient features (Bons et al., 2009; Kisters et al., 2009) and the preserved leucogranites are likely to have been sampled at differing stages of inflation and/or deflation. This is clearly recorded by the presence of collapsed shear-band-hosted and high-angle leucogranite sheets and pucker structures in the outcrops (see Fig. 5). Hence, size–frequency distributions only record snapshots taken at different times during the magma transport episode.

In addition, the interpretation of results and even the selection of parameters for the image analysis of migmatites through, for example, the box counting-method is ambiguous and controversial. For instance, the analyses of Marchildon and Brown (2003) are, like this study, based on the analysis of contours representing the outlines of leucocratic veins. This means that the perimeter

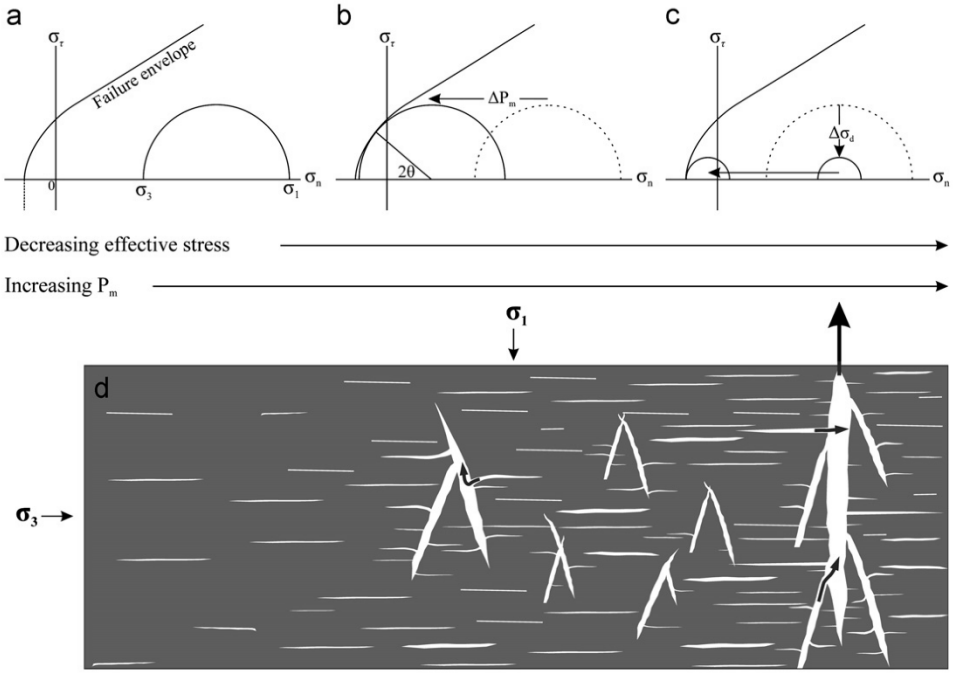

Fig. 9. The development of the observed leucogranite network can qualitatively be described through Mohr diagrams (see text for detailed discussion). (a) At low melt pressures and melt volumes melt flow is accommodated by foliation-parallel stringers. (b) At increasing melt volumes and pressures, lowering of the effective stress promotes shear failure and melt accumulation in shear bands if the stress circle touches the failure envelope in the tensile field of the Mohr diagram. (c) At high melt volumes, a decrease in differential stress due to the presence of a low-viscosity melt phase causes the formation of extensional fractures; the stress circle touches the origin of the failure envelope indicating the formation of extensional fractures perpendicular $\sigma 3$ ($2\theta=0$). Fracture dilatancy causes the flow of melt into the extensional fracture, followed by an almost instantaneous drop in P_m, allowing the system to revert to its initial state (a). (d) Schematic sketch illustrating the prevalence of leucogranite geometries at progressively increasing melt volumes and pressures from left to right.

length of the leucogranites is measured and the results describe distributions in physical space (Bonamici and Duebendorfer, 2010). In contrast, Tanner (1999) analysed images of filled leucosomes by counting boxes containing any amount of leucosome whereas Bonamici and Duebendorfer (2010) used similar images and counted boxes containing only leucosome, effectively measuring the size of leucosomes.

So far then, we have established that leucogranites in the outcrops of the Swakop River display a crudely defined inverse size–frequency distribution and that the box-counting image analysis of leucogranites on selected pavements hints at some degree of a scale-invariant or fractal behaviour, which is a characteristic of self-organised systems. This part of the study also suggests that the statistical analysis of leucogranite networks may be taken as an indication of the scale-invariant distribution and possibly self-organised nature of the networks. However, this is not always as conclusive as some of the literature suggests (Bons and Arnold, 2003; Soesoo et al., 2004; Tanner, 1999).

5. Controls of granite sheeting and fracture formation

The morphology, relative orientation and controls of the leucogranites exposed in the Swakop River correspond with the intersecting net-structured leucosome pods and sheets documented from migmatites and high-grade terrains worldwide (diktyonitic migmatites, after Sederholm (1907); deformation-band hosted leucosomes after Brown (2007); net-structured leucosomes after Sawyer (2008)). Melt migration in these networks is commonly considered to follow local stress gradients, from large numbers of melt concentrations in sites of compaction, such as axial planar foliations (e.g. Vernon and Paterson, 2001), into rather spaced dilational sites such as shear bands, interboudin partitions and extensional fractures (Brown, 2007). However, whereas net-structured migmatites are commonly developed in layered and anisotropic rocks, the net-structured leucogranites in the Swakop River are developed in largely homogenous gneisses. The boudinage of foliation-parallel stringers within the axial planar S2 foliation is consistent with the emplacement of these leucogranites along a weakly developed anisotropy and into the plane of finite shortening, but is the only evidence that layer anisotropies exerted any control on the occurrence of the leucogranites. It seems, therefore, that while the orientations of the leucogranites are closely controlled by D2 strains, the formation of contemporaneous, intersecting leucogranite sets is not determined by rheological contrasts and wall-rock anisotropies, but rather by other factor(s).

In lower-crustal rocks, where deformation is generally ductile, brittle behaviour is promoted by the presence of lithostatically pressured melts (Brown and Solar, 1998b; Davidson et al., 1994; Roering et al., 1995). This can either occur during partial melting reactions that are associated with a positive volume change and/or where the rates of melt production exceed the rates of melt extraction (Davidson et al., 1994). In such situations an increase in melt pressure is analogous to an increase in pore fluid pressure, effectively lowering the differential stress required to induce brittle behaviour (Davidson et al., 1994). The mode of fracturing is dependent on a combination of factors and fractures can take the form of compressive or extensional shear fractures, or dilatant tensile fractures (opening mode I fractures). Mohr diagrams constructed for a particular set of conditions are commonly used to model fracture formation, even in visco-elastic lower-crustal

rocks (e.g. Brown and Solar, 1998b; Davidson et al., 1994; Lucas and St-Onge, 1995).

In the present outcrops, the volume of granite increases dramatically towards the crest of the F2 antiform. This ponding in antiformal structures capped by metasedimentary and, in particular, marble units is a commonly observed feature in the Damara Belt and is a result of the blunting and arrest of granite sheets and dykes against the highly-ductile marble units that prevent further ascent of the granitic magmas (Johnson et al., 2006; Kisters et al., 2009; Miller, 1983). The arrest of melt filled fractures and ponding of melt in the crest of the antiform impedes melt extraction from the system and will result in an increase in melt volume and transiently increased melt pressures as well as a decrease in the overall viscosity of the rocks.

The increased proportion of leucogranites in the crest of the F2 antiform and the minor control of wall-rock anisotropies on the formation of the leucogranites suggest that the formation of the leucogranite network in the outcrops may have been primarily driven by variations in melt pressure (Fig. 9). At low melt volumes, melt flow is accommodated mainly by foliation parallel stringers. This scenario is realised in the lower parts of the cliff section where the small-scale foliation-parallel granite stringers are abundant. An increase in melt pressure will lower the effective stress and promote the formation of foliation oblique shear band structures. This situation is illustrated in Fig. 9b, where the stress circle makes contact with the failure envelope. The angle 2θ describes the acute angle between the set of conjugate shear fractures that form and, ideally, is bisected by σ_1. In the case of extensional shear bands ($2\theta \leq 45^{\circ}$), the dilational component along the shear bands creates a gradient in magmastatic head from the wall rocks and the foliation parallel stringers and veins into the shear bands, focusing melt into the newly formed shear bands. Further increase in melt volume and pressure will result in a decrease of the mean stress and a lowering of wall-rock viscosities. The combined results of this are illustrated in Fig. 9c, where the Mohr circle moves toward and beyond the origin, into the tensional field of the diagram. This condition promotes extensional failure perpendicular to the least compressive stress when the circle makes contact with the failure envelope at $\sigma_\tau = 0$. This situation is realised in the upper parts of the cliff section and in the crest of the antiform, documented by the formation of the large leucogranite sheets that occupy extensional fractures. This would imply that the development of differently orientated, intersecting granite pathways may be promoted by subtle variations in melt pressure and that the formation of the leucogranite networks is driven by the melt itself. The extensional fractures are ideally suited to accommodate the rapid extraction of melt during times of high-melt production. They are by far the largest structures, combining the largest magma volumes and the purely dilational component along the fractures creates the largest gradients in magmastatic head. This enables the focusing of melt from the rather small-scale network of foliation-parallel and shear band hosted stringers in the wall rocks into spaced fractures or fracture sets. The opening and drainage of melt from the surroundings into the extensional fracture will lead to a lowering of the melt pressure, and the system will revert to the state that existed prior to the build-up of melt pressure.

In all these considerations, it should be noted that differential stresses in the highly ductile rocks that contain partial melts are likely to be very low, probably < 1 MPa (Rutter and Neumann, 1995) and the variations in melt pressure and differential stress considered here describe a very delicate balance. Hence, exceedingly small fluctuations in melt supply may cause dramatic changes in the way in which the melt moves through the system. The arrival of new bursts of melt will result in transiently elevated melt pressures and an effective switch from melt transport along low-volume stromatic or shear-band-hosted conduits to high-volume, high-angle extensional fractures. This process may be repeated for as long as new melt enters the system. Cross-cutting relationships between different, but also within individual leucogranites, indicate multiple episodes of melt transport during which earlier melt conduits may be reactivated (Hasalová et al., 2011) or new structures may form. In either case, stromatic and shear-band-hosted granite stringers and veins occupy structures that form in response to regional strains. The rate at which melt is transferred along these structures is, thus, likely to be slow and is unlikely to exceed regional strain rates, even though strain localization along the melt-filled structures may conceivably increase deformation rates locally. This also means that stromatic and shear-band-hosted geometries cannot account for any far-field melt transfer, particularly if melt ascent is through mostly subsolidus crust where the transport needs to be sufficiently fast to prevent the melt from freezing (Clemens and Mawer, 1992; Petford et al., 2000). Accordingly, the general absence of stromatic gneisses from low-grade metamorphic terrains reflects their formation restricted to high grade and/or anatectic regions (see Sawyer (2008) for examples).

Extensional fractures, in contrast, form at high-strain rates (e.g. Dell'angelo and Tullis, 1988) irrespective of regional tectonic rates at the lower crustal levels, in the presence of transiently supralithostatic melt pressures. The formation of structures that allow rapid extraction of melt is a prerequisite for any far-field melt transport. Melt transport out of the anatectic region is most efficient when the fracture systems have steep or vertical orientations that assist the largely buoyancy-driven melt ascent. In the present case, the steep regional stretch (L2) and shallow orientation of the extensional fractures have most likely contributed to the preservation of the leucogranite sheets in the outcrops along the Swakop River. Provided that the fracture orientation is steep, extensional fractures originating in net-structured leucogranite systems could provide the transition from segregation at the source to fast melt extraction out of the anatectic region. This agrees with Sawyer's (2008, p. 156) observation that a net-like leucosome structure "…*appears to be a necessary step in the extraction of large volumes of melt from anatectic terranes*…," which, we suggest, relates directly to the formation of extensional fractures rooted within the net-structured leucogranite systems.

5.1. *Are granitic melt networks self-organised?*

Bak et al. (1988) concluded that systems that tend to develop towards a self-organised critical state evolve to a particular stable state regardless of initial conditions or subsequent perturbations. Moreover, self-organised systems should exhibit features that display temporal as well as spatial scale-invariance and, thus, power-law distributions. The occurrence of net-structured leucogranite sheets described in high-grade terrains worldwide underlines the fact that this specific arrangement of granite sheets and stringers represents a particularly robust, stable and efficient configuration for the initial segregation and subsequent transport of melt out of its source region (Brown, 2007; Mehnert, 1968; Sawyer, 2008; Sederholm, 1907). High-grade sequences in anatectic regions are commonly heterogeneous and wall-rock anisotropies will facilitate the formation of differently orientated sheet geometries. However, the lithological layering will also tend to obscure features of self-organisation, since different flow strengths of the rocks or the scales of the lithological layering, combined with regional strains will determine the formation (spacing and size) of leucogranite veins. Clearly, this will impact on any results of an image analysis and obscure power-law distributions, the scale-invariance of leucogranite veins in

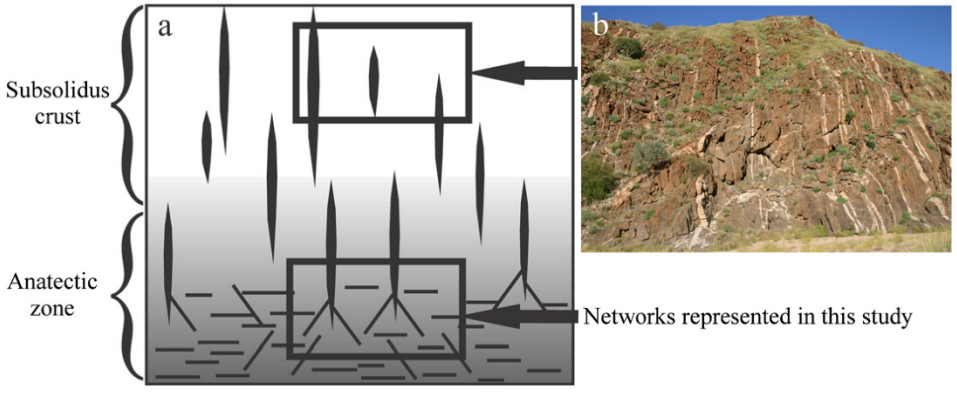

Fig. 10. (a) The leucogranite networks illustrated in this study are interpreted to represent the transition from local-scale segregation of melt within and close to the anatectic source to large-scale vertical transfer conduits. The formation of the extraction and transfer network is driven by the melt pressure, but influenced by pre-existing anisotropies and regional stresses. The high-angle leucogranites represent the end member of this network formed at high melt volumes. In a vertical orientation, these features are able to both create pressure gradients that drain melt from the wall rocks and/or tributary networks, as well as provide ascent conduits that can accommodate the rapid buoyancy driven ascent of magmas through subsolidus upper crustal levels. (b) The photograph shows swarms of vertical leucogranite sheets in lower-amphibolite biotite–cordierite schists, approximately 50 km along strike and some 10–12 km above (*P* ca. 2–3 kbar, *T* ca. 550–600 °C; Wulff et al., 2010) the crustal sections studied here in the lower Swakop River. These dyke swarms are common in upper crustal levels of the Damara Belt and although these sheets cannot be directly connected to the lower migmatitic crust, they represent ascent conduits of granitic magmas in the subsolidus crust.

outcrops and, hence, whether or not melt-flow networks are self-organised. Nevertheless, the granite networks in relatively homogenous gneisses of the Khan Formation documented here tend to display spatial power-law distributions, suggesting that the networks may be self-organised.

6. Conclusions

Field evidence and statistical data analysing the distribution of leucogranite stringers, veins and sheets in net-structured high-grade gneisses point towards self-organisation of the melt transfer system. Variations in melt pressure represent a key, internally derived control on the development of the leucogranite networks. Two main end members of leucogranite geometries can be distinguished. The pervasively developed stromatic and shear-band-hosted parts of the leucogranite network accommodate the metre-scale segregation of melt from the grain-scale framework close to the anatectic source. This closely spaced and more pervasive melt network feeds into spaced extensional fractures that are only activated during periods of high supply and when melt volumes cannot be accommodated by the stromatic parts of the network. This stage represents the transition from melt segregation near the source to far-field melt transport out of the anatectic region (Fig. 10). Rapid propagation rates and large melt volumes combined in extensional fractures allow for the rapid and efficient extraction of melt and further transport through the subsolidus crust, in vertically propagating hydrofractures or dykes. Regional strains exert a control on the orientation of the networks. An efficient extraction of granitic magmas from anatectic regions seems feasible only in steeply inclined fracture conduits that can assist the largely buoyancy-driven ascent of the melts. The hierarchical arrangement of melt conduits in net-structured vein networks seems to be able to concentrate melt and initiate large-scale migration by means of simple variations in melt pressure/melt supply only.

Acknowledgements

We would like to thank Bannerman Resources for permission to access the area and additional logistical support during the field work. Detailed comments on an earlier version of the manuscript by John Clemens are greatly appreciated. The critical and constructive reviews by Mike Brown and Roberto Weinberg helped to clarify many aspects of this paper. Additional financial support to DH through the South African National Research Foundation Grant to Ian Buick (Grant no.: 69858:2009) is gratefully acknowledged.

References

Bak, P., Tang, C., Wiesenfeld, K., 1988. Self-organized criticality. Phys. Rev. A 38, 364–374.
Bonamici, C.E., Duebendorfer, E.M., 2010. Scale-invariance and self-organized criticality in migmatites of the southern Hualapai Mountains, Arizona. J. Struct. Geol. 32, 1114–1124.
Bons, P.D., Arnold, J., 2003. Accumulation and self-organization in hydrofracture transport of fluids. J. Geochem. Explor. 78–79, 667–670.
Bons, P.D., Arnold, J., Elburg, M.A., Kalda, J., Soesoo, A., van Milligen, B.P., 2004. Melt extraction and accumulation from partially molten rocks. Lithos 78, 25–42.
Bons, P.D., Becker, J.K., Elburg, M.A., Urtson, K., 2009. Granite formation: stepwise accumulation of melt or connected networks? Earth Environ. Sci. Trans. R. Soc. Edinburgh 100, 105–115.
Bons, P.D., van Milligen, B.P., 2001. New experiment to model self-organized critical transport and accumulation of melt and hydrocarbons from their source rocks. Geology 29, 919–922.
Brown, M., 1994. The generation, segregation, ascent and emplacement of granite magma: the migmatite-to-crustally-derived granite connection in thickened orogens. Earth Sci. Rev. 36, 83–130.
Brown, M., 2007. Crustal melting and melt extraction, ascent and emplacement in orogens: mechanisms and consequences. J. Geol. Soc. London 164, 709–730.
Brown, M., 2010. The spatial and temporal patterning of the deep crust and implications for the process of melt extraction. Philos. Trans. R. Soc. A 368, 11–51.
Brown, M., Averkin, Y.A., McLellan, E.L., Sawyer, E.W., 1995. Melt segregation in migmatites. J. Geophys. Res. 100, 15655–15679.
Brown, M., Solar, G.S., 1998a. Shear-zone systems and melts: feedback relations and self-organization in orogenic belts. J. Struct. Geol. 20, 211–227.
Brown, M., Solar, G.S., 1998b. Granite ascent and emplacement during contractional deformation in convergent orogens. J. Struct. Geol. 20, 1365–1393.
Brown, M., Solar, G.S., 1999. The mechanism of ascent and emplacement of granite magma during transpression: a syntectonic granite paradigm. Tectonophysics 312, 1–33.
Clauset, A., Shalizi, C.R., Newman, M.E.J., 2009. Power-law distributions in empirical data. SIAM Rev. 51, 661–703.
Clemens, J.D., 2005. Granites and granitic magmas: strange phenomena and new perspectives on some old problems. Proc. Geol. Assoc. 116, 9–16.
Clemens, J.D., Mawer, C.K., 1992. Granitic magma transport by fracture propagation. Tectonophysics 204, 339–360.
Collins, W.J., Sawyer, E.W., 1996. Pervasive granitoid magma transfer through the lower-middle crust during non-coaxial compressional deformation. J. Metamorph. Geol. 14, 565–579.

Coward, M.P., 1983. The tectonic history of the Damara belt. In: Miller, R.M. (Ed.), Evolution of the Damara Orogen of South West Africa/Namibia. Geological Society of South Africa Special Publication, Vol. 11, pp. 409–421.
Davidson, C., Schmid, S.M., Hollister, L.S., 1994. Role of melt during deformation in the deep crust. Terra Nova 6, 133–142.
Dell'angelo, L.N., Tullis, J., 1988. Experimental deformation of partially melted granitic aggregates. J. Metamorph. Geol. 6, 495–515.
Gonzato, G., Mulargia, F., Marzocchi, W., 1998. Practical application of fractal analysis: problems and solutions. Geophys. J. Int. 132, 275–282.
Guernina, S., Sawyer, E.W., 2003. Large-scale melt-depletion in granulite terranes: an example from the Archean Ashuanipi subprovince of Quebec. J. Metamorph. Geol. 21, 181–201.
Hasalová, P., Weinberg, R.F., MacRae, C., 2011. Microstructural evidence for magma confluence and reusage of magma pathways: implications for magma hybridization, Karakoram Shear Zone in NW India. J. Metamorph. Geol. 29, 875–900.
Jacob, R.E., 1974. Geology and metamorphic petrology of part of the Damara orogen along the lower Swakop River, South West Africa. Precambrian Res. Unit Bull. 17, 185.
Johnson, S.D., Poujol, M., Kisters, A.F.M., 2006. Constraining the timing and migration of collisional tectonics in the Damara Belt, Namibia: U–Pb zircon ages for the syntectonic Salem-type Stinkbank granite. S. Afr. J. Geol. 109, 611–624.
Jung, S., Mezger, K., 2001. Geochronology in migmatites—a Sm–Nd, U–Pb and Rb–Sr study from the Proterozoic Damara belt (Namibia): implications for polyphase development of migmatites in high-grade terranes. J. Metamorph. Geol. 19, 77–97.
Jung, S., Mezger, K., 2003. Petrology of basement-dominated terranes: I. Regional metamorphic T–t path from U–Pb monazite and Sm–Nd garnet geochronology (Central Damara orogen, Namibia). Chem. Geol. 198, 223–247.
Karperien, A. 1999–2012. FracLac for ImageJ, version 2.5. 〈http://rsb.info.nih.gov/ij/plugins/fraclac/FLHelp/Introduction.htm〉.
Kisters, A.F.M., Jordaan, L.S., Neumaier, K., 2004. Thrust-related dome structures in the Karibib district and the origin of orthogonal fabric domains in the south Central Zone of the Pan-African Damara belt, Namibia. Precambrian Res. 133, 283–303.
Kisters, A.F.M., Ward, R.A., Anthonissen, C.J., Vietze, M.E., 2009. Melt segregation and far-field melt transfer in the mid-crust. J. Geol. Soc. London 166, 905–918.
Kriegsman, L.M., 2001. Quantitative field methods for estimating melt production and melt loss. Phys. Chem. Earth A: Solid Earth Geod. 26, 247–253.
Lucas, S.B., St-Onge, M.R., 1995. Syn-tectonic magmatism and the development of compositional layering, Ungava Orogen (northern Quebec, Canada). J. Struct. Geol. 17, 475–491.
Marchildon, N., Brown, M., 2003. Spatial distribution of melt-bearing structures in anatectic rocks from Southern Brittany, France: implications for melt transfer at grain- to orogen-scale. Tectonophysics 364, 215–235.
Masberg, H.P., 2000. Garnet growth in medium pressure granulite-facies metapelites from the central Damara Orogen: igneous versus metamorphic history. Commun. Geol. Surv. Namib. 12, 115–124.
Mehnert, K.R., 1968. Migmatites and the Origin of Granitic Rocks. Elsevier, Amsterdam, Netherlands.
Miller, R.M., 1983. The Pan-African Damara Orogen of South West Africa/Namibia. In: Miller, R.M. (Ed.), Evolution of the Damara Orogen of South West Africa/Namibia, 11 ed, Geological Society of South Africa Special Publication, Vol. 11, pp. 431–515.
Miller, R.M., 2008. Neoproterozoic and early palaeozoic rocks of the Damara Orogen. In: Miller, R.M. (Ed.), The Geology of Namibia. Ministry of Mines and Energy, Windhoek.
Petford, N., Cruden, A.R., McCaffrey, K.J.W., Vigneresse, J., 2000. Granite magma formation, transport and emplacement in the Earth's crust. Nature 408, 669–673.
Petford, N., Koenders, M.A., 1998. Self-organisation and fracture connectivity in rapidly heated continental crust. J. Struct. Geol. 20, 1425–1434.
Petford, N., Lister, J.R., Kerr, R.C., 1994. The ascent of felsic magmas in dykes. Lithos 32, 161–168.
Poli, L.C., Oliver, G.J.H., 2001. Constrictional deformation in the Central Zone of the Damara Orogen, Namibia. J. Afr. Earth Sci. 33, 303–321.
Rasband, W.S.. 1997–2012. ImageJ, U.S. National Institutes of Health. Bethesda, Maryland, USA 〈http://imagej.nih.gov/ij/〉.
Roering, C., Van Reenen, D.D., Smit, C.A., Du Toit, R., 1995. Deep crustal embrittlement and fluid flow during granulite metamorphism in the Limpopo Belt, South Africa. J. Geol. 103, 673–686.
Rutter, E.H., Neumann, D.H.K., 1995. Experimental deformation of partially molten Westerly granite under fluid-absent conditions, with implications for the extraction of granitic magmas. J. Geophys. Res. 100, 15697–15715.
Sawyer, E.W., 2008. Atlas of Migmatites, 9th ed. NRC Research Press, Ottawa, Ontario, Canada.
Sederholm, J.J., 1907. On Granite and Gneiss: Their Origin, Relations and Occurrence in the Pre-Cambrium Complex of Fennoscandia. Bulletin, Community of Geology, Finlande, 23.
Soesoo, A., Kalda, J., Bons, P., Urtson, K., Kalm, V., 2004. Fractality in geology: a possible use of fractals in the studies of partial melting processes. Proc. Est. Acad. Sci. Geol. 53, 13–27.
Tack, L., Bowden, P., 1999. Post-collisional granite magmatism in the central Damaran (Pan-African) Orogenic Belt, western Namibia. J. Afr. Earth Sci. 28, 653–674.
Tanner, D.C., 1999. The scale-invariant nature of migmatite from the Oberpfalz, NE Bavaria and its significance for melt transport. Tectonophysics 302, 297–305.
Turcotte, D.L., 1997. Fractals and Chaos in Geology and Geophysics, 2nd ed. Cambridge University Press, Cambridge.
Urtson, K., Soesoo, A., 2009. Stepwise magma migration and accumulation processes and their effect on extracted melt chemistry. Est. J. Earth Sci. 58, 246–258.
Vanderhaeghe, O., 1999. Pervasive melt migration from migmatites to leucogranite in the Shuswap metamorphic core complex, Canada: control of regional deformation. Tectonophysics 312, 35–55.
Vernon, R.H., Paterson, S.R., 2001. Axial-surface leucosomes in anatectic migmatites. Tectonophysics 335, 183–192.
Ward, R.A., Stevens, G., Kisters, A.F.M., 2008. Fluid and deformation induced partial melting and melt volumes in low-temperature granulite-facies metasediments, Damara Belt, Namibia. Lithos 105, 253–271.
Weinberg, R.F., 1996. Ascent mechanism of felsic magmas: news and views. Trans. R. Soc. Edinb. Earth Sci. 87, 95–103.
Weinberg, R.F., 1999. Mesoscale pervasive felsic magma migration: alternatives to dyking. Lithos 46, 393–410.
Weinberg, R.F., Mark, G., 2008. Magma migration, folding, and disaggregation of migmatites in the Karakoram Shear Zone, Ladakh, NW India. Geol. Soc. Am. Bull. 120, 994–1009.
Weinberg, R.F., Regenauer-Lieb, K., 2010. Ductile fractures and magma migration from source. Geology 38, 363–366.
Wulff, K., Dziggel, A., Kolb, J., Vennemann, T., Böttcher, M.E., Michael Meyer, F., 2010. Origin of mineralizing fluids of the sediment-hosted navachab gold mine, Namibia: constraints from stable (O, H, C, S) isotopes. Econ. Geol. 105, 285–302.

Chapter 4: Magma accumulation and ascent

This chapter constitutes a presentation of the research paper: ***Covering their tracks – episodic accumulation and drainage of granitic magma batches in the mid-crust***[1] by Hall and Kisters, which has undergone a first revision and has been resubmitted to the Journal of Metamorphic Geology.

This manuscript was first authored by Duncan Hall with standard supervision entailing academic guidance and editorial support from Alex Kisters. The following aspects were carried out independently by Duncan Hall: (1) field work and data collection, (2) interpretation of the field data (3) conceptual integration of the field data with theoretical models of fracture-controlled magma transport (4) preparation and submission of the manuscript.

[1] Hall, D.J. & Kisters, A.F.M., first revision *J. Met. Geol.* [under review]. ***Covering their tracks – episodic accumulation and drainage of granitic magma batches in the mid-crust.*** [assigned manuscript no: JMG-15-0086]

J. metamorphic Geol. ***first revision,*** **manuscript number:** ***JMG-15-0086.***

Covering their tracks – episodic accumulation and drainage of granitic magma batches in the mid-crust

D.J. HALL[1], A.F.M. KISTERS[1]

[1]Department of Earth Sciences, University of Stellenbosch, Matieland 7602, South Africa (duncanh11@gmail.com)

ABSTRACT The processes of long-range granitic magma transfer from mid- and lower-crustal anatectic zones to upper-crustal pluton emplacement sites remain controversial in the literature, partly because the feeder networks that could have accommodated this large-scale magma transport remain elusive in the field. Granite ascent models are thus based largely on numerical and theoretical studies that seek to demonstrate the viability of fracture-controlled magma transport through dykes or self-propagating hydrofractures with little supporting field evidence, such as sufficiently voluminous magma accumulations near- or within the anatectic source, to support their basic premises.

We document large (deca- to hectometre-scale), steeply-dipping and largely homogeneous granite lenses in suprasolidus (P ~5 kbar, T ~750 ºC) mid-crustal rocks in the Damara Belt in Namibia. The lenses are surrounded by and connected to shallowly dipping networks of stromatic leucogranites in the well-layered gneisses of the deeply incised Husab Gorge. The outcrops sketch a four-stage process from (1) initial formation and growth of large magma-filled lenses as extension fractures formed at high angles to the subhorizontal regional extension in relatively competent wall-rock layers, followed by (2) the simultaneous lateral inflation and (3) vertical growth of the lenses to a critical size that (4) results in the destabilization and buoyancy-driven upward mobilization of the fractures and, consequently, vertical magma transport.

These field observations are compared with existing numerical models and are used to constrain, by referring to the dimensions of the largest in situ leucogranite lens, an estimate of the minimum fracture length (~100 m) and volume (~2.4×105 m3) required to initiate buoyancy-driven brittle fracture propagation in this particular mid-crustal section. The critical values and field relationships compare favourably with theoretical models of magma ascent along vertical self-propagating hydrofractures which close at their tails during propagation. This process leaves behind subtle wake-like structures and thin leucogranite trails that mark the path of magma ascent and the repeated inflation and drainage of the fracture-controlled conduits is consistent with the episodic accumulation and removal of magma from the mid-crust, as is reflected in the sheeted nature of many granitoid plutons.

Key words: granite; magma ascent; self-propagating hydrofractures; magma buoyancy; magma transport, magma batches

INTRODUCTION

The transport of crustally-generated granitic magma from sites of anatexis in the mid- to deep continental crust to shallower emplacement levels is an important mechanism of intracrustal mass and heat transfer. The first stage in this transfer is accomplished by the extraction of partial melts from sites of partial melting along grain triple junctions in fertile source rocks (e.g. Jurewicz and Watson, 1984) and their concentration, driven by deformation-induced stress/pressure gradients (Brown, 1994; Rutter and Neumann, 1995), into the secondary melt/magma networks that are represented by leucosome/leucogranite networks in migmatite terrains worldwide (e.g. Marchildon and Brown, 2003; Sawyer, 2008; Hall and Kisters, 2012; Weinberg et al., 2013). This manuscript deals with the drainage of these secondary storage networks and the relatively poorly understood mechanism whereby the long-range transport of magma through the continental crust is initiated.

Ubiquitous upper crustal granitoid plutons attest to the effectiveness of long-range granitic magma transport in the continental crust, but apart from a few examples (e.g. Sawyer, 1998; Weinberg and Searle, 1998), field evidence of large-scale, long-range magma ascent through the crust between deep granite source regions and shallow crustal plutons remains elusive (Reichardt and Weinberg, 2012). Moreover, plutons are increasingly being recognized as composite bodies (e.g. Hutton, 1992; Miller and Paterson, 2001; Coleman, et al., 2004; Glazner et al., 2004; Rocchi et al., 2010; Miller et al., 2011; Leuthold et al., 2014; Olivier et al., 2015) that are assembled batch-by-batch at cumulative rates much slower than the rates necessary to prevent magma from freezing during transport through subsolidus crust (Menand et al., 2015). This suggests that magma ascent is episodic and that near- and within-source magma volumes must vary in space and time in response to distinct episodes of accumulation and draining (Brown, 2013).

Much of our understanding of long-range magma ascent is based on conceptual, analogue and numerical models of buoyancy-driven magma ascent along fracture-controlled conduits (dykes sensu lato; e.g. Weertman, 1971; Lister and Kerr, 1991; Clemens and Mawer, 1992; Petford et al., 1993; Rubin, 1995; Nunn, 1996; Dahm, 2000; Bons and van Milligen, 2001; see comprehensive review by Rivalta et al., 2015). Magma-filled fractures may develop within- or close to source regions where sufficiently elevated magma pressures and low differential stresses (σ_1-σ_3 with $\sigma_1>\sigma_2>\sigma_3$) promote extensional (mode I) failure of the wall rocks, focusing nearby magma towards the newly-formed dilatant sites (Davidson et al., 1994). The models suggest that once sufficient magma has accumulated within steep fractures formed in this way, the buoyancy of the magma and the geometry of the fracture tips can induce tensile stresses large enough to overcome the tensile strength of the overlying wall rocks, allowing the fractures to propagate upwards (Ida and Kumazawa, 1986; Clemens and Mawer, 1992). Two endmember models of fracture-controlled magma ascent exist, namely dykes (sensu stricto) and self-propagating hydrofractures (Nakashima, 1993). In their original formulation dykes are tabular bodies of magma with very high aspect ratios whose propagation is driven by the buoyancy of the contained magma as well as supralithostatic magma pressures within source reservoirs to which the dykes remain connected during propagation (e.g. Lister and Kerr, 1991; Roper and Lister, 2007; Taisne and Jaupart, 2009). Compelling field evidence for dyking is abundant in upper-crustal and subvolcanic environments where sufficiently large magma chambers are known to form suitable source reservoirs. However, dyke transport directly from source rocks has been questioned, because

a sufficient volume of hydraulically connected magma may not be available in the source to establish a growing dyke (Bons et al., 2001; Diener et al., 2014).

Magma ascent within self-propagating hydrofractures has been suggested as an alternative mechanism for the ascent of magma from source (Bons and van Milligen, 2001; Bons et al., 2009), since they can develop independently of large source reservoirs/connected networks. Once formed, the density contrast between the granitic magma (2.3-2.4 g/cm3) and the wall rocks (~2.7 g/cm3) produces a pressure differential within subvertical magma-filled fractures that results in supralithostatic and sublithostatic magma pressures in the fracture tips and tails respectively (Sleep, 1988; Bons et al., 2001; Kisters et al., 2009). Buoyancy-driven propagation of the fracture tip occurs in response to the tensile stress generated in the wall rocks by the supralithostatic magma pressures in the upper parts of the fracture (Clemens and Mawer, 1992). The magnitude of this tensile stress is dependent on the vertical height of the magma column and the density contrast between the magma and the wall rocks (Weertman, 1971; Secor and Pollard, 1975). Pressure-dependent density is usually not considered and propagation of the fracture tip is dependent only on the magma-filled fracture reaching some critical length so that the tensile stress generated ahead of the fracture exceeds the tensile strength of the wall-rock. Once propagation starts, the sublithostatically-pressured tail of the hydrofracture begins to close, resulting in the wholesale ascent of a now isolated magma-filled fracture that maintains a constant magma volume. This process leaves behind very little evidence in the rock record and could account for the elusive nature of long-range magma ascent conduits in the middle continental crust (Bons et al., 2001).

As outlined above, the development of efficient dykes and self-propagating hydrofractures requires that magma is somehow able to accumulate in source reservoirs/networks or the hydrofractures themselves prior to the onset of ascent (Diener et al., 2014). However, former anatectic terrains are typically characterized by low-volume and, commonly,

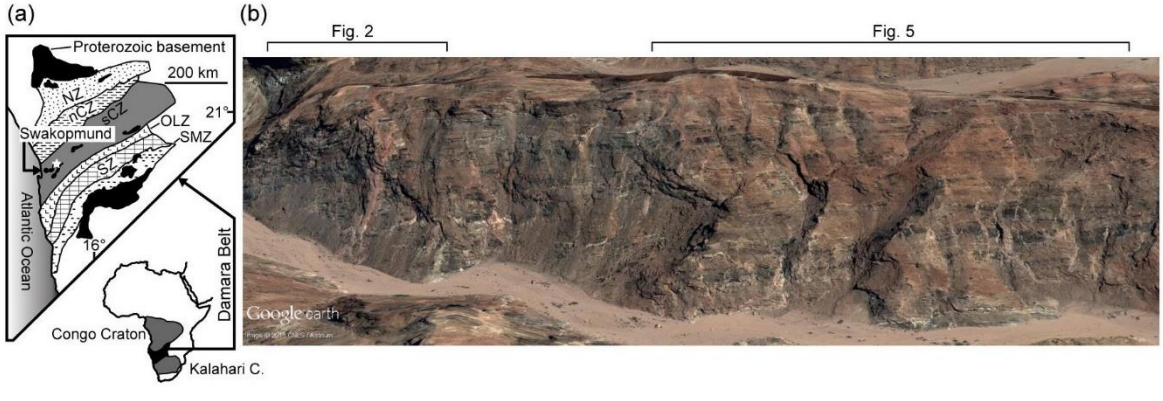

Fig. 1 (a) The high-grade south Central Zone of the Damara Belt (sCZ) represents the magmatic arc of the NE-trending suture that joined the Kalahari and Congo Cratons during the Pan-African (c. 550-500 Ma) assembly of Gondwana. Location of the study area indicated by star. Modified after Miller (2008) and Kisters et al. (2009); tectonostratigraphic zoning after Miller (1983): NZ = Northern Zone, nCZ = north Central Zone, OLZ = Okahandja Lineament Zone, SZ = Southern Zone, SMZ = Southern Marginal Zone. (b) Oblique 3D view towards the NW (Google Earth) of the lower ~1.8 km of the study area in the Husab Gorge (1.5x vertical exaggeration; 22° 45.181' S, 15° 4.189' E). Locations of the panels illustrated in figures 2 and 5 are indicated.

only shallowly-dipping leucosome/leucogranite veins and dykes contained within networks that represent the remnants of local magma transport within- and close to the source. Steeply orientated near/within-source leucogranites that represent coherent former magma bodies large enough to ascend out of the anatectic zone under their own buoyancy (several- to several hundred metres long and up to several metres wide; Petford et al., 1993; Nunn, 1996; Bons et al., 2001) are not commonly preserved (Diener et al., 2014) and the intrusive features within and close to high-grade source regions are typically much smaller. This paper aims to help clarify the link between the low volume magma networks that typically develop within or close to partially molten source rocks and the processes that initiate long-range magma ascent through the overlying subsolidus crust. We base our interpretations and conclusions on field observations from superbly exposed leucogranite networks in the suprasolidus (T ~750 °C, P ~5 kbar) mid-crust of the Pan-African (c. 550-500 Ma) Damara Belt in central Namibia. Intrusive networks along the steep slopes of the >100 m deep Husab Gorge (Fig. 1) are for the most part characterized by evenly distributed cm- to dm-thick leucogranite stringers and sheets developed parallel to the wall-rock layering. However, the cliff sections also contain much larger, subvertical lens-like leucogranites that demonstrate not only the local accumulation, but also the passage of large magma volumes, underlining the importance of the episodic accumulation within and extraction of magma from structurally-controlled sites in high-grade, near-source wall rocks. The outcrops in the Husab Gorge will be presented and discussed with reference to theoretical, experimental and numerical models in order to characterize the mechanisms of magma accumulation and extraction and to assess the implications for the long-range vertical transport of granitic magmas in the continental crust.

GEOLOGICAL SETTING

Tectonic framework

The northeast-trending Damara Belt in central Namibia represents the suture formed during the convergence and eventual soft collision between the Kalahari and Congo cratons during Gondwana assembly in the latest Proterozoic and early Phanerozoic (Fig. 1a; Coward, 1983; Oliver, 1994; Meneghini et al., 2014). The belt can be divided into several tectonostratigraphic zones (Fig. 1a; Miller, 1983). The highest grade Central Zone is thought to represent the magmatic arc of the belt (Meneghini et al., 2014) and is further subdivided into the relatively lower grade north Central Zone and the higher grade south Central Zone (sCZ). The present study area forms part of the deeply eroded, high-grade western parts of the sCZ (Fig. 1). The lithological inventory of the western sCZ includes a Paleoproterozoic (c. 2.0-1.8 Ga; Jacob et al., 1978; Longridge et al., 2014) basement comprised mainly of quartzofeldspathic gneisses and minor supracrustal rocks collectively referred to as the Abbabis Metamorphic Complex. This basement is unconformably overlain by the Neoproterozoic (c. 780-600 Ma) Damara Supergroup, which represents a sequence of mixed carbonate-siliciclastic metasedimentary and minor metavolcanic units. The supracrustal rocks document the evolution of the belt from initial rifting between c. 800 and 750 Ma, through spreading, convergence and the onset of subduction at c. 580 Ma to final collision between c. 540 and 515 Ma (De Kock et al., 2000; Gray et al., 2008; Miller, 2008).

Structural geology of the western sCZ

Paleoproterozoic basement rocks of the Abbabis Metamorphic Complex are exposed as regional-scale basement uplifts or windows through the overlying Damara Supergroup. The basement gneisses contain earlier Proterozoic fabrics that

are variably overprinted by later Pan-African strains (e.g. Jacob, 1974; Brandt, 1987; Kisters et al., 2004; Miller, 2008; Longridge et al., 2011; 2014). The details of the Pan-African structural evolution are controversially discussed, but most studies have identified regionally widespread bedding-parallel or low-angle fabrics (S1 and L1) and structures as the earliest fabric elements in the Damara Belt. These fabrics are assigned to a D1 phase of deformation. D1 structures include outcrop- to regional-scale recumbent folds (F1) and associated low-angle thrusts (Jacob, 1974; Miller, 1983; Kisters et al., 2004). Earlier D1 structures and fabrics have been refolded by later, more or less upright, northeast-trending regional-scale folds (D2/F2) and associated thrusts. D2 structures dominate the structural pattern of the Damara Belt. F2 folding and thrusting are associated with relatively consistent and, in places, pervasive northeast-trending fabrics (S2/L2). The steep, northeast-trending S2 foliation is axial-planar to F2 folds, while the L2 lineation shows north-easterly trends and mostly shallow plunges, parallel to the hinges of F2 folds. Constrictional fabrics (L2) in the higher-grade south-western parts of the sCZ are interpreted to indicate the lateral extrusion of the mid-crustal levels during high-angle northwest-southeast convergence (Poli and Oliver, 2001; Kisters et al., 2004). Irrespective of the different interpretations of the detailed structural evolution of the belt, structural and geochronological studies suggest that D1/D2 strains formed during a prolonged period (550-515 Ma) of northwest-directed, subhorizontal, largely co-axial shortening (Poli and Oliver, 2001; Kisters et al., 2004, 2012), probably related to the high-angle convergence and shallow subduction of the Kalahari below the Congo Craton.

Metamorphism and partial melting in the western sCZ

In the western sCZ of the HTLP Damara Belt (Miller, 1983; Puhan, 1983, Masberg et al., 1992) D2 was accompanied and outlasted by upper amphibolite- to lower granulite-facies P-T conditions (5-6 kbar and ~750 °C; e.g. Jung and Mezger, 2003; Ward et al., 2008). The deeply-incised dry riverbeds of the Khan and Swakop Rivers in the western sCZ superbly expose extensive networks of both in situ leucosomes and intrusive leucogranites that are interpreted to have accommodated the within- and near-source transport of magma (e.g. Hall and Kisters, 2012) as well as the mobilization of magma out of the source- and near-source region (Kisters et al., 2009). Low-volume, in-situ partial melting of metapelitic rocks is locally recorded (e.g. Jung et al., 1998; Ward et al., 2008; Miller, 2008; Kisters et al., 2009), but is rare in the largely quartzofeldspathic basement rocks of the Abbabis Metamorphic Complex (e.g. Jung et al., 1998; Nex et al., 2001; Miller, 2008; Longridge et al., 2011). Isotope geochemistry indicates the extensive networks of intrusive leucogranites in basement and cover rocks to be derived by low-volume partial melting of the deeper levels of the underlying basement (e.g. Jung et al., 2002; Ostendorf et al., 2014; Stammeier et al., 2015).

Geology of the Husab Gorge

This study focuses on leucogranites that intrude the Abbabis Metamorphic Complex along the lower reaches of the northeast-trending Husab Gorge, which forms a tributary to the Swakop River ~60 km east of its mouth at Swakopmund (Fig. 1). The gorge exposes a longitudinal section through a well-layered sequence of moderately northwest-dipping (30°-70°) grey quartzofeldspathic augen- and paragneisses and interlayered dark amphibolites (collectively referred to as basement gneisses). The quartzofeldspathic gneisses contain a well-developed layer-parallel foliation, the preservation of which underlines the minimal

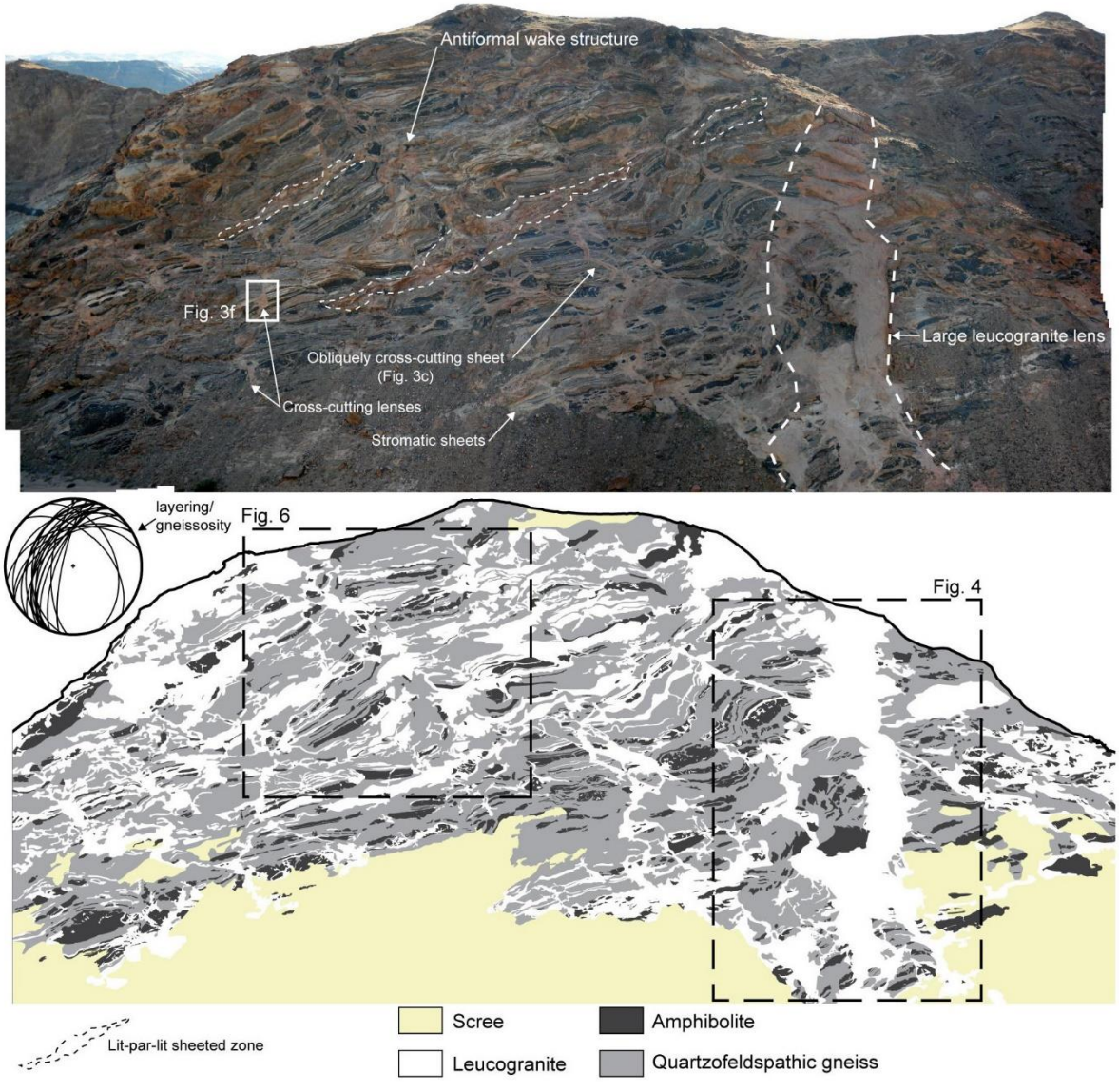

Fig. 2 Digital image composite and sketch map of the cliffs along the NW slope of the lower reaches of the Husab Gorge as viewed from the SE (for location see figure 1). The cliffs contain well-layered, moderately NW-dipping quartzofeldspathic gneisses and intercalated amphibolite horizons (gneissosity indicated by lower hemisphere equal area stereonet) that are intruded by extensive networks of concordant and cross-cutting leucogranites. The cliff section as viewed measures ~300 m along the dry riverbed of the Husab River and is >~100 m tall. The locations of the large, lens-like leucogranite (Fig. 4) and antiformal wake structure (Fig. 6) discussed below are indicated.

overprinting of the original Paleoproterozoic basement fabrics by later Pan-African strains.

The basement gneisses along the Husab Gorge host networks of millimetre- to decametre-wide sheet- and lens-like leucogranites that span at least five orders of magnitude in scale. Marked colour contrasts between the pale to pinkish granites and the darker basement rocks allowed granites thicker than a few 10s of cm to be mapped remotely using digital image composites (Fig. 2). The leucogranites appear homogeneous at the scale of these base images, but gradual

compositional and pronounced textural contrasts develop at outcrop-scale. Despite this, markedly distinct granite phases cross-cut one another only in places and consistent cross-cutting relationships between leucogranite bodies of different composition or macroscopic internal structure could not be identified. The granites are compositionally similar overall and petrographic continuity across granite intersections is common (e.g. Figs 3a, b, c, d). In contrast, the contacts between the granites and the wall rocks are knife-sharp throughout, and the diffuse contacts common in partially melted high-grade rocks are not developed. Furthermore, thin (mm-wide) biotite-rich mafic selvedges, such as those typically developed along the contacts between injected leucogranites and their host rocks (Sawyer, 2008), are common (e.g. Fig. 3b). Evidence of in-situ partial melting, such as the presence of peritectic phases, is not developed. The relatively biotite-poor gneisses and amphibolites thus appear largely unmelted and, if present, the volumetric contribution of any in situ partial melting to the volume of leucogranite present in the Husab Gorge is likely to be very small. The lack of evidence of widespread in-situ partial melting and the sharp intrusive contacts together indicate that the networks very likely record the accumulation and passage of magma close to, but outside of the partially melted source of the leucogranites. Thus, the rocks in the Husab Gorge are injection migmatites made up of networks of near-source leucogranites. The lack of pervasive solid state fabrics in the granites and the undeformed nature of the intrusive contacts points to the preservation of the original leucogranite geometries and suggests leucogranite development during the later stages of the Pan-African tectonism.

LEUCOGRANITE NETWORKS

The cliff sections along the lower reaches of the Husab Gorge contain leucogranites in laterally extensive mm- to several m-thick stromatic sheets and generally larger (up to ~30 m wide), more widely spaced cross-cutting sheets and lenses (Fig. 2). Together, these geometries form near-pervasive and largely interconnected leucogranite networks.

Stromatic leucogranite sheets and stringers

Foliation and/or layer-parallel leucogranite stringers and sheets from a few mm- to a few cm-thick are the most abundant and, cumulatively, the least voluminous granite geometry developed along the Husab Gorge. Development of the stromatic leucogranites is limited to the quartzofeldspathic gneisses, within which they define a mm- to dm-scale stromatic layering (Fig. 3e). Wider stromatic leucogranite sheets from ~10 cm (Figs 3c, e) up to ~2 m (Fig. 2) thick show sharp intrusive contacts against the wall rocks and a much wider spacing of up to several metres. Subtle pinch and swell morphologies along the stromatic leucogranites are common and probably reflect a small degree of post-crystallization, layer-normal shortening as well as the original emplacement geometries parallel to the gently undulating gneissosity. The largest concordant leucogranite features are somewhat indistinct, granite-rich zones up to 5 m wide that are commonly developed along lithological contacts. These zones are characterized by multiple lit-par-lit granite sheets emplaced parallel to the wall-rock layering/foliation that result in the peeling off of layer-parallel wall-rock slivers, highlighting, in places, the loss of wall-rock cohesion during granite injection (Fig. 2).

Cross-cutting leucogranite sheets and lenses

The stromatic granite stringers and sheets described above are connected by variably-sized granite lenses and sheets that cut across the wall-rock and stromatic layering obliquely or at high-angles. The cross-cutting leucogranites can be

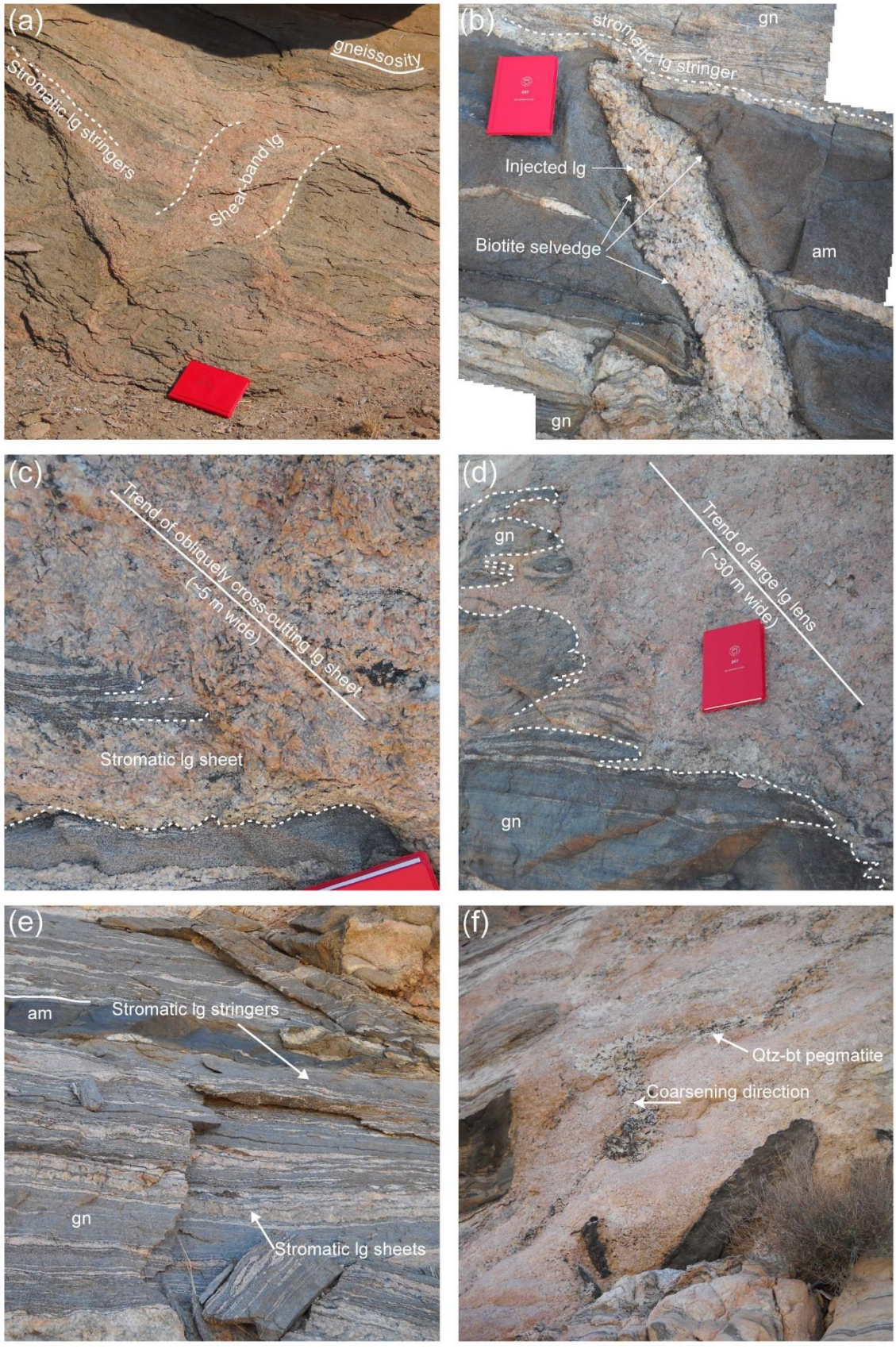

Fig. 3 (a) Petrographic continuity within small-scale network of shear-band and stromatic leucogranites. Notebook is ~15 cm wide. (b) Intersection and arrest/rotation of cross-cutting leucogranite lens along lithological contact between amphibolite and gneiss. Note the presence of melanocratic selvedges along the granite/wall-rock contacts (c) Petrographic continuity across the contact between a stromatic leucogranite sheet and a large (~5 metre wide) obliquely cross-cutting leucogranite sheet (location of oblique sheet indicated in figure 2). (d) Typical field-relationships recorded along the lateral margin of the large leucogranite lens (see figures 2 and 4) commonly include sharply cross-cutting contacts against the wall-rock gneisses and continuous intersections with stromatic leucogranites sheets and stringers. (e) Oblique view showing stromatic layering within quartzofeldspathic gneiss. The layering is defined by leucogranite stringers and sheets from mm- to dm-thick. Concordant stringers/sheets are absent from the amphibolite layer. Foreground field of view is ~2 m. (f) Cross-cutting granite lens (3-4 m wide; for location see figure 2) showing pronounced inward-coarsening textures. gn = quartzofeldspathic gneiss, am = amphibolite, lg = leucogranite.

distinguished based on size, geometry and wall-rock relationships.

Small-scale cross-cutting leucogranite sheets

The smallest cross-cutting leucogranites are cm- to dm-wide sheets and lenses sporadically developed within extensional (mode I) fractures and conjugate shear-band sets in the quartzofeldspathic gneisses (Fig. 3a). Typically larger cross-cutting lenses and pods (up to ~1 m wide) orientated at high angles to the layering are preferentially developed within the amphibolites (Figs 2, 3b). Still larger oblique- to high-angle cross-cutting leucogranite sheets, lenses and pods up to 4 m wide and several tens of metres long cut across the outcrops at regular intervals of between ~5 and 20 m (Fig. 2). Several of these larger features show textures that coarsen inwards towards central margin-parallel pegmatite bands that contain increased proportions of quartz and biotite compared to the surrounding leucogranite (Fig. 3f).

Large-scale cross-cutting leucogranite lenses

The m-scale granite geometries described up to this point form extensive networks of largely interconnected layer-parallel and cross-cutting leucogranite sheets and lenses (Fig. 2). These networks also contain several much larger subvertical lens-like leucogranites that cut across the wall rocks, but largely maintain intrusive continuity with adjacent leucogranite networks. The largest of these is a northwest-striking subvertical lens-like feature that sharply cross-cuts the wall-rock layering at high angles within the cliff section along the lower reaches of the gorge (Figs 2, 4). The lowest parts of the lens are not exposed, but the preserved cross-sectional dimensions of 100 by 30 m define a channel that narrows upwards and bifurcates near the crest of the cliffs (Fig. 4d). An extent of at least 150 m is indicated along strike to the northwest beyond the cliff section (Fig. 4d). Using these dimensions, and by approximating the volume of the large leucogranite lens to that of a similarly sized ellipsoid, a minimum intrusive volume of ~2.36 × 105 m3 is indicated. The leucogranite contained within the lens is largely homogeneous, but marked textural and slight compositional variations develop within widely-spaced pockets and margin-parallel bands of pegmatite (Fig. 4). The lateral contacts of the lens dip steeply southwest/northeast at high angles to the regional stretching direction and define the northwest-strike of the lens overall (Fig. 4c), but describe an irregular and/or jagged surface in detail (Figs 3d, 4a, b) that results from the combination of sharply cross-cutting contacts against the wall rocks and the connectivity

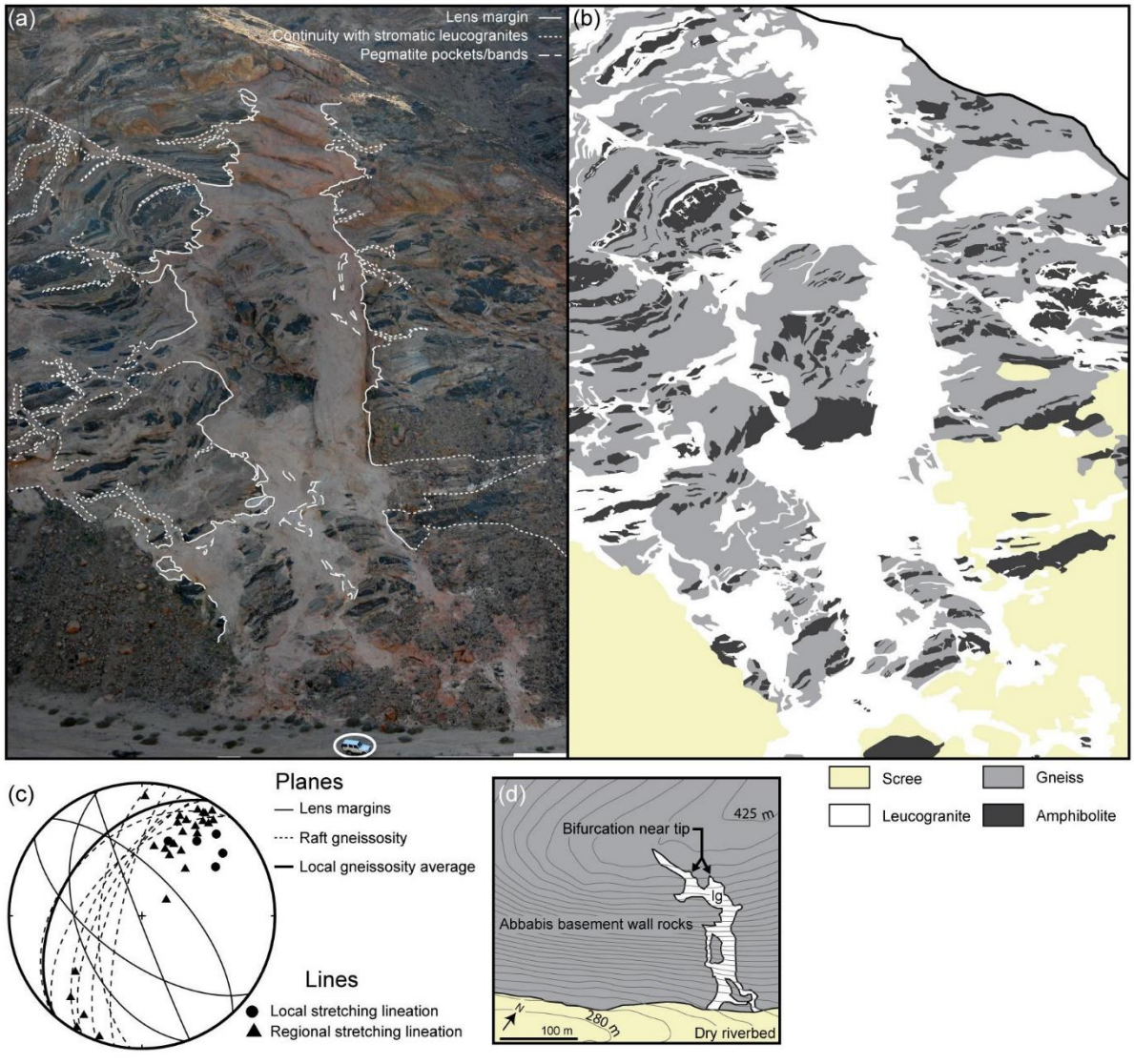

Fig. 4 (a-b) Composite image and sketch map showing a SE-facing cross section through the large lens-like leucogranite contained within the cliff section along the lower reaches of the Husab Gorge (see figure 2 for location). The lens is ~100 m tall and up to ~30 m wide as exposed. Four-wheel drive vehicle circled for scale (~5 m long). Note the widened intersections between m-scale stromatic leucogranite sheets in the wall rocks and the leucogranite contained within the lens. (c) Lower hemisphere, equal area stereonet illustrating the orientation of the lens (striking NW), the local and regional stretching lineations and a comparison between the foliations within the large wall-rock rafts in the lower parts of the lens and the average orientation of the wall-rock layering/gneissosity. Regional stretching fabric data provided for reference was recorded in the nearby Hollands Dome. (d) Simplified plan view of the leucogranite lens illustrating the vertical and along-strike extents of the lens. Elevation contours with intervals of 5 m are shown; lg = leucogranite.

between the adjacent stromatic leucogranites and the main body of the lens (Fig. 4). Intrusive continuity between the stromatic leucogranites and the leucogranites contained within the large lens is also indicated by the widening of the stromatic leucogranite sheets towards the lens and also by petrographic and textural continuity at outcrop-scale (Figs 3d, 4). In the lower parts of the lens, this zigzag contact morphology is manifested in the separation of wall-rock rafts up to 15 m in diameter. The rafts themselves are separated from one another by swathes of leucogranite up to several metres across, yet their internal structure is retained and remains subparallel to that of the wall-rocks outside the lens (Fig. 4c).

The lack of rotation even of small (m-wide) wall-rock rafts that are separated from adjacent wall rocks by several metres of homogenous granite and are probably completely suspended within the large lens underlines the progressive dismemberment of the wall rocks during passive leucogranite emplacement. An intermediate stage in the accumulation of such large magma volumes is illustrated by the development of a series of subvertical leucogranite lenses within steep cliffs ~1 km upstream of the large lens described above (Figs 1, 5). In this area, northwest-striking granite lenses are preferentially developed within and centred around a prominent, ~15 m thick amphibolite layer. The lenses occur with a spacing of ~20-50 m and preserve cross-sectional lengths and widths of 50-100 m and up to ~25 m respectively. These dimensions describe convex geometries overall that are widest at their vertical centres and gradually taper towards rotated tip and tail sections within the bounding gneisses, defining a pronounced bilateral symmetry about the central amphibolite layer (Fig. 5). The sharply discordant and parallel-sided subvertical central sections of the lenses within the amphibolites

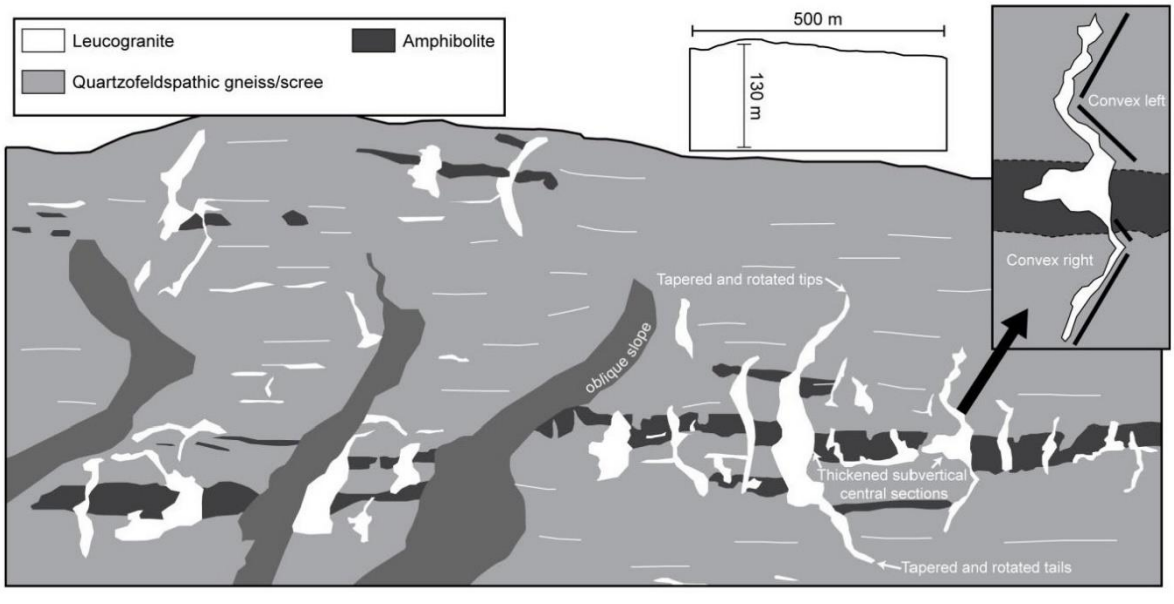

Fig. 5 Sketch map showing a SE-facing cross section through a series of large convex leucogranite lenses ~1 km upstream from the cliff section illustrated in figure 2. Leucogranite development is closely associated with the relatively competent amphibolite horizons. The right hand inset details the alternating symmetry and zigzag contacts of the granite lenses, highlighting different modes of fracture in the more competent amphibolites and less competent quartzofeldspathic gneisses. The panel illustrated is ~500 m long and ~130 m high. For location see figure 1.

indicate that the lenses formed as extensional fractures that nucleated within relatively competent wall-rock layers. In detail however, where the lenses intersect the gneisses, they are comprised of en echelon segments with opposite senses that result in zigzag contacts, pronounced alternating convex-left and convex-right symmetries in some cases (Fig. 5 inset) and the rotation by up to 30-40° of the tips and tails of the lenses with respect to their vertical central sections. This highlights a change in failure mechanism across the mechanical anisotropy associated with the change in wall-rock lithology from mode I extension fracturing in the amphibolites to mode II conjugate shear failure in the gneisses. In places, the termination of the lenses within the gneisses is defined by the rotation of the tips and tails of the lenses into parallelism with the lithological layering or wall-rock foliation, producing T- or L-shaped geometries that underline the continuity between leucogranite lenses and the stromatic leucogranite sheets in the wall rocks.

The above observations illustrate a role during the development of the cross-cutting leucogranite geometries for the interaction between three distinct anisotropies. The first is the competence anisotropy between the mechanically-distinct wall-rock layers that initiates lens formation within the competent amphibolites. The second is the regional stress anisotropy that determines the direction of fracture propagation, i.e. normal/at high angles to the regional stretching direction during extensional fracturing of the amphibolites and alternating, likely conjugate segments that are bisected by the regional stretching direction during mode II fracturing of the less competent gneisses. The third anisotropy, namely the wall-rock gneissosity, is responsible for the capture of propagating fracture tips and the arrest of fracture propagation in the gneisses.

Antiformal wake structure

A characteristic upward deflection of the wall-rock layering defines an antiformal, cusp-like structure along the cliff face ~150 m southwest of the large lens described above (Figs 2, 6). The subvertical central line of the cusp extends to the crest of the cliffs, 80 m above its lower bounding surface along a layer-parallel detachment defined by the intrusion of several stromatic leucogranite sheets which interfinger with and dismember the wall-rock layering and gneissosity. The central line of the cusp is pierced along its 80 m length by an up to 8 m wide, but highly irregular leucogranite band that truncates the wall-rock layering overall, but interfingers with the wall rocks locally (Fig. 6). Together, the central leucogranite and the flanking cusp produce a wake-like geometry formed by the unidirectional drag of the wall-rock layering on either side of the leucogranite. The leucogranite contains several m-scale fragments of amphibolite and smaller fragments of quartzofeldspathic gneiss. The fragments have been displaced and rotated with respect to the bounding wall rocks (Fig. 6) and some are large (up to ~5 m diameter) relative to the width of leucogranite, indicating that more magma was present than is recorded by the preserved volume of leucogranite. The smaller, and generally more elongate fragments have been displaced upwards and rotated so that the internal gneissosity is at high angles to that of the surrounding wall rocks, but parallel to the central axis of the wake structure (Fig. 6), highlighting a rotation of the fragments during their upward displacement.

MAGMA ACCUMULATION AND EXTRACTION

Field evidence of magma extraction

An important consideration for the following discussion is that leucogranites in this part of the sCZ intruded into suprasolidus crust. At wall-rock temperatures of ~700-750 °C, the granitic magmas may have contained as much as 40-50 % melt (e.g., Clemens and Wall, 1981). This

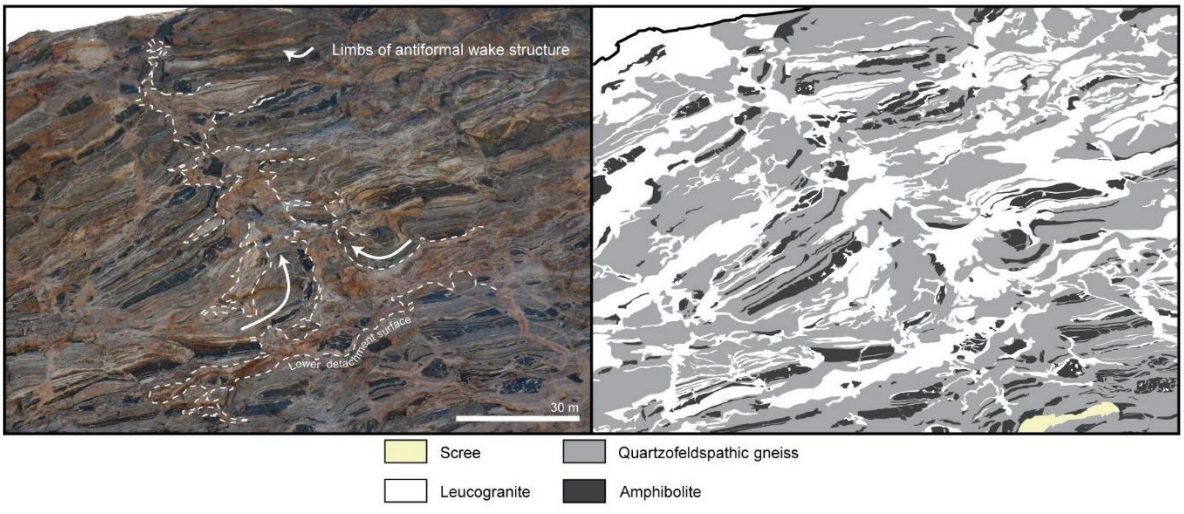

Fig. 6 Digital image composite and sketch map showing the antiformal wake structure developed within the cliff section illustrated in figure 2, some 150 m southwest of the large leucogranite lens in figure 4. The digital image shows the rough outline of the leucogranite contained within the antiformal wake structure as well within its lower, layer-parallel detachment surface.

implies the presence, in the western sCZ, of a low-viscosity melt phase for a protracted period and before the terrain cooled to solidus temperatures much later (Gray et al., 2006) or melts were extracted by deformation. The homogeneity of the large leucogranite lens and its continuity with the stromatic leucogranites in the wall rocks further suggest it represented a large and fairly contiguous magma body connected with the smaller magma sheets in the adjacent suprasolidus wall rocks. Wall-rock deformation and the much lower volumes of leucogranite in the antiformal wake structure, in contrast, appear to record the collapse of a more voluminous precursor structure (e.g. Bons et al., 2008). Smaller-scale features with similar geometries and wall-rock relationships to the antiformal wake structure have been described as post-deformation melt/magma flow channels in migmatites at Kangaroo Island (Weinberg et al., 2013). Similar geometries are also produced by computer simulations of the deformation imparted on migmatitic wall rocks by rising magma bodies (Koyi et al., 2013). Both of these studies relate the unidirectional bending of the wall rocks to the drag exerted by the flow of viscous magma in the direction of the cusp of the wake. This would suggest the vertical movement and extraction of magma along the antiformal wake structure in the Husab Gorge.

Fracture-controlled magma accumulation and extraction

We propose that the large-leucogranite lens and antiformal wake structure preserve different stages in the inflation and subsequent draining of fracture-controlled sites within which magma was temporarily stored in the larger-scale complex of leucogranite networks in the Husab Gorge area.

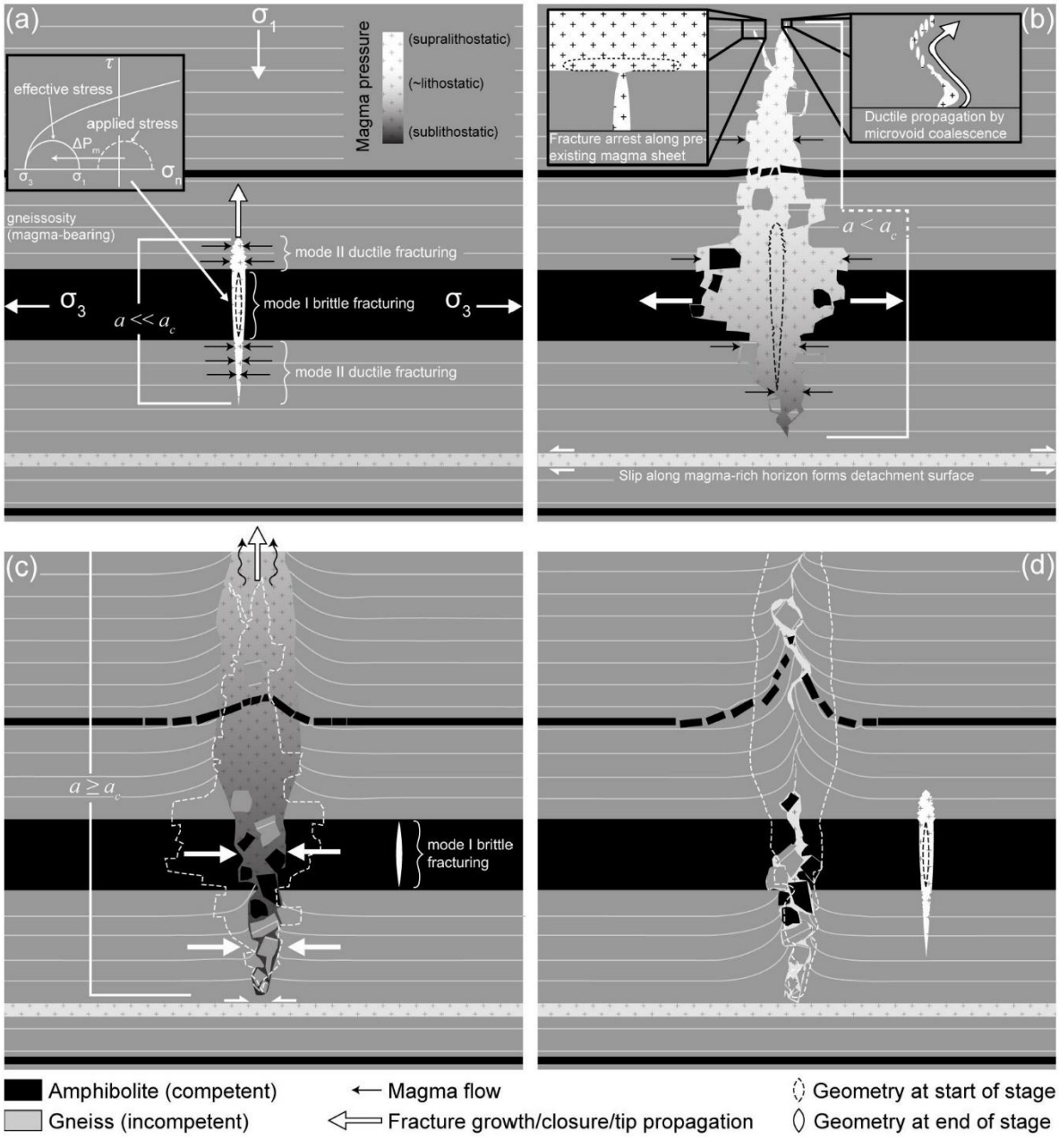

Fig. 7 Schematic model illustrating the inflation and drainage of subvertical magma-filled fractures in the Husab Gorge. (a) Initial extensional fracturing within the relatively competent amphibolite occurs under conditions of low differential and effective stress (illustrated by Mohr diagram; ΔPm represents increasing melt pressure) and results in a penny-shaped magma-filled fracture orientated at high angles to the regional stretch. (a-b) Regional extension is partitioned into the newly-formed magma-filled fracture, resulting in lateral as well as vertical growth. Vertical growth within the relatively incompetent (ductile) gneisses occurs by ductile fracturing that follows mode II shear bands. (b) Vertical ductile fracturing occurs by the coalescence of en echelon microvoids that form obliquely to the fracture tip (right-hand inset; modified after Sawyer, 2014), but remains sensitive to the mechanical anisotropies in the wall rock and may be arrested, for instance, where the propagating fracture tip intersects a pre-existing magma sheet (left-hand inset). (b-c) When the upwards propagation of the fracture tip results in the fracture attaining some critical length (a = ac) the tail of the fracture begins to close and the entire fracture and its contents are mobilized. (c-d) The viscosity of the magma prevents complete closure of the tail and the magma crystallizes to anneal the fracture, resulting in the preservation of a leucogranite trail within which relatively large rotated and displaced blocks of wall-rock are preserved. Extension in the adjacent wall rocks due to fracture closure ($\Delta\sigma 3$) may result in the development of fractures in the adjacent wall rocks.

Below we outline a four-stage process that includes (1) the initial formation of magma-filled extension fractures within relatively competent amphibolite layers, via (2) the progressive lateral inflation and coeval vertical growth of the fractures to form subvertical magma-filled lenses that (3) on becoming sufficiently buoyant are mobilized, resulting in (4) the evacuation of magma, the collapse of the original magma-bearing geometries and the decoupling of ascending magma-filled fractures from their source networks. The filling of the fractures is inferred to occur by the flow of magma along the adjacent magma network, which is interpreted to be in hydraulic connectivity with similar, but increasingly smaller-scale networks closer to the source of partial melting (Sawyer, 2014). This flux is envisaged to be driven by dilatancy-induced pumping associated initially with extensional fracturing of the amphibolites and later with the partitioning of strain into the magma-filled fractures during extension as detailed below.

This discussion aims to elaborate on the process outlined above by comparing the available field evidence with conceptual and/or numerical models of fracture-controlled magma ascent along self-propagating hydrofractures (e.g. Weertman, 1971; Secor and Pollard, 1975; Clemens and Mawer, 1992; Nunn, 1996; Dahm, 2000; Bons et al., 2009; see Rivalta et al., 2015).

Stage 1: fracture initiation

Networks of stromatic and obliquely cross-cutting leucogranites such as those developed along the Husab Gorge reflect the geometries of leucogranite networks in migmatite terrains worldwide (Sederholm, 1907; Mehnert, 1968; McLellan, 1988; Sawyer, 1991; 2008; 2010; Brown, 1994; 2004; Marchildon and Brown, 2003; Weinberg and Mark, 2008; Weinberg and Regenauer-Lieb, 2010; Morfin et al., 2013). The orientations of the magma-bearing geometries within the networks are controlled by planar anisotropies in the wall rocks and the orientation of the regional stress field that determines the orientation of dilatant sites produced during fluid-induced wall-rock failure (Davidson et al., 1994; Lucas and St-Onge, 1995; Bons et al., 2012). In the Husab Gorge, the convex leucogranite lenses illustrated in figure 5 record fracturing at high angles to the regional stretch and at right angles to the compositional layering within competent amphibolite horizons. This

suggests an origin of the granite lenses as extensional fractures that nucleated within the amphibolites. Such fractures form initially as sharp-tipped and roughly penny-shaped features (e.g. Heimpel and Olson, 1994) that grow in both directions (Dahm et al., 2010). This initially symmetrical bidirectional phase of growth within the plane of the fracture (Fig. 7a) is, in this case, limited to the relatively competent amphibolites.

Stage 2: fracture inflation

The pronounced inward-coarsening textures in some of the cross-cutting leucogranite lenses in the Husab Gorge may be a result of the relative abundance of potential nucleation sites along the wall-rock contacts, but may also highlight the availability of space during crystallization of the granites and suggest a component of dilation during their formation. Progressive dilation in response to regional extension normal to the leucogranite lenses results in the lateral migration of magma down gradients in magmastatic head from leucogranite stromata contained in the wall rocks into the dilating magma-filled extensional fractures. Since the dilation of the high-angle lenses is determined by the regional stretch, the inflation rates are likely to reflect tectonic strain rates, as is suggested by the lack of shortening strains in the wall-rocks adjacent to the large lens, despite dilation of >30 m.

Stage 3: vertical fracture growth

The lateral inflation of the magma-filled fractures is accompanied by growth along the plane of the original extensional fracture as the fracture tip and tail propagate into the wall rocks (Fig. 7b). However, the contact between the amphibolites and gneisses marks a pronounced change in the morphology of the fracture-controlled leucogranite lenses (Fig. 5), suggesting a change in failure mechanism where the lenses extend across the wall-rock competence anisotropy into the less viscous gneisses. The reduction in the viscosity contrast between the magmas and their wall rocks within the gneisses results in the blunting of the fracture tip and the dissipation of the tensile stresses generated ahead of the fracture. This process may result in fracture arrest (Figs 5, 7b) or a change in fracture mode from brittle to ductile fracturing (e.g. Eichhubl and Aydin, 2003; Brown, 2007; Weinberg and Regenauer-Lieb, 2010; Sawyer, 2014).

Ductile fracturing has been suggested as a mechanism of magma transport in high-grade within and near-source rocks as well as a mechanism for the initiation of the brittle dykes that are required for rapid long-range magma transport through subsolidus crust (Brown, 2007; Weinberg and Regenauer-Lieb, 2010). Ductile fractures exhibit zigzagging lateral contacts that are thought to result from propagation of the fractures along mode II shear bands (Fig. 7b) formed at low shear strains (2-3 %) and, as a result, do not always preserve an association with shear zones in the field (Weinberg and Regenauer-Lieb, 2010). Brittle fractures propagate by intra- and intergranular cracking in the region of the fracture tip. In contrast, ductile fractures are characterized, at the microscale, by the presence of alternately left- and right-stepping, arrays of en echelon elliptical microvoids that are oblique to the fracture tip (Fig. 7b; Sawyer, 2014). The oblique microvoids form due to dilation at grain triple boundaries in response to microscale shear displacement by, for example, grain-boundary sliding (Weinberg and Regenauer-Lieb, 2010). Macroscale ductile fracture propagation results from the coalescence of melt/magma-filled microvoids that trace the patterns of conjugate shear bands. This produces the final zigzag fracture geometries recorded along the large-scale leucogranite lenses in the Husab Gorge (Fig. 7b; Eichhubl and Aydin, 2003; Sawyer, 2014).

Stage 4: fracture mobilization and decoupling from the source

The buoyancy-driven brittle propagation of vertical, magma-filled fractures occurs when the fracture toughness (K_c) is equal to the stress intensity factor K^+ or K^- defined as

$$K^+ = \sqrt{\pi a}\left(p_0 + \frac{a}{2}\frac{dp}{dz_{tot}}\right)$$

and

$$K^- = \sqrt{\pi a}\left(p_0 - \frac{a}{2}\frac{dp}{dz_{tot}}\right)$$

at the upper and lower tips of the fracture respectively. The stress intensity factors are controlled by the fracture length (a), the (over)pressure at the fracture midpoint (p_0) and the pressure gradient within the fracture ($\frac{dp}{dz_{tot}}$; Rivalta et al., 2015). The internal pressure gradient is determined by the balance between the buoyancy of the magma, represented by $\Delta\rho g$ – where $\Delta\rho$ represents the density contrast between the magma and the wall rock (typically 300-400 kg m^{-3} for granitic magmas in the mid-crust) and g the gravitational acceleration– and the viscous pressure drop in the fracture (Rubin, 1995). In many models of self-propagating hydrofractures, the viscous pressure drop is ignored or simplified as a linear gradient (Rivalta et al., 2015). In the case of this conceptual model, the viscous pressure drop within the magma-filled fractures is neglected for simplicity and the internal pressure gradients in the steep/subvertical magma-filled fractures are, for the purposes of illustrating the main controls involved, related simply to magma buoyancy by the relationship $\frac{dp}{dz_{tot}} = \Delta\rho g$.

Should a growing magma-filled fracture, which extends vertically by ductile processes at its fracture tip, reach a such that $K^+/K^- < K_c$, the fracture will begin to grow by brittle processes at one or both of the fracture tips. Once initiated, this buoyancy-driven brittle propagation at the tip is magnified as the fracture continues to grow and will eventually result in unidirectional upward fracture growth once $K^- < K_c$ (Fig. 7b; Dahm, 2010). The extent to which this buoyancy feedback effect can occur is limited by instability at the fracture tail as $K^- \to 0$ (Weertman, 1971; Secor and Pollard, 1975; Nakashima, 1993; Dahm, 2000). At this point, K^- can be used to constrain the critical length at which the underpressured tail region of the fracture becomes unstable and begins to close. This closure squeezes the magma upwards out of the tail and the entire magma-filled fracture and its contents ascend together in the form of an isolated, self-propagating hydrofracture (Fig. 7c). During this process, the increasing viscous resistance at the tail prevents complete closure of the fracture (Fig. 7d; Stevenson, 1982; Lister and Kerr, 1991; Roper and Lister, 2007) and the hydraulic decoupling of the ascending fracture from the magma in the tail occurs only as the magma begins to solidify (Dahm, 2000). This process is recorded by the leucogranite contained in the central parts of the antiformal wake structure (Figs 6, 7d). The loss of volume due to the trapping of magma in the tail is usually assumed to be minor compared to the volume of magma in the fracture (Dahm, 2000) and may be partially compensated for by magma influx from the wall rocks (Kisters et al., 2009) if the fracture originates within the anatectic zone. The Husab Gorge wake structure also contains blocks of rotated gneiss and amphibolite trapped up to several tens of metres above/below their original stratigraphic positions. This is due to the sinking of large blocks in the pre-existing magma-filled fracture or the upward displacement and rotation of smaller blocks as a result of the drag exerted by the viscous magma during evacuation as the bottom of the hydrofractures closes (Fig. 7d).

The closure or collapse of the originally up to 30 m wide lens filled with granitic magma will result in extension of the adjacent wall rocks (Figs 7c, d) and may initiate the formation of new extensional fractures (Fig. 7d), the drawing in of magma from the adjacent networks and the development of an incipient successor ascent conduit in a manner similar to dilatancy pumping. The proximity of the large leucogranite lens and antiformal wake structure may, thus, not be coincidental, but rather a consequence of the closure of the antiformal wake structure initiating the growth and progressive inflation of the adjacent granite lens (Fig. 7d). The overall effect therefore resembles a concertina-like magma pump arrangement operated by the sequential closure and opening of closely-spaced magma-filled extensional fractures that draw in magma from below.

Critical parameters for buoyancy-driven ascent

Numerical models of self-propagating hydrofractures predict the critical length at which the buoyancy-driven fracture ascent described above is initiated, relating the onset of ascent to

$$a_c = \left(\frac{K_c}{\sqrt{\pi}\Delta\rho g}\right)^{\frac{2}{3}}$$

where a_c is the critical length (Rivalta et al., 2015). However, the effective fracture toughness of mid-crustal rocks remains unconstrained. Typical experimentally determined values of rock fracture toughness are within an order of magnitude of 1 MPa $m^{½}$ (e.g. Atkinson and Meredith, 1987) whereas standalone numerical modelling and inverse numerical modelling of real fractures in the field suggests values of effective fracture toughness in nature generally within an order of magnitude of 100 MPa $m^{½}$ (e.g. Rivalta and Dahm, 2006; Jin and Johnson, 2008; Bunger and Cruden, 2011). For the purposes of illustration the values for the critical fracture length – given magma/wall-rock density contrasts of ~400 kg m^{-3} and assuming mode I extensional fracturing – for the self-driven propagation a granitic magma-filled fracture for wall-rock fracture toughness values of 1, 10 and 100 MPa $m^{½}$ are 27, 125 and to 583 m respectively. The presence of the large, cross-cutting lens in the Husab Gorge suggests that a fracture length of ~100 m and magma volumes of ~2.4×10^5 m^3 are below the critical length and magma volume for magma-filled hydrofractures to separate from their source networks within the gneisses. The comparably large antiformal wake structure that is truncated along the crest of the Husab cliff section probably contained magma volumes slightly in excess of ~2.4×10^5 m^3 within a fracture longer than ~100 m in order to drain from the section. Notably, although this minimum critical length is consistent with the predictions from the basic models of self-propagating hydrofractures (Bons et al., 2001), the dyke-diapir hybrids and two-dimensional tear-shaped geometries produced by analogue models (Sumita and Ota, 2011) and numerical solutions that incorporate fluid flow within the fracture (Dahm, 2000) are not realized in the Husab cliff sections. Instead, the geometries are highly irregular and the width and volume of the critical fractures are much larger than predicted by the models (Clemens and Mawer, 1992; Petford et al., 1993; Clemens, 1998). This could be related to the high fracture toughness of mid-crustal rocks or the low viscosity contrast between the magma and the wall-rock, both of which control three dimensional fracture geometries (Rubin, 1993; Sumita and Ota, 2011), or the fact that in situ fracture growth prior to extraction was likely to have been by ductile rather than brittle fracturing of the wall rocks.

Fate of the hydrofractures in the overlying crust

The outcrops in the Husab Gorge are suggested to represent the conditions and critical magma

volumes required to initiate long-range granitic magma ascent out of the anatectic source along self-propagating hydrofractures. A persistent problem with fracture-controlled models of magma ascent is that regional stress fields in most convergent settings promote the formation of subhorizontal rather than subvertical fracture-controlled permeabilities. Steeply dipping transcurrent or transpressional shear zones, in particular, are commonly invoked to facilitate the large-scale ascent of granitic magmas. The steep shear zones are common in obliquely convergent settings and many studies describe a close spatial and temporal relationships between granites and shear zones, for a number of reasons (e.g., D'lemos et al., 1992; Collins and Sawyer, 1996; Neves et al., 1996; Brown and Solar, 1998a, b; Weinberg et al., 2004; 2009; Demartis et al., 2011). Large finite strains suggest that the ductile shear zones were weaker than surrounding wall rocks and represented areas of reduced mean stress (Rosenberg, 2004). This would promote lateral magma focussing from the wall rocks into the shear zones following gradients in magmastatic head. More importantly, subvertical shear zone fabrics and anisotropies combined with the shear-zone kinematics are likely to result in preferentially vertical permeability structures. Dilational jogs or releasing bend geometries during strike-slip shearing create at least transient vertical permeabilities, both on a local and a regional scale (Reichardt and Weinberg, 2012). The ascent of relatively low viscosity magmas along the shear zone rocks further lowers the strength of the shear zones and creates a positive feedback loop between strain localization and foliation/shear zone parallel magma ascent (Brown and Solar, 1998b; Solar et al., 1998).

The role of lithological contacts and mechanical contrasts in granite emplacement around the brittle-ductile transition has been illustrated by many field studies (e.g. Vigneresse, 1995; Hogan et al., 1998; Brown and Solar, 1999; Acocella and Rosetti, 2002; Hall and Kisters, 2016) and is supported by inferences from analogue and numerical modelling (e.g. Benn et al., 2000; Gudmundsson and Brenner, 2001; Kavanagh et al., 2006; Sumita and Ota, 2011). Differential stresses reach a maximum at and above the brittle-ductile transition and the ascent path of hydrofractures becomes increasingly influenced by the orientation of the regional stress field (σ_3 commonly subvertical in convergent settings). As a result, lithological heterogeneities in the layered crust above the brittle-ductile transition increasingly act as mechanical barriers and, thus, magma traps. The arrest of ascending buoyancy-driven hydrofractures is largely controlled by wall-rock rigidity and rheological anisotropies that are commonly associated with lithological contacts (Kavanagh et al., 2006; Menand, 2008; Gudmundsson, 2011). The deflection of the fractures into sills is promoted by the stress orientation and may follow facture arrest provided the strength of the arresting lithological interface is low (Kavanagh et al., 2006). This deflection represents the first stage of pluton emplacement and results in the generation of new mechanical anisotropies in the form of ductile magma-rich horizons (e.g. Wiebe and Collins, 1998) or rigid crystallized granite sheets along which later phases may be emplaced. Thus, the repeated emplacement of the relatively small magma batches suggested here for hydrofracture-controlled ascent, could result in the assembly of composite sheeted plutons, which themselves record perhaps the most compelling evidence for episodic, fracture-controlled magma ascent.

Covering their tracks – how elusive is the evidence?

Implicit in the model of melt ascent through self-propagating hydrofractures is the closure of wall-

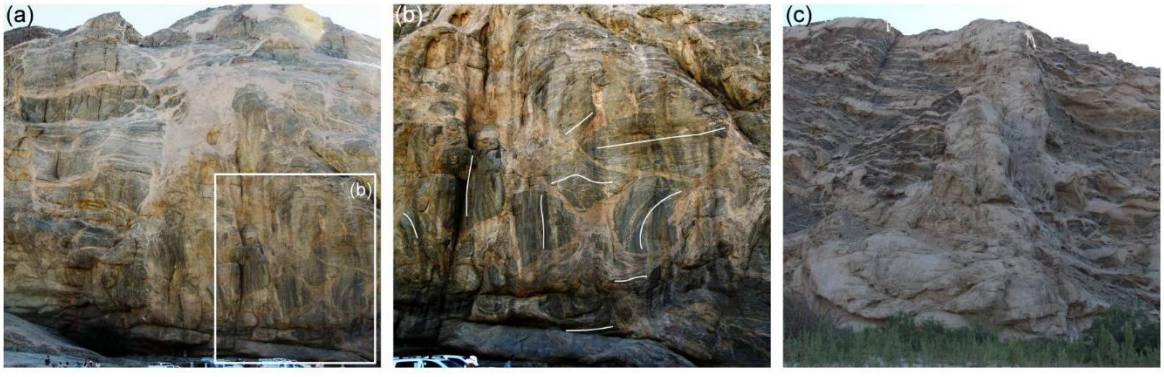

Fig. 8 Several features similar to those described along the Husab Gorge are exposed elsewhere in the Damara Belt. (a) A large subvertical leucogranite along the lower reaches of the Khan River contains (b) large, rotated (internal foliation indicated) and displaced blocks of wall-rock in its lower parts. Roofs of vehicles for scale. (c) Large inflated leucogranite lens hosted within networks of conjugate leucogranite sheets in the Swakop River ~6 km downstream of the Husab Gorge. Photos (a) and (b) used with permission from Dave Waters.

rock strata behind ascending melt-filled hydrofractures, a process that leaves behind only subtle features such as the narrow leucogranite trail and antiformal wake structure preserved in the Husab Gorge. Importantly, the break in wall-rock continuity marked by the wake structure (Figs 6; 7d) lowers locally the wall-rock fracture toughness, creating an anisotropy along which the ascent of subsequent, likely smaller batches of magma is promoted for as long as magma supply to the section continues, possibly for the duration of the tectonometamorphic event. This allows, potentially, for multiple reutilisation of ascent pathways, thus contributing to the focusing of magmas derived from voluminous source regions towards much more focused long-range conduits. Reutilisation of preferred ascent pathways in this manner may also be important given that several hundred- to several thousand batches with volumes of ~2.4×10^5 m^3 would be required to account for the volume and the internal compositional complexity of average-sized sheeted plutons in the upper crust. The preservation of the features described in the outcrops from the Husab Gorge requires also that they form late during tectonism, since the preferential partitioning of strain into magma rich horizons will destroy similar features developed earlier during the evolution of the belt. Thus, the elusive nature of potential granite conduits is twofold; the already subtle evidence is highly likely to be overprinted where their formation predates deformation and single conduits may be able to account for the flux of far greater magma volumes than can be conducted upwards in a single ascent event. Yet, lens-like magma accumulations similar to those along the Husab Gorge have been documented from other high-grade anatectic terrains (e.g. Kisters et al., 1998). Moreover, several subvertical lens-like leucogranite up to ~100 m long and ~25 m wide are exposed in layered metasediments some 20 km northwest of the confluence between the Husab and Swakop Rivers (Figs 8a, b) as well as closer by, in the Swakop River (Fig. 8c), suggesting that these dimensions roughly record the maximum size for stable subvertical leucogranite lenses in the western sCZ of the Damara Belt.

CONCLUSION

Fracture-controlled long-range magma ascent requires the accumulation of magma volumes large enough to initiate buoyancy-driven ascent. This manuscript describes large (10^1-10^2 m long), vertical lens-like leucogranites that record both inflated (incipient; Figs 4, 5) and collapsed (drained; Fig. 6) fracture-controlled sites of former magma accumulation in the mid-crustal wall rocks of the Husab Gorge. Magma accumulation is driven by the formation of subvertical extension fractures that fill with magma and extend along their long-axes during regional extension. Magma extraction is buoyancy driven and occurs when the volume of magma contained in the fractures reaches some critical length/volume which promotes brittle failure of the wall rocks and the formation of self-propagating hydrofractures. We tentatively suggest that the features described here from the Husab Gorge provide a field-based constraint on the minimum critical lengths (>~100 m) and volumes (~2.4×10^5 m^3) required to initiate long-range, buoyancy-driven magma ascent along self-propagating hydrofractures from a natural magma-transport network in this ductile mid-crustal section. The process leaves only subtle and easily overprinted evidence of the original magma accumulation and transport pathways in the rock record, and may explain the dichotomy between recorded magma volumes in granite plutons and the apparent lack of conduits that could have accommodated the transfer of these magma volumes through the crust. Repeated, episodic ascent of relatively small magma volumes from granite sources agrees with the documented incremental growth of granite plutons at shallower crustal levels through the progressive accretion/amalgamation of multiple distinct magma batches.

ACKNOWLEDGEMENTS

We would like to thank Swakop Uranium for support and access to the Husab Gorge during field work. Dave Waters is thanked for granting permission to use photographs of the outcrops along the lower Khan River (Figs 8a, b) from his online collection (accessed November 2015: http://www.earth.ox.ac.uk/~oesis/teaching/Namib15/damara/index.html). Tolene Kruger is thanked for sharing data from the nearby Hollands Dome. Ed Sawyer and Roberto Weinberg are thanked for thorough and insightful reviews, which helped to improve the context and broaden the scope of the manuscript. Mike Brown is thanked for prompt editorial handling of the manuscript.

REFERENCES

Acocella, V. & Rossetti, F., 2002. The role of extensional tectonics at different crustal levels on granite ascent and emplacement: an example from Tuscany (Italy). Tectonophysics, 354(1), 71-83.

Atkinson, B.K. & Meredith, P.G., 1987. Experimental fracture mechanics data for rocks and minerals. In: Atkinson, B.K. (Ed.), Fracture Mechanics of Rock. Academic Press, London, 477–525.

Benn, K., Odonne, F., Lee, S.K.Y. & Darcovich, K., 2000. Analogue scale models of pluton emplacement during transpression in brittle and ductile crust. Transactions of the Royal Society of Edinburgh, Earth Sciences, 91(1-2), 111-121.

Bons, P. D. & van Milligen, B. P., 2001. New experiment to model self-organized critical transport and accumulation of melt and hydrocarbons from their source rocks. Geology, 29(10), 919-922.

Bons, P. D., Dougherty-Page, J. & Elburg, M. A., 2001. Stepwise accumulation and ascent of

magmas. Journal of Metamorphic Geology, 19(5), 627-633.

Bons, P. D., Druguet, E., Castaño, L. M. & Elburg, M. A., 2008. Finding what is now not there anymore: recognizing missing fluid and magma volumes. Geology, 36(11), 851-854.

Bons, P. D., Becker, J. K., Elburg, M. A. & Urtson, K., 2009. Granite formation: Stepwise accumulation of melt or connected networks?. Earth and Environmental Science Transactions of the Royal Society of Edinburgh, 100(1-2), 105-115.

Bons, P. D., Elburg, M. A. & Gomez-Rivas, E. 2012. A review of the formation of tectonic veins and their microstructures. Journal of Structural Geology, 43, 33-62.

Brandt, R., 1987. A revised stratigraphy for the Abbabis Complex in the Abbabis Inlier, Namibia. South African journal of geology, 90(3), 314-323.

Brown, M., 1994. The generation, segregation, ascent and emplacement of granite magma: the migmatite-to-crustally-derived granite connection in thickened orogens. Earth-Science Reviews, 36(1), 83-130.

Brown, M., 2004. The mechanism of melt extraction from lower continental crust of orogens. Geological Society of America Special Papers, 389, 35-48.

Brown, M., 2007. Crustal melting and melt extraction, ascent and emplacement in orogens: mechanisms and consequences. Journal of the Geological Society, 164(4), 709-730.

Brown, M., 2013. Granite: From genesis to emplacement. Geological Society of America Bulletin, 125(7-8), 1079-1113.

Brown, M. & Solar, G. S. 1998a. Granite ascent and emplacement during contractional deformation in convergent orogens. Journal of Structural Geology, 20(9), 1365-1393.

Brown, M. & Solar, G. S., 1998b Shear-zone systems and melts: feedback relations and self-organization in orogenic belts. Journal of Structural Geology, 20(2), 211-227.

Brown, M. & Solar, G. S., 1999. The mechanism of ascent and emplacement of granite magma during transpression: a syntectonic granite paradigm. Tectonophysics, 312(1), 1-33.

Bunger, A.P. & Cruden, A.R., 2011. Modeling the growth of laccoliths and large mafic sills: role of magma body forces. Journal of Geophysical Research: Solid Earth, 116(B2).

Clemens, J. D., 1998. Observations on the origins and ascent mechanisms of granitic magmas. Journal of the Geological Society, 155(5), 843-851.

Clemens, J. D. & Mawer, C. K., 1992. Granitic magma transport by fracture propagation. Tectonophysics, 204(3), 339-360.

Clemens, J.D. & Wall, V.J., 1981. Origin and crystallization of some peraluminous (s-type) granitic magmas. Canadian Mineralogist, 19, 111-131.

Coleman, D. S., Gray, W., & Glazner, A. F., 2004. Rethinking the emplacement and evolution of zoned plutons: Geochronologic evidence for incremental assembly of the Tuolumne Intrusive Suite, California. Geology, 32(5), 433-436.

Collins, W. J. & Sawyer, E. W., 1996. Pervasive granitoid magma transfer through the lower–middle crust during non-coaxial compressional deformation. Journal of Metamorphic Geology, 14(5), 565-579.

Coward, M. P., 1983. The tectonic history of the Damara belt. Evolution of the Damara Orogen. Special Publication of the Geological Society of South Africa, 11, 409-421.

D'lemos, R. S., Brown, M. & Strachan, R. A., 1992. Granite magma generation, ascent and emplacement within a transpressional orogen. Journal of the Geological Society, 149(4), 487-490.

Dahm, T., 2000. On the shape and velocity of fluid-filled fractures in the Earth. Geophysical Journal International, 142(1), 181-192.

Dahm, T., Hainzl, S. & Fischer, T., 2010. Bidirectional and unidirectional fracture growth during hydrofracturing: role of driving stress gradients. Journal of Geophysical Research: Solid Earth (1978–2012), 115(B12).

Davidson, C., Schmid, S. M. & Hollister, L. S., 1994. Role of melt during deformation in the deep crust. Terra Nova, 6(2), 133-142.

De Kock, G.S., Eglington, B., Armstrong, R.A., Harmer, R.E. & Walraven, F., 2000. U-Pb and Pb-Pb ages of the Naauwpoort rhyolite, Kawakeup leptite and Okongava Diorite: implications for the onset of rifting and of orogenesis in the Damara belt, Namibia. Communications of the Geological Survey of Namibia, 12, 81-88.

Demartis, M., Pinotti, L. P., Coniglio, J. E., D'Eramo, F. J., Tubía, J. M., Aragón, E. & Insúa, L. A. A., 2011. Ascent and emplacement of pegmatitic melts in a major reverse shear zone (Sierras de Córdoba, Argentina). Journal of Structural Geology, 33(9), 1334-1346.

Diener, J. F., White, R. W. & Hudson, T. J., 2014. Melt production, redistribution and accumulation in mid-crustal source rocks, with implications for crustal-scale melt transfer. Lithos, 200, 212-225.

Eichhubl, P. & Aydin, A., 2003. Ductile opening-mode fracture by pore growth and coalescence during combustion alteration of siliceous mudstone. Journal of Structural Geology, 25(1), 121-134.

Glazner, A. F., Bartley, J.M., Coleman, D.S. & Gray, W., Taylor, R.Z., 2004. Are plutons assembled over millions of years by amalgamation from small magma chambers? GSA Today, 14, 4-12.

Gray, D.R., Foster, D.A., Goscombe, B., Passchier, C.W. & Trouw, R.A., 2006. 40 Ar/39 Ar thermochronology of the Pan-African Damara Orogen, Namibia, with implications for tectonothermal and geodynamic evolution. Precambrian research, 150(1), 49-72.

Gray, D. R., Foster, D. A., Meert, J. G., Goscombe, B. D., Armstrong, R., Trouw, R. A. J. & Passchier, C. W., 2008. A Damara orogen perspective on the assembly of southwestern Gondwana. Geological Society, London, Special Publications, 294(1), 257-278.

Gudmundsson, A., 2011. Deflection of dykes into sills at discontinuities and magma-chamber formation. Tectonophysics, 500(1), 50-64.

Gudmundsson, A. & Brenner, S. L., 2001. How hydrofractures become arrested. Terra Nova, 13(6), 456-462.

Hall, D. & Kisters, A., 2012. The stabilization of self-organised leucogranite networks—Implications for melt segregation and far-field melt transfer in the continental crust. Earth and Planetary Science Letters, 355, 1-12.

Hall, D. & Kisters, A., 2016. From steep feeders to tabular plutons–Emplacement controls of syntectonic granitoid plutons in the Damara Belt, Namibia. Journal of African Earth Sciences, 113, 51-64.

Heimpel, M. & Olson, P., 1994. Buoyancy-driven fracture and magma transport through the lithosphere: models and experiments. in Ryan, M. (ed), Magmatic Systems, Academic Press, New York, 223-240.

Hogan, J. P., Price, J. D. & Gilbert, M. C., 1998. Magma traps and driving pressure: consequences for pluton shape and emplacement in an extensional regime. Journal of Structural Geology, 20(9), 1155-1168.

Hutton, D. H., 1992. Granite sheeted complexes: evidence for the dyking ascent mechanism. Geological Society of America Special Papers, 272, 377-382.

Ida, Y. & Kumazawa, M., 1986. Ascent of magma in a deformable vent. Journal of Geophysical Research: Solid Earth (1978–2012), 91(B9), 9297-9301.

Jacob, R.E., 1974. Geology and metamorphic petrology of part of the Damara Orogen along the lower Swakop River, South West Africa. Precambrian Res. Unit Bull. 17, 201.

Jacob, R. E., Kröner, A. & Burger, A. J., 1978. Areal extent and first U-Pb age of the pre-Damaran Abbabis Complex in the central Damara belt of South West Africa (Namibia). Geologische Rundschau, 67(2), 706-718.

Jin, Z.H. & Johnson, S.E., 2008. Magma-driven multiple dike propagation and fracture toughness of crustal rocks. Journal of Geophysical Research: Solid Earth, 113(B3).

Jung, S., Masberg, P., Hoffer, E. & Hoernes, S., 1998. Petrology of an intrusion-related high-grade migmatite: implications for partial melting of metasedimentary rocks and leucosome-forming processes. Journal of metamorphic Geology, 16(3), 425-445.

Jung, S., Hoernes, S. & Mezger, K., 2002. Synorogenic melting of mafic lower crust: constraints from geochronology, petrology and Sr, Nd, Pb and O isotope geochemistry of quartz diorites (Damara orogen, Namibia). Contributions to Mineralogy and Petrology, 143(5), 551-566.

Jung, S. & Mezger, K, 2003. Petrology of basement-dominated terranes: I. Regional metamorphic T–t path from U–Pb monazite and Sm–Nd garnet geochronology (Central Damara orogen, Namibia). Chemical Geology, 198(3), 223-247.

Jurewicz, S. R. & Watson, E. B., 1984. Distribution of partial melt in a felsic system: the importance of surface energy. Contributions to Mineralogy and Petrology, 85(1), 25-29.

Kavanagh, J. L., Menand, T. & Sparks, R. S. J., 2006. An experimental investigation of sill formation and propagation in layered elastic media. Earth and Planetary Science Letters, 245(3), 799-813.

Kisters, A. F., Gibson, R. L., Charlesworth, E. G. & Anhaeusser, C. R., 1998. The role of strain localization in the segregation and ascent of anatectic melts, Namaqualand, South Africa. Journal of structural geology, 20(2), 229-242.

Kisters, A.F., Jordaan, L.S. & Neumaier, K., 2004. Thrust-related dome structures in the Karibib district and the origin of orthogonal fabric domains in the south Central Zone of the Pan-African Damara belt, Namibia. Precambrian research, 133(3), 283-303.

Kisters, A. F. M., Ward, R. A., Anthonissen, C. J. & Vietze, M. E., 2009. Melt segregation and far-field melt transfer in the mid-crust. Journal of the Geological Society, 166(5), 905-918.

Kisters, A.F.M., Vietze, M.E. & Buick, I., 2012. Deformation and age of the Stinkbank pluton and implications for the correlation of tectonometamorphic episodes in the Pan-African Damara Belt. South African Journal of Geology, 115(3), .309-326.

Koyi, H., Schmeling, H., Burchardt, S., Talbot, C., Mukherjee, S., Sjöström, H. & Chemia, Z., 2013. Shear zones between rock units with no relative movement. Journal of Structural Geology, 50, 82-90.

Leuthold, J., Müntener, O., Baumgartner, L. P. & Putlitz, B., 2014. Petrological constraints on the recycling of mafic crystal mushes and intrusion of braided sills in the Torres del Paine mafic complex (Patagonia). Journal of Petrology, 55(5), 917-949.

Lister, J. R. & Kerr, R. C., 1991. Fluid-mechanical models of crack propagation and their application to magma transport in dykes. Journal of Geophysical Research: Solid Earth (1978–2012), 96(B6), 10049-10077.

Longridge, L., Gibson, R.L., Kinnaird, J.A. & Armstrong, R.A., 2011. Constraining the timing of deformation in the southwestern Central Zone of the Damara Belt, Namibia.

Geological Society, London, Special Publications, 357(1), 107-135.

Longridge, L., Kinnaird, J. A., Gibson, R. L. & Armstrong, R. A., 2014. Amphibolites of the Central Zone: new SHRIMP U-Pb ages and implications for the evolution of the Damara Orogen, Namibia. South African Journal of Geology, 117(1), 67-86.

Lucas, S. B. & St-Onge, M. R., 1995. Syn-tectonic magmatism and the development of compositional layering, Ungava Orogen (northern Quebec, Canada). Journal of Structural Geology, 17(4), 475-491.

Marchildon, N. & Brown, M., 2003. Spatial distribution of melt-bearing structures in anatectic rocks from Southern Brittany, France: implications for melt transfer at grain- to orogen-scale. Tectonophysics, 364(3), 215-235.

Masberg, H.P., Hoffer, E. & Hoernes, S., 1992. Microfabrics indicating granulite-facies metamorphism in the low-pressure central Damara Orogen, Namibia. Precambrian research, 55(1), 243-257.

McLellan, E. L., 1988. Migmatite structures in the Central Gneiss Complex, Boca de Quadra, Alaska. Journal of Metamorphic Geology, 6(4), 517-542.

Menand, T., 2008. The mechanics and dynamics of sills in layered elastic rocks and their implications for the growth of laccoliths and other igneous complexes. Earth and Planetary Science Letters, 267(1), 93-99.

Menand, T., Annen, C. & de Saint Blanquat, M., 2015. Rates of magma transfer in the crust: Insights into magma reservoir recharge and pluton growth. Geology, 43, 199-202.

Meneghini, F., Kisters, A., Buick, I. & Fagereng, Å., 2014. Fingerprints of late Neoproterozoic ridge subduction in the Pan-African Damara belt, Namibia. Geology, 42(10), 903-906.

Mehnert, K. R., 1968. Migmatites and the origin of granitic rocks (Vol. 1). Elsevier, Amsterdam, 393 pp.

Miller, C. F., Furbish, D. J., Walker, B. A., Claiborne, L. L., Koteas, G. C., Bleick, H. A. & Miller, J. S., 2011. Growth of plutons by incremental emplacement of sheets in crystal-rich host: evidence from Miocene intrusions of the Colorado River region, Nevada, USA. Tectonophysics, 500(1), 65-77.

Miller, R. B. & Paterson, S. R., 2001. Construction of mid-crustal sheeted plutons: Examples from the North Cascades, Washington. Geological Society of America Bulletin, 113(11), 1423-1442.

Miller, R.M., 1983. The Pan-African Damara Orogen of South West Africa/Namibia.In: Miller, R.M. (Ed.), Evolution of the Damara Orogen of South West Africa/Namibia, vol. 11. Geological Society of South Africa Special Publication, Johannesburg,South Africa, pp. 431-515.

Miller, R.M., 2008. The Geology of Namibia volume 2: Neoproterozoic to Lower Paleozoic. Geological Survey of Namibia, Windhoek, Namibia.

Morfin, S., Sawyer, E. W. & Bandyayera, D., 2013. Large volumes of anatectic melt retained in granulite facies migmatites: An injection complex in northern Quebec. Lithos, 168, 200-218.

Nakashima, Y., 1993. Static Stability and Propagation of a Fluid-Filled Edge Crack in Rock: Implication for Fluid Transport in Magmatism and Metamorphism. Journal of Physics of the Earth, 41(3), 189-202.

Neves, S. P., Vauchez, A. & Archanjo, C. J. 1996. Shear zone-controlled magma emplacement or magma-assisted nucleation of shear zones? Insights from northeast Brazil. Tectonophysics, 262(1), 349-364.

Nex, P. A. M., Oliver, G. J. H. & Kinnaird, J. A., 2001. Spinel-bearing assemblages and PT-t

evolution of the Central Zone of the Damara Orogen, Namibia. Journal of African Earth Sciences, 32(3), 471-489.

Nunn, J. A., 1996. Buoyancy-driven propagation of isolated fluid-filled fractures: Implications for fluid transport in Gulf of Mexico geopressured sediments. Journal of Geophysical Research, 101(B2), 2963-2970.

Oliver, G. J., 1994. Mid-crustal detachment and domes in the central zone of the Damaran orogen, Namibia. Journal of African Earth Sciences, 19(4), 331-344.

Olivier, P., Druguet, E., Castaño, L. M. & Gleizes, G., 2015. Granitoid emplacement by multiple sheeting during Variscan dextral transpression: the Saint-Laurent-La Jonquera pluton (Eastern Pyrenees). Journal of Structural Geology.

Ostendorf, J., Jung, S., Berndt-Gerdes, J. & Hauff, F., 2014. Syn-orogenic high-temperature crustal melting: Geochronological and Nd–Sr–Pb isotope constraints from basement-derived granites (Central Damara Orogen, Namibia). Lithos, 192, 21-38.

Petford, N., Kerr, R. C. & Lister, J. R., 1993. Dike transport of granitoid magmas. Geology, 21(9), 845-848.

Poli, L. C. & Oliver, G. J. H., 2001. Constrictional deformation in the Central Zone of the Damara Orogen, Namibia. Journal of African Earth Sciences, 33(2), 303-321.

Puhan, D., 1983. Temperature and pressure of metamorphism in the Central Damara orogen. In: Miller, R.McG. (Ed.), Evolution of the Damara Orogen of South West Africa/Namibia, vol. 11. Geolological Society of South Africa Special Publication, 219-223.

Reichardt, H. & Weinberg, R. F., 2012. The dike swarm of the Karakoram shear zone, Ladakh, NW India: Linking granite source to batholith. Geological Society of America Bulletin, 124(1-2), 89-103.

Rivalta, E. & Dahm, T., 2006. Acceleration of buoyancy-driven fractures and magmatic dikes beneath the free surface. Geophysical Journal International, 166(3), 1424-1439.

Rivalta, E., Taisne, B., Bunger, A. P. & Katz, R. F., 2015. A review of mechanical models of dike propagation: Schools of thought, results and future directions. Tectonophysics, 638, 1-42.

Rocchi, S., Westerman, D. S., Dini, A. & Farina, F., 2010. Intrusive sheets and sheeted intrusions at Elba Island, Italy. Geosphere, 6(3), 225-236.

Roper, S. M. & Lister, J. R., 2007. Buoyancy-driven crack propagation: the limit of large fracture toughness. Journal of Fluid Mechanics, 580, 359-380.

Rosenberg, C. L., 2004. Shear zones and magma ascent: a model based on a review of the Tertiary magmatism in the Alps. Tectonics, 23(3).

Rubin, A. M., 1993. Tensile fracture of rock at high confining pressure: implications for dike propagation. Journal of Geophysical Research: Solid Earth (1978–2012), 98(B9), 15919-15935.

Rubin, A. M., 1995. Propagation of magma-filled cracks. Annual Review of Earth and Planetary Sciences, 23, 287-336.

Rutter, E. H. & Neumann, D. H. K., 1995. Experimental deformation of partially molten Westerly granite under fluid-absent conditions, with implications for the extraction of granitic magmas. Journal of Geophysical Research: Solid Earth (1978–2012), 100(B8), 15697-15715.

Sawyer, E. W., 1991. Disequilibrium melting and the rate of melt–residuum separation during migmatization of mafic rocks from the Grenville Front, Quebec. Journal of Petrology, 32(4), 701-738.

Sawyer, E.W., 1998. Formation and evolution of granite magmas during crustal reworking: the

significance of diatexites. Journal of Petrology, 39(6), 1147-1167.

Sawyer, E.W., 2008. Atlas of Migmatites. The Canadian Mineralogist, Special Publication 9. NRC Research Press, Ottawa, Ontario, Canada. 371 p.

Sawyer, E. W., 2010. Migmatites formed by water-fluxed partial melting of a leucogranodiorite protolith: microstructures in the residual rocks and source of the fluid. Lithos, 116(3), 273-286.

Sawyer, E.W., 2014. The inception and growth of leucosomes: microstructure at the start of melt segregation in migmatites. Journal of Metamorphic Geology, 32(7), 695-712.

Secor, D. T. & Pollard, D. D., 1975. On the stability of open hydraulic fractures in the Earth's crust. Geophysical Research Letters, 2(11), 510-513.

Sederholm, J. J., 1907. On Granite and gneiss: their origin, relations and occurrence in the Pre-Cambrium complex of Fennoscandia. Bulletin, Community of Geology, Finlande, 23.

Sleep, N.H., 1988. Tapping of melt by veins and dykes. Journal of Geophysical Research 93,10255–10272.

Solar, G. S., Pressley, R. A., Brown, M. & Tucker, R. D., 1998. Granite ascent in convergent orogenic belts: testing a model. Geology, 26(8), 711-714.

Stammeier, J., Jung, S., Romer, R. L., Berndt, J. & Garbe-Schönberg, D., 2015. Petrology of ferroan alkali-calcic granites: Synorogenic high-temperature melting of undepleted felsic lower crust (Damara orogen, Namibia). Lithos, 224, 114-125.

Stevenson, D. J., 1982. Migration of fluid-filled cracks: Applications to terrestrial and icy bodies. Lunar Planet. Sci. XIII, 768–769.

Sumita, I. & Ota, Y., 2011. Experiments on buoyancy-driven crack around the brittle–ductile transition. Earth and Planetary Science Letters, 304(3), 337-346.

Taisne, B. & Jaupart, C., 2009. Dike propagation through layered rocks. Journal of Geophysical Research: Solid Earth (1978–2012), 114(B9).

Vigneresse, J. L., 1995. Control of granite emplacement by regional deformation. Tectonophysics, 249(3), 173-186.

Ward, R., Stevens, G. & Kisters, A., 2008. Fluid and deformation induced partial melting and melt volumes in low-temperature granulite-facies metasediments, Damara Belt, Namibia. Lithos, 105(3), 253-271.

Weertman, J., 1971. Theory of water-filled crevasses in glaciers applied to vertical magma transport beneath oceanic ridges. Journal of Geophysical Research, 76(5), 1171-1183.

Weinberg, R.F. & Searle, M.P., 1998. The Pangong Injection Complex, Indian Karakoram: a case of pervasive granite flow through hot viscous crust. Journal of the Geological Society, 155(5), 883-891.

Weinberg, R.F. & Mark, G., 2008. Magma migration, folding, and disaggregation of migmatites in the Karakoram Shear Zone, Ladakh, NW India. Geological Society of America Bulletin, 120(7-8), 994-1009.

Weinberg, R.F. & Regenauer-Lieb, K., 2010. Ductile fractures and magma migration from source. Geology, 38(4), 363-366.

Weinberg, R. F., Sial, A. N. & Mariano, G., 2004. Close spatial relationship between plutons and shear zones. Geology, 32(5), 377-380.

Weinberg, R. F., Mark, G. & Reichardt, H., 2009. Magma ponding in the Karakoram shear zone, Ladakh, NW India. Geological Society of America Bulletin, 121(1-2), 278-285.

Weinberg, R., Hasalova, P., Ward, L. & Fanning, C., 2013. Interaction between deformation and magma extraction in migmatites: Examples from Kangaroo Island, South

Australia. Geological Society of America Bulletin, 125, 1282-1300.

Wiebe, R. A. & Collins, W. J., 1998. Depositional features and stratigraphic sections in granitic plutons: implications for the emplacement and crystallization of granitic magma. Journal of Structural Geology, 20(9), 1273-1289.

Chapter 5: Pluton emplacement levels in the mid-crust

This chapter constitutes a presentation of the published research paper: From steep feeders to tabular plutons – ***Emplacement controls of syntectonic granitoid plutons in the Damara Belt, Namibia***[1] by Hall and Kisters.

This paper was first authored by Duncan Hall with standard supervision entailing academic guidance and editorial support from Alex Kisters. The following aspects were carried out independently by Duncan Hall: (1) field work and data collection during detailed mapping of the Kubas granite, (2) processing and interpretation of the structural data from the Kubas granite to determine the controls on the level of emplacement (3) entirely new interpretations of the controls on the emplacement of the Mon Repos and Stinkbank intrusions based on regional mapping by Chris Anthonissen and Martin Vietze as part of their unpublished Masters degrees (cited in the paper) (4) preparation and submission of the manuscript and (5) manuscript revision and successful resubmission.

[1] Hall, D. & Kisters, A., 2016. ***From steep feeders to tabular plutons–Emplacement controls of syntectonic granitoid plutons in the Damara Belt, Namibia***. *Journal of African Earth Sciences*, 113, 51-64.

Journal of African Earth Sciences 113 (2016) 51–64

Contents lists available at ScienceDirect

Journal of African Earth Sciences

journal homepage: www.elsevier.com/locate/jafrearsci

From steep feeders to tabular plutons – Emplacement controls of syntectonic granitoid plutons in the Damara Belt, Namibia

Duncan Hall*, Alexander Kisters

Department of Earth Sciences, University of Stellenbosch, Private Bag X1, Matieland 7602, South Africa

ARTICLE INFO

Article history:
Received 22 July 2015
Received in revised form
6 October 2015
Accepted 8 October 2015
Available online 22 October 2015

ABSTRACT

Granitoid plutons in the deeply eroded south Central Zone of the Damara Belt in Namibia commonly show tabular geometries and pronounced stratigraphic controls on their emplacement. Subhorizontal, sheet-like pluton geometries record emplacement during regional subhorizontal shortening, but the intrusion of spatially and temporally closely-related granitoid plutons at different structural levels and in distinct structural settings suggests independent controls on their levels of emplacement. We describe and evaluate the controls on the loci of the dyke-to-sill transition that initiated the emplacement of three syntectonic (560–530 Ma) plutons in the basement-cover stratigraphy of the Erongo region. Intrusive relationships highlight the significance of (1) rigidity anisotropies associated with competent sedimentary packages or pre-existing subhorizontal granite sheets and (2) rheological anisotropies associated with the presence of thick ductile marble horizons. These mechanical anisotropies may lead to the initial deflection of steep feeder conduits as well as subsequent pluton assembly by the repeated underaccretion of later magma batches. The upward displacement of regional isotherms due to the heat advection associated with granite emplacement is likely to have a profound effect on the mechanical stratification of the upper crust and, consequently, on the level at which granitoid pluton emplacement is initiated. In this way, pluton emplacement at progressively shallower crustal depths may have resulted in the unusually high apparent geothermal gradients recorded in the upper crustal levels of the Damara Belt during its later evolution.

1. Introduction

Granitoid plutons (granites sensu lato) are increasingly being recognized as subhorizontal, tabular bodies with high length: thickness ratios (e.g. Benn et al., 1999; Vigneresse et al., 1999; Westraat et al., 2005; Burchardt et al., 2010) formed through the under- or overaccretion of multiple intrusive sheets (e.g. Blenkinsop and Treloar, 2001; Coleman et al., 2004; Westraat et al., 2005; de Saint-Blanquat et al., 2006; Morgan et al., 2008; Farina et al., 2010; Miller et al., 2011; Leuthold et al., 2012; Saumur and Cruden, 2015). In contrast, the ascent of magma from lower-crustal sources to mid-to upper-crustal sinks must take place along conduits steep enough to allow buoyancy-driven magma ascent to occur sufficiently rapidly to prevent the freezing of magma within the subsolidus sections of crust along the ascent path (Clemens and Mawer, 1992; Hutton, 1992; Brown, 1994; Vigneresse and Clemens, 2000; Kisters et al., 2009; Diener et al., 2014; Menand et al., 2015). Conduits suitable for successful far-field ascent are now widely believed to be fracture-controlled and probably take the form of rooted dykes/dyke networks or self-driven magma-filled (hydro) fractures that have separated from the zones of partial melting (Lister and Kerr, 1991; Hutton, 1992; Petford et al., 1993; Rubin, 1995; Bons et al., 2001, 2009). Both dykes and hydrofractures are commonly extension fractures that open against the least compressive stress (σ_3 with $\sigma_1 \geq \sigma_2 \geq \sigma_3$; Anderson, 1951). Deviations from this general rule allow fracture-controlled magma ascent to take place at high angles to σ_1 in the mid-crust of convergent orogens where the temperature-dependent plasticity of most rock-forming minerals means that differential stresses are low ($\sigma_1 - \sigma_3 \leq 20$ MPa; Davidson et al., 1994; Behr and Platt, 2011). In such cases, anisotropies such as bedding or foliation planes can promote fracture propagation at high angles to the commonly subhorizontal tectonic compression (e.g. Lucas and St-Onge, 1995; Brown and Solar, 1998; Kisters et al., 2009).

Pluton emplacement is initiated with the deflection from steep

* Corresponding author.
E-mail address: duncanh11@gmail.com (D. Hall).

http://dx.doi.org/10.1016/j.jafrearsci.2015.10.005
1464-343X/

ascent conduit to subhorizontal sheet that is commonly referred to as the dyke-to-sill transition. Analogue and numerical modelling commonly relate this process to mechanical anisotropies that are commonly associated with changes in wall-rock lithologies along the ascent path of the magmas (e.g., Kavanagh et al., 2006; Gudmundsson, 2011; Menand, 2011; Taisne et al., 2011). For example, wall-rock mechanical anisotropies such as marked rigidity or rheological contrasts initiate emplacement by affecting the stresses ahead of the fracture-tips due to local stress variations that result from the interaction of regional stress fields with the presence and orientation of the lithological layering (Gudmundsson and Brenner, 2001). Emplacement continues by lateral propagation along the arresting interface provided the conduit internal pressure exceeds the interface strength (Kavanagh et al., 2006; Kavanagh and Pavier, 2014). Vertical growth pluton is accomplished by the repeated under- or overaccretion of later magmatic phases (e.g. Leuthold et al., 2012). Together, the initial stages of conduit arrest and interface-parallel growth probably account for the stratigraphic and/or lithological control on tabular pluton emplacement suggested by the models (see comprehensive review in Menand, 2011), but these controls have not commonly been described for pluton emplacement in the field.

The Central Zone of the Pan-African (ca. 550–500 Ma) Damara Belt in Namibia preserves a layered succession within which granite emplacement is largely stratigraphically controlled (Jacob, 1974; Miller, 2008). Previously, the physical aspects of the emplacement of the multitude of syn-to late-tectonic granitoid plutons that intrude the Central Zone were neglected and the granites were depicted on regional sections as steep-sided balloon- or tear-drop shaped intrusions (e.g., Lehtonen et al., 1995). More recent studies have emphasized tabular- (e.g. Ameglio et al., 2000; Kisters et al., 2012) or lopolithic geometries (Miller, 2008). Geophysical and/or field evidence suggest the plutons to be associated with and underlain by steeply inclined sheets/sheeted complexes that may represent feeder zones of the plutons (Ameglio et al., 2000; Kisters et al., 2009, 2012). Internal compositional heterogeneities in Damaran granitoids have traditionally been interpreted as the results of assimilation and fractionation both within-source and at the level of emplacement (e.g. Jacob, 1974; Miller, 1983, 2008; Stammeier et al., 2015), but recent field and geochronological evidence have also highlighted pluton assembly through the addition of multiple compositionally distinct magma batches, commonly in the form of subhorizontal sheets (e.g. Johnson et al., 2006; Kisters et al., 2012).

In this field-based case study, we examine three spatially and temporally closely associated tabular granitoid plutons from the south Central Zone of the Damara Belt (Fig. 1). The petrological and geochronological aspects of the plutons have previously been described, but, like most plutons in the Damara Belt, the physical controls on pluton emplacement have been neglected. The three plutons are preserved at different stratigraphic levels – from within the basement to within the uppermost formation of the covering metasediments – and display concordant to highly discordant intrusive relationships with their wall rocks, suggesting distinct controls on the level of the dyke-to-sill transition in each case. Unlike most studies of the controls on the level emplacement, many of which are based on models or field data from shallow-crustal (e.g. Leuthold et al., 2012) or subvolcanic environments (e.g. Burchardt et al., 2010), the uniquely exposed plutons provide an opportunity to describe the physical controls on the level of pluton emplacement in the mid-crust. We aim to do this by means of presenting new and established data on the pluton geometries and intrusive relationships and by, within the framework of existing theoretical and analogue models of pluton emplacement, characterizing the controls that determined the location of the dyke–sill transition at each emplacement level.

2. Geology of the Erongo region

The NE-trending Damara Belt formed in response to the subduction of the Kalahari below the Congo Craton between ca. 580 and 520 Ma (Meneghini et al., 2014; Fig. 1B). Several tectonostratigraphic zones delineate the belt (Fig. 1C; Miller, 2008), with the former magmatic arc being represented by the Central Zone, which is in turn divided into a north- and south Central Zone (sCZ; Fig. 1C). The sCZ exposes deeply eroded sections of this magmatic arc and is comprised of Paleoproterozoic (2.0–1.8 Ga) basement gneisses and an unconformably overlying, lithologically heterogeneous Neoproterozoic (ca. 750–600 Ma) cover sequence known as the Damara Supergroup (DSG). Upper amphibolite-to lower granulite facies regional peak metamorphism (P 4–5 kbar T > 650 °C) is recorded between 530 and 520 Ma in the higher grade western parts of the sCZ (Jung and Mezger, 2003), where both basement and cover rocks are intruded by a multitude of syn-to late- and post-tectonic granites as well as in-situ and near-source migmatite networks (e.g. Miller, 2008; Ward et al., 2008; Kisters et al., 2009). Further east, in the lower grade central parts of the sCZ, intrusive activity is defined by the emplacement of numerous Pan-African granite plutons largely into the DSG (Miller, 2008).

Structural and intrusive relationships between several plutons and their wall rocks are particularly well exposed in the semi-arid Erongo region between the towns of Karibib, Usakos and Otjimbingwe, situated ~200 km west of the Namibia's capitol, Windhoek (Fig. 1A). In this area, the basement rocks, which are throughout the Damara Belt collectively referred to as the Abbabis Metamorphic Complex (AMC), are preserved in a central NE-trending basement uplift known as the Abbabis High (Fig. 1A), which is comprised of undifferentiated quartzofeldspathic augen- and banded gneisses and subordinate supracrustal rocks (Brandt, 1985). Fabrics in the AMC are commonly considered to record a pre-Damaran, probably Paleoproterozoic fabric-forming event that has not been overprinted by pervasive Pan-African strains (Brandt, 1987; Kisters et al., 2004; Longridge et al., 2011, 2014). This interpretation is consistent with the distinctly discordant fabric relationships between the AMC and DSG as well as the generally well-preserved basement-cover unconformity (Miller, 2008). Around much of its perimeter, the Abbabis High is unconformably overlain by the locally >2000 m thick, folded DSG. In the Erongo region the lower DSG is dominated by the basal, rift-type coarse-clastic Etusis Formation, the overlying glaciomarine Chuos Formation and a mixed schist-marble sequence dominated by the thick (300–800 m) marble units of the Karibib Formation. Locally and regionally, the upper DSG is dominated by the >1000 m thick metaturbiditic succession of the Kuiseb Formation. The northern and northwestern contact of the Abbabis High against the DSG is tectonic in nature and is marked by the Mon Repos Thrust Zone (Fig. 1A; Kisters et al., 2004). For most of its strike extent, thrusting is localized within marble units of the Karibib Formation and records a top-to-the-NW throw of both basement rocks and the lower parts of the DSG onto rocks of the upper DSG (Kisters et al., 2004).

Pan-African deformation in the sCZ records a prolonged period of NW-SE directed subhorizontal shortening between ca. 560 and 520 Ma related to the high-angle convergence between the Kalahari and Congo Cratons (Oliver, 1994; Poli and Oliver, 2001; Longridge et al., 2011; Kisters et al., 2012). Related fabrics and structures in the DSG describe a progression from early, low-angle fabrics, thrusts and associated recumbent folds to later, NE-trending, upright to NW-verging folds and thrusts (D3 after Miller, 1983). First-order F3 folds are the most prominent regional-scale structural feature of the sCZ (Fig. 1A). The commonly doubly

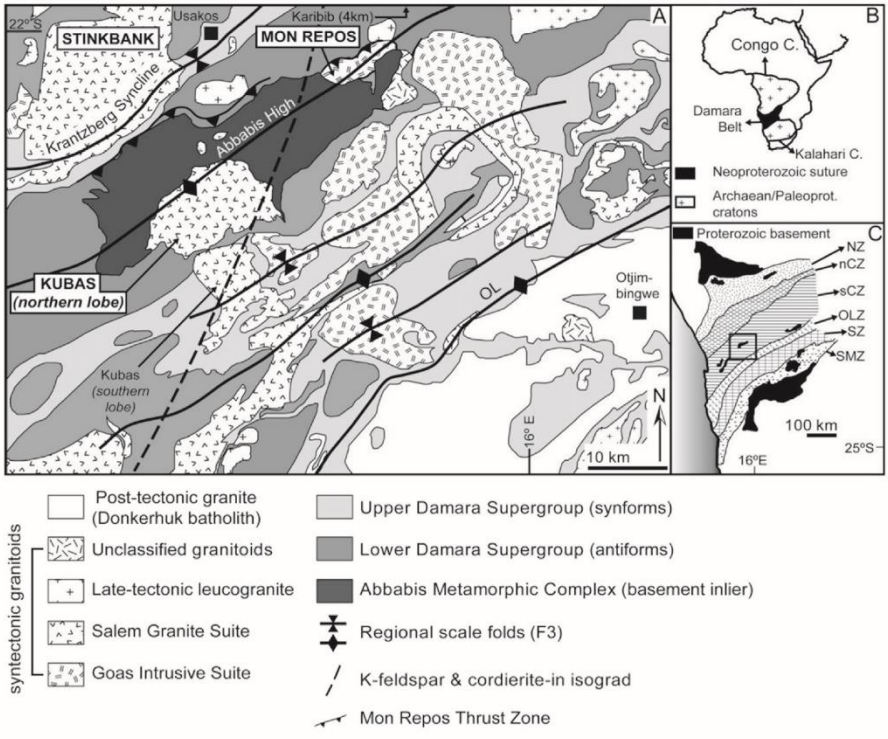

Fig. 1. (A) Simplified geological map of granitoid plutons in the Erongo region. The plutons that form this case study (Mon Repos, Stinkbank and Kubas; highlighted) were emplaced during NW-SE directed convergence between the Congo and Kalahari Cratons. Modified after Miller (2008); cordierite-in isograd after Hartmann et al. (1983). (B) Position of the Neoproterozoic Damara Belt between the Congo and Kalahari Cratons. Modified after Kisters et al. (2009). (C) The location of the Erongo region within the south Central Zone (sCZ) of the Damara Belt is indicated by the dark rectangle. NZ = Northern Zone; nCZ = north Central Zone; OLZ = Okahandja Lineament Zone, SZ = Southern Zone, SMZ = Southern Marginal Zone. Modified after Miller (2008).

plunging folds show wavelengths of up to >10 km and individual folds can be traced for >50 km along their axial planes. F3 folds are associated with near-upright foliations (S3) and shallowly plunging, NE-trending lineations (L3). Many of the commonly sheet-like granitoids in the DSG are folded parallel to F3 and contain magmatic and solid-state fabrics parallel to the NE-trending S3 foliation (Jacob, 1974; Miller, 1983, 2008; Johnson et al., 2006; Kisters et al., 2012), underlining the syn-tectonic emplacement of the granites during regional shortening and convergence. Despite this deformation intrusive contact relationships are mostly well preserved. Local P–T conditions in the Erongo region of 3 ± 1 kbar and ~555–645 °C (Puhan, 1983; Dziggel et al., 2009) are consistent with the results of isotope fractionation and garnet growth zoning at the nearby Navachab gold mine (Dziggel et al., 2009; Wulff et al., 2010). Thus, syntectonic granite emplacement in the Erongo region into relatively hot mid- and upper crustal amphibolite facies rocks during the late stages of D2/3 (530–520 Ma; Steven, 1993; Wulff et al., 2010) may account for the lack of contact metamorphic effects in the region. The lack of contact metamorphism also underlines a relatively low magma flux during emplacement and highlights the fact that the increments of assembly of the plutons were likely to have been relatively small (Annen et al., 2015).

3. Granitoid plutons

The three plutons discussed here, namely the Mon Repos diorite, the Stinkbank granite and the Kubas granite all show round-to oval-shaped outcrop patterns that underlie areas ranging from ~40 km^2 for the Mon Repos diorite to >600 km^2 for the Stinkbank granite (Fig. 1A). Field evidence suggests thicknesses of no more than a few hundred metres for the Mon Repos and Stinkbank plutons, very crudely constraining the intrusive volumes of the intrusions as ~6 and ~90 km^3 respectively. In the case of the 150 km^2 northern lobe of the Kubas granite (see below), whose lower contacts are not exposed, a minimum intrusive volume of ~60 km^3 is indicated by the up to 400 m thickness as exposed.

The geometries and wall-rock relationships of the upper parts of all three plutons can be easily constrained based on the available outcrop. Existing age data and deformation document emplacement of the plutons early during regional D2/3 shortening between ca. 560 and 530 Ma (e.g. De Kock et al., 2000; Johnson et al., 2006; Miller, 2008; Ostendorf et al., 2014), largely prior to the local peak of metamorphism. Petrogenesis of the Kubas granite and Goas Intrusive Suite, of which the Mon Repos diorite is a member, involved high temperature (T > 900 °C) partial melting and assimilation of the heterogeneous lower crust (8–10 kbar; >30–35 km; e.g. Jung et al., 2002; Ostendorf et al., 2014), placing the level of partial melting ~15–20 km below the emplacement level of the plutons.

The three plutons intrude at markedly different stratigraphic levels in the sCZ, suggesting different controls on the dyke–sill transition in each case. In the following, we provide a brief characterization of the geometry, stratigraphic position and intrusive relationships for each pluton. Detailed accounts of their geochronology, petrology and geochemistry can be found in, amongst others, Brandt (1985), Lehtonen et al. (1995), Jacob et al. (2000), Johnson et al. (2006), Kisters et al. (2012) and Ostendorf et al.

(2014) and the comprehensive summary of Damaran granitoids by Miller (2008).

3.1. The Mon Repos diorite

The Mon Repos diorite is a member of the Goas Intrusive Suite, a calc-alkaline series of gabbroic to granodioritic and tonalitic rocks that form a cluster of round-to oval shaped plutons mainly south of the Abbabis High (Figs. 1 and 2). Rocks of the Goas suite intruded the Damara Belt during the early stages of crustal convergence between ca. 580 and 545 Ma (Lehtonen et al., 1995; De Kock et al., 2000; Jung et al., 2002; Jacob et al., 2000; Milani et al., 2014). Existing U–Pb zircon ages of 563 ± 4 Ma and 558 ± 8–546 ± 6 Ma (Jacob et al., 2000; Milani et al., 2014) for the Mon Repos indicate a protracted multi-phase assembly. Despite this, internal intrusive relationships between individual phases are not evident and the pluton displays only a gradual compositional zonation from diorite along its margins to granodiorite and monzonite in its centre (Ameglio et al., 2000). Notwithstanding the early timing, the Mon Repos diorite contains only a weakly developed NE-trending, steep SE-dipping S3-parallel solid-state foliation defined by the preferred orientation of biotite and/or hornblende. A weak margin-parallel magmatic foliation is locally developed (Fig. 2A) and a steeply plunging magnetic lineation has been identified by AMS analysis in the southwestern parts of the pluton (Ameglio et al., 2000).

The Mon Repos diorite is preserved as a ~40 km^2 NE-trending reniform feature overlying the AMC, south of the Mon Repos Thrust Zone (Fig. 2B, D). In this area the basal clastic sequences of the DSG are not developed and bright white recrystallized marbles of the Karibib Formation overlie gneisses of the AMC. The diorites intrude along and parallel to the subhorizontal contact between basement gneisses that form the floor and the marbles of the Karibib Formation that form the roof of the pluton. The sharp roof contact between the diorite and Karibib marbles is exposed for ~ 5 km along a prominent ridge that traces the southern and southwestern perimeter of the pluton (Fig. 2B). This contact describes a gently undulating shallow (<5°) SW-dipping surface. Notably, the unconformity between basement gneisses and Karibib Formation marbles does not appear to have been affected by the regional-scale folding (Fig. 2B) and represents a planar, subhorizontal surface. For the most part, Karibib Formation marbles are pervasively recrystallized, but where bedding is preserved along the southern margin of the subhorizontal diorite sheet the intrusive rocks can be seen to cross-cut the steep primary layering at high angles (Fig. 2A–B). Intrusion/wall-rock relationships along the northern and northwestern margin of the pluton are obscured by the localization of thrusting into the marbles. The floor of the Mon Repos diorite is exposed in places in erosional windows through the diorites. In all of these exposures, the diorites are highly discordant to the subvertical, N-trending basement

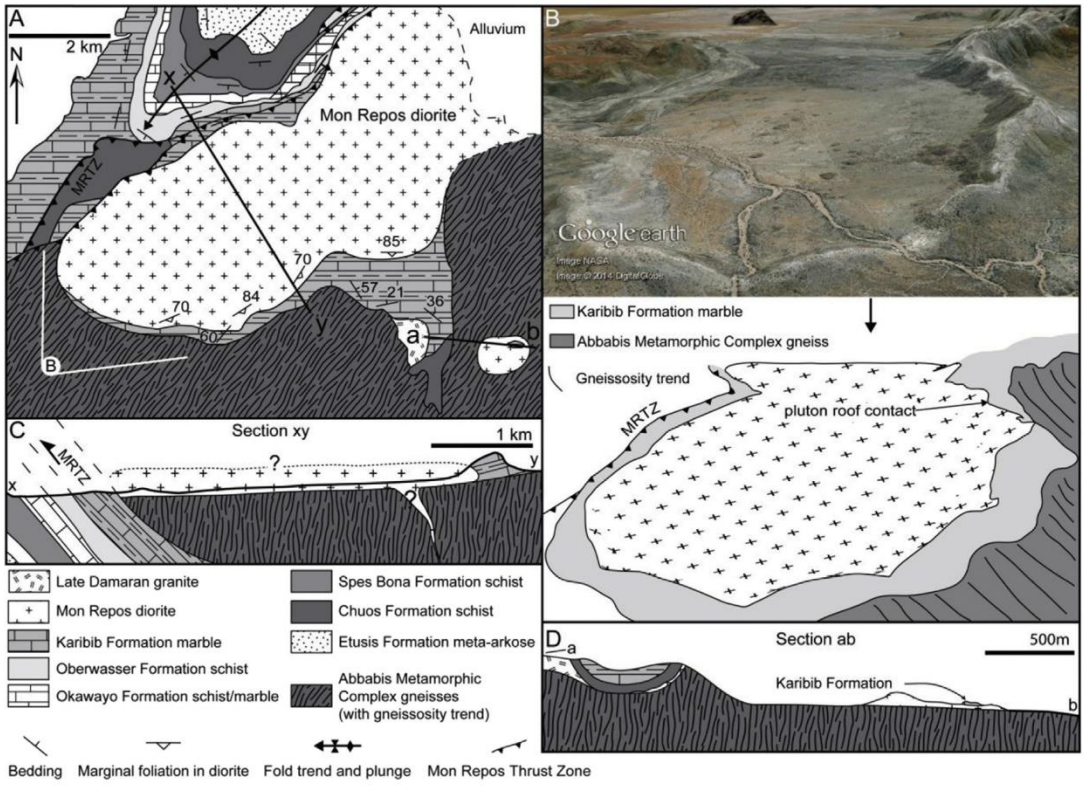

Fig. 2. (A) Simplified geological map of the Mon Repos diorite showing the position of the 40 km^2 pluton along the local basement-cover interface northeast of the Abbabis High and south of the Mon Repos Thrust Zone (MRTZ). Partly adapted from Kisters et al. (2004) and Anthonissen (2009). (B) Oblique 3D view and schematic map looking towards the northeast over the Mon Repos diorite, showing the preservation of the basement-cover interface and the pluton roof contact around the southern and southwestern perimeter of the pluton (Image data: Google, DigitalGlobe, NASA). This view emphasizes the sheet-like geometry as well as the restriction of the pluton to the basement-cover contact. Field of view indicated by spot and line symbol in (A); terrain is depicted with vertical exaggeration of 1.5×. (C) Schematic section to highlight the relationships between the diorites and their wall rocks along the southwestern perimeter of the pluton. The roof geometry and location of the feeder are speculative. Vertical exaggeration is 1.5×. (D) An outlier of the Mon Repos illustrates the very thin (~60 m in this locality) nature of parts of the pluton. Vertical exaggeration is 1.5×; modified after Anthonissen (2009).

gneissosity and indicate a flat-lying, sheet-like geometry that is no more than 100–150 m thick. A complete cross section through the diorites, overlain by Karibib Formation marble and underlain basement gneisses, is exposed in an isolated inselberg in the eastern parts of the pluton. Here, the thickness is only ca. 60 m (Fig. 2D; Anthonissen, 2009). In summary, field relationships around the margins of the Mon Repos diorite document a very thin (maximum preserved thickness ~150 m), laterally extensive (~9 by 4 km) subhorizontal sheet-like geometry that is confined to the unconformable basement-cover contact, but has sharply discordant contacts against both the gneissosity of the underlying basement and the bedding of the marble units in the roof.

There are no obvious feeders within or around the Mon Repos diorite. Longridge et al. (2014) identified ca. 550–560 Ma amphibolite dykes in the AMC that they related to possible feeders of the Goas Suite, but without any direct contacts with the mafic-to intermediate plutons. The steep magnetic lineation identified through the AMS study by Ameglio et al. (2000) is tentatively interpreted to indicate the position of a steep feeder zone underlying the southwestern parts of the diorite sheet (Fig. 2C).

3.2. The Stinkbank granites

The Stinkbank pluton is located north of the Abbabis High (Figs. 1 and 3) where it forms a ~600 km^2, compositionally and texturally heterogeneous sheet-like granite body. The granites are emplaced into biotite-cordierite schists of the lower Kuiseb Formation that are preserved in the core of the regional-scale (F3) Krantzberg syncline (Fig. 3C; Jacob, 1974; Marlow, 1983; Johnson et al., 2006; Vietze, 2009; Kisters et al., 2012), a typical emplacement level for the 550–540 Ma Salem granite suite (Smith, 1965; Jacob, 1974; Miller, 1983). Folding (F3) of the sheet-like granites and associated magmatic and solid-state fabrics (S3, L3) underline the syntectonic emplacement of the Stinkbank granites during D3 shortening (Figs. 3B and 4D–E).

The well exposed southwestern parts of the Stinkbank pluton reveal the internal structure and wall-rock contact relationships of the pluton. Here, the pluton consists of three vertically stacked granite sheets. The roof zone is made up of K-feldspar megacrystic biotite granites which are underlain by a volumetrically subordinate megacrystic leucogranite. Fine-to medium-grained, garnet- and tourmaline-bearing leucogranites form the lowermost phase (Fig. 3A–B; Kisters et al., 2012). The megacrystic varieties belong to the Salem Granite Suite, whereas the leucogranites form part of a later suite of S-type granites that intruded the Damara Belt between 540 and 520 Ma (Marlow, 1983; Miller, 2008; Vietze, 2009). Recent U–Pb zircon and monazite geochronology confirm this arrangement by showing an up to 20 Ma age gap between the older Salem granites (549 ± 10 Ma, 547.5 ± 4.7 Ma) and the younger leucogranites (529 ± 4 Ma) in the Stinkbank pluton (Johnson et al., 2006; Kisters et al., 2012).

On a regional scale, the uppermost megacrystic biotite granite forms a subconcordant sheet within the lower Kuiseb Formation. The actual roof contacts against the Kuiseb Formation are only locally exposed, but the proximity of the roof against the biotite granite is indicated by an abundance of cm-to decimetre-sized wall-rock xenoliths (Fig. 4C). The xenoliths populations include calc-silicate felses and metapsammites in addition to the dominant biotite-cordierite schists of the Kuiseb Formation. For the most part, xenoliths are elongated defining well developed NE-trends, parallel

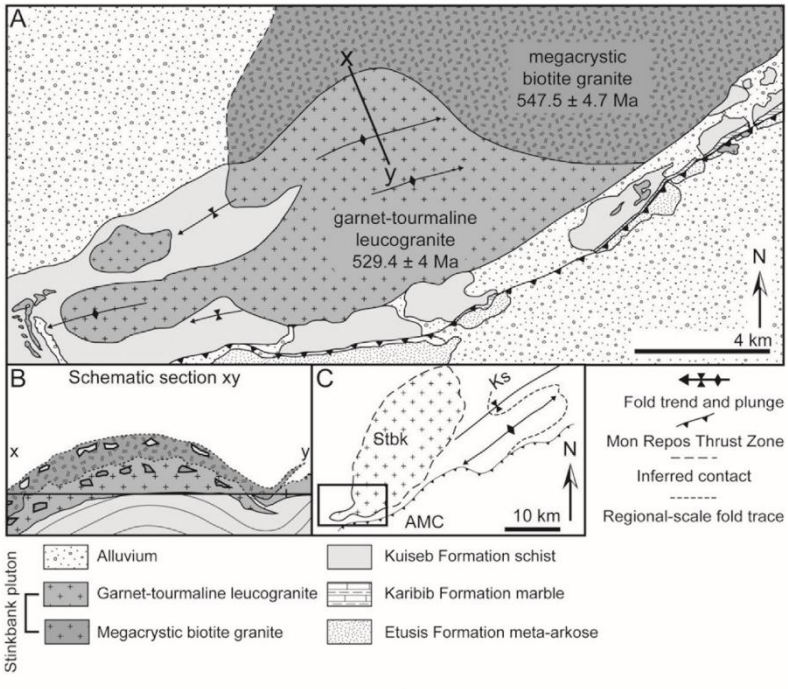

Fig. 3. (A) Simplified geological map of the Stinkbank granite. The majority of the 600 km^2 pluton is hosted within the lower Kuiseb Formation, but is only poorly exposed (dashed contact in lower inset). A well-exposed corridor in the southwest (rectangle in inset) clearly preserves internal contact relationships that show the Stinkbank pluton to be comprised of a biotite granite phase stacked over two later leucogranite phases (only one shown at map scale). (B) Schematic section to highlight the large-scale sheeting in the southwestern parts of the Stinkbank granite. Note the presence of fragments of the overlying rocks near the roof of each of the sheets (see text, Fig. 4A–B). The top-down intrusion sequence suggested by these intrusive relationships is supported by existing geochronological data (see text). (C) Regional position of the Stinkbank pluton along the Krantzberg Syncline (Ks). AMC = Abbabis Metamorphic Complex; Stbk = Stinkbank pluton. Maps and sections modified after Kisters et al. (2012) and Vietze (2009).

Fig. 4. Stinkbank granite photo panel showing (A) a sharp intrusive contact between the Salem biotite granite phase and a later underlying sheet-like leucogranite phase that illustrates the development of elongate, contact-parallel biotite granite xenoliths along the intrusive contact. The leucogranites are internally sheeted and show sharp, margin parallel internal contacts between texturally distinct granites. (B) Intrusive breccia beneath the contact between overlying biotite granite and underlying leucogranite. Several, in this case, widely-spaced xenoliths of biotite granite suspended in leucogranite define what we refer to here as the intrusive breccia. (C) Elongate xenoliths of the Kuiseb Formation (arrows) in the upper biotite granite phase of the Stinkbank pluton. The xenoliths are developed parallel to S3. Pen circled for scale. (D) Decimetre-scale folded leucogranite sheets (contacts marked) near the contact of the Stinkbank granite with Kuiseb Formation. The granite sheet beneath the lower dashed line is ~50 cm thick. (E) Decimetre-scale sheeting (contacts marked) in biotite granite of the Stinkbank pluton. (F) Small-scale internal leucogranite sheets truncate one another at low angles (arrows). Dashed line highlights prominently cross-cutting sheet. Pen circled for scale. (G) Bedding-parallel sheet swarm that compositionally resembles the main tourmaline-bearing leucogranite phase of the Stinkbank pluton. Sheet thickness varies from ~decimetre-to m-scale. (H) 3D exposure of the chocolate tablet boudinage of syntectonic tourmaline-bearing leucogranite sheets interpreted to be a feeder network exposed SW of the Stinkbank granite.

to the regional S3 fabric and axial planar to F3 folds. Contacts may also be discordant on a more local scale and the granite can be seen to truncate folded Kuiseb Formation rocks along sharp, sub-horizontal contacts (Johnson et al., 2006). The thickness of the upper megacrystic granite sheet does not exceed 100 m and the granite sheet thins towards the SW of the pluton where it pinches out completely. The megacrystic biotite granite is intruded and underlain by a megacrystic leucogranite (not shown at the scale of

Fig. 3). This lower phase has a maximum thickness of up to 10 m and shows a somewhat patchy and discontinuous development at the base of the overlying megacrystic biotite granite. The megacrystic leucogranite is, in turn, intruded along its lower contact by fine-grained leucogranites and, where the former is not developed, the fine grained leucogranites are in direct contact with the megacrystic biotite granite. In places, the leucogranites can be seen to be made up of compositionally and texturally distinct sheets (Fig. 4A, F). Granite sheeting is best developed along the margins of the main leucogranite phase where individual outcrops may preserve up to 20 vertically stacked, texturally and compositionally distinct sheets (Fig. 4D–E). The gently dipping, openly folded sheets are from 10 to 200 cm thick and can be followed laterally beyond individual outcrops for distances >50–100 m. Compositional variations define smaller-scale (cm-to decimetre-scale) granite sheeting within large granite sheets (Fig. 4F) that show distinct, and in places, truncating contacts between compositionally distinct sheets. This small-scale sheeting is preserved particularly well in the leucogranites demonstrates that even individual phases are made up of smaller internal sheets (Fig. 4F). Intrusive timing and relationships between the main phases are indicated by 3–10 m thick, contact parallel horizons characterized by the presence of large (up to m-scale) fragments of the overlying phase that are suspended in the underlying phase (Figs. 4A–B, 3B), which we refer to as intrusive breccias. The breccias contain angular fragments of the overlying granite phase that document the growth of the Stinkbank pluton by the underaccretion of successively younger granite sheets to the base of earlier emplaced, probably largely solidified sheets.

Within ~300–500 m of the main leucogranite body in the southwestern parts of the Stinkbank pluton, the Kuiseb Formation wall rocks are intruded by a multitude of subvertical tourmaline-bearing leucogranite sheets (Fig. 4G–H; Vietze, 2009; Kisters et al., 2012) that compositionally resemble the lowermost leucogranites of the Stinkbank pluton. The sheets range in thickness between 0.1 and 10 m and are, for the most part, parallel to the subvertical bedding of the tightly folded wall-rock sequence. Wider examples are internally sheeted and can be followed for >2 km along strike. Many of these NE-trending, bedding-parallel sheets have experienced chocolate tablet boudinage indicating their emplacement during D2/3 shortening and at high-angles to the regional shortening strain. These sheets can be seen, in places, to connect with the compositionally similar lowermost Stinkbank leucogranites that were emplaced during the later stages of folding and regional deformation and may thus represent granite feeders. However, potential feeders to the earlier megacrystic Salem-type phases could not be identified.

3.3. The Kubas granite

The Salem-type Kubas granite consists of two roughly equally sized lobes separated by a prominent NE-striking ridge that together cover an area of ~300 km^2 (Figs. 1 and 5). The southern lobe intrudes the lower parts of the Kuiseb Formation in the core of a regional-scale, NE-trending synform (F3) to the south of the Abbabis High (Figs. 1 and 5; Jacob, 1974; Brandt, 1985; Miller, 2008; Ostendorf et al., 2014). Here it forms a subconcordant sheet in the gently folded metaturbidites of the Kuiseb Formation and occupies a characteristic position for Salem granites in the sCZ (Jacob, 1974; Miller, 1983, 2008). We focus on the better exposed northern lobe of the Kubas granite that is, for the most part, discordantly intrusive into basement gneisses of the Abbabis High and thus occupies a structural position that is highly unusual in a region within which most other plutons are emplaced into the covering Damara Supergoup.

The Kubas (Figs. 1 and 5) has been labelled as an anomalously undeformed member of the Salem Granite Suite. Unlike most other Salem granites the Kubas is largely devoid of macroscopic fabrics, leading previous workers to suggest a late-to post-tectonic emplacement (Brandt, 1985; Miller, 2008). However, recent U–Pb zircon crystallization ages of 553.3 ± 8.4 Ma (Ostendorf et al., 2014) demonstrate a syntectonic (D2/3) emplacement of the main body of the granite as well as the presence of a much younger phase of ca. 510 Ma (Ostendorf et al., 2014). These ages indicate the Kubas granite is broadly contemporaneous with most other Salem granites and that pluton assembly was protracted, similar to the macroscopically composite Stinkbank granite. However, the main phase of the Kubas granite lacks the obvious textural and compositional heterogeneity of the other Stinkbank granites and is made up of compositionally and texturally homogeneous medium-grained, porphyritic biotite granite. Swarms and trains of granitic and dioritic to gabbroic magmatic enclaves are commonly developed and represent the only macroscopic evidence of heterogeneity in the Kubas (Fig. 6). Sporadically developed sharp intrusive contacts between texturally distinct enclave-rich and enclave-poor granite phases further support indicate the presence distinct intrusive phases in the otherwise homogeneous pluton (Fig. 6).

The granites of the northern lobe show highly discordant wall-rock relationships that crosscut gneisses of the AMC, the basement-cover contact as well as the rocks of the moderate-to steeply (50–70°) SE-dipping lower Damara Supergoup at high angles (Figs. 5 and 7A–E). Intrusive relationships between the pluton roof and overlying DSG are exposed for ~10 km along the strike of the ridge that divides the Kubas granite into its northern and southern lobes (Fig. 7A, C, E). Along this transect, the roof contact defines a shallow (<20°), SE-dipping surface overall, with only gentle vertical undulations of ≤120 m along its 10 km length. In detail the roof surface describes a far more irregular, staircase-like geometry in which concordant, moderately SE-dipping bedding-parallel sections alternate with sharply discordant NW-dipping sections (Figs. 5A and 7A, C, E). Discordant contacts are most common against basement gneisses and the massively bedded quartzites and meta-arkoses of the Etusis Formation (Fig. 7A–E), whereas concordant contacts are more prominent against strongly foliated, quartz-biotite schists and marble units (Fig. 7F). Both concordant and discordant contacts along the roof are knife sharp (Fig. 7) and suggest a fracture-controlled emplacement of the granites against the roof rocks. The southwestern sidewall contacts are sharp and highly discordant, showing steep outward dips of 60–80° where directly exposed (Fig. 5). The shallowly-dipping, gently undulating roof contact and steep sidewall contacts describe a piston-like geometry for the northern lobe of the Kubas granite. The floor of the pluton is not exposed, despite vertical exposure of up to 400 m of the upper parts of the Kubas granite. As a result, the floor geometry and any potential feeders remain concealed.

4. Discussion

4.1. Controls on the dyke–sill transition

Horizontal shortening promotes lateral sheet propagation (Anderson, 1951) and the tabular geometries of the Mon Repos, Stinkbank and Kubas plutons are thus broadly consistent with granite emplacement during crustal convergence and regional shortening (Menand et al., 2010). However, this condition does not promote buoyancy-driven, fracture-controlled ascent unless suitably orientated anisotropies exist (lithological contacts, bedding planes, foliations) and differential stresses are low. More specifically, ascent along anisotropies occurs where the differential stress is smaller than difference between the tensile strength of the wall

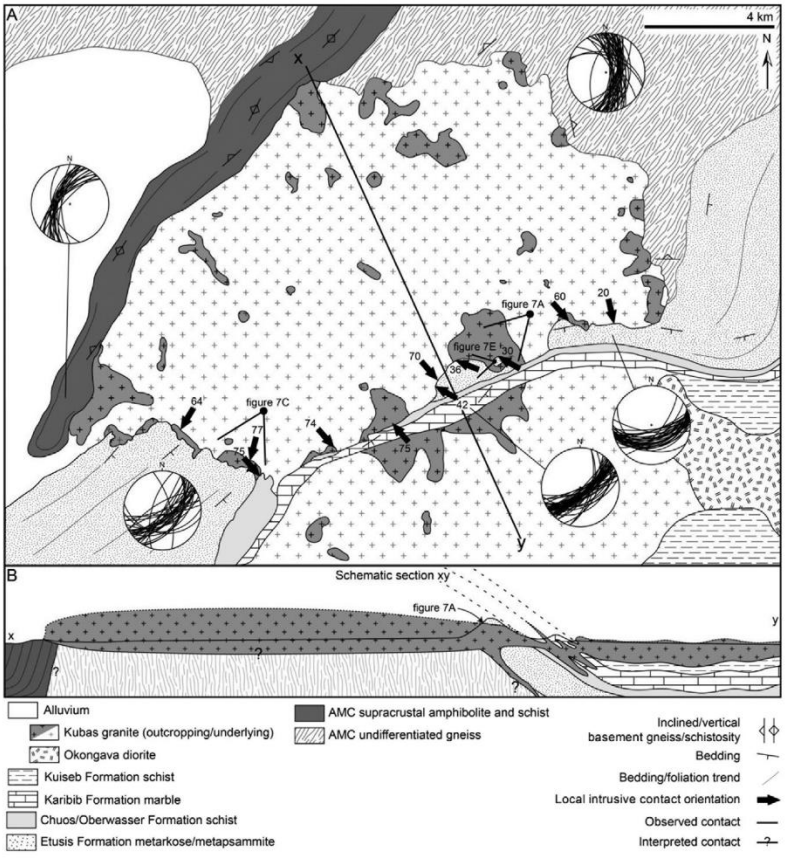

Fig. 5. (A) Simplified geological map of the 300 km^2 Kubas granite, which consists of two roughly equally-sized lobes within and along the southern flank of the Abbabis High. The pluton intrudes basement and cover lithologies, occupying an emplacement site that is unusual for this part of the Damara Belt. Equal area, lower hemisphere stereonets show bedding and bedding-parallel foliations in metasedimentary wall rocks and the gneissosity/layering of the basement rocks. Fields of view for Fig. 7A, C and E are indicated by the spot and line indicators. (B) Schematic section to highlight the relationships between the Kubas granite and its roof and wall-rocks along a central NE-striking ridge (see text). The location of the feeder along the basement-cover contact and floor geometries are speculative. Vertical exaggeration is 1.5×.

Fig. 6. Compositional variations within the Kubas granite are preserved as multitudes of enclaves with compositions from granitic and dioritic to gabbroic. Crosscutting relationships between texturally distinct enclave-rich and enclave-poor phases suggest the presence of distinct intrusive phases. Dashed line delineates contact between distinct phases. Notebook is 20 cm long.

rocks along and across their anisotropies ($\sigma_1 - \sigma_3 < T_{||} - T_{\perp}$; Lucas and St-Onge, 1995; Kisters et al., 2009). This formulation describes a delicate balance which, if upset, will reverse and promote the development of subhorizontal fractures in convergent settings.

4.1.1. The effect of rigidity anisotropies — the cases of the Stinkbank and Kubas granites

Small-scale strain variations in the rocks of the DSG reflect variations in the Young's moduli (E) of individual layers. Depending on the orientation of this mechanical layering and the orientation and intensity of the applied stress field, these contrasts may lead to local stress variations large enough to influence fracture propagation and affect the location of the dyke–sill transition (Gudmundsson and Brenner, 2001). During horizontal shortening of a horizontally layered sequence, stiffer layers (high E) experience higher differential stresses and more compression than softer layers (Fig. 8). Magma-filled fractures ascend where the magnification of tensile stresses ahead of their tips (Clemens and Mawer, 1992) exceeds the fracture toughness of the wall-rock in addition to any compressive tectonic stress normal to the fracture (Fig. 8A lower inset). Where the compressive stress build-up in the stiffer layers is greater than the tensile stresses generated ahead of ascending magma-filled fractures, the stiff layers may form stress barriers that prohibit further magma ascent (e.g. Gudmundsson

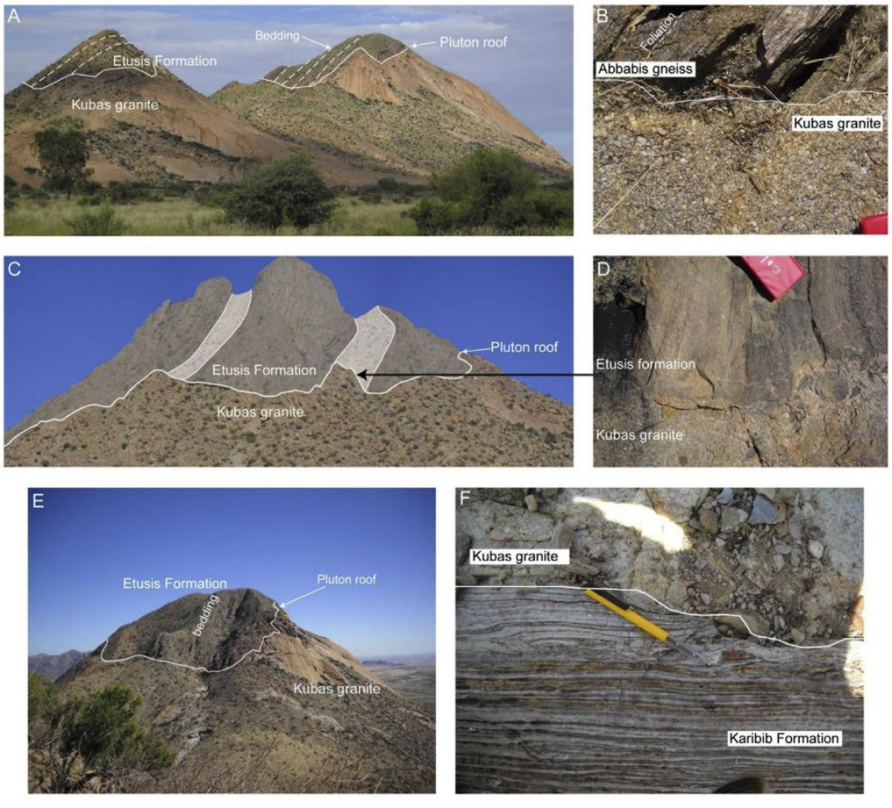

Fig. 7. Photo panel illustrating the contact relationships of the Kubas granite. (A, C, E) In detail, the roof of the pluton is comprised of alternating concordant and discordant contact sections that together described the overall gentle southwest dip of the pluton roof. For rough scale see fields of view indicated on Fig. 5A. (B) Small-scale discordant contact between the Kubas granite and Abbabis basement gneiss. Corner of ~20 cm long notebook for scale. (D) Small-scale discordant contact between the Kubas granite and Etusis Formation meta-arkose. ~20 cm long notebook for scale; for photo location see (C). (F) Small-scale concordant contact between a sheet of Kubas granite and marbles of the Karibib Formation.

and Brenner, 2001; Rivalta et al., 2005). In such cases, the low-cohesion along the contacts between mechanically distinct layers and the horizontally compressive stress field may result in dyke deflection and contact-parallel propagation provided the driving pressure in the ascent conduit is greater than the cohesion of the interface (Kavanagh et al., 2006; Gudmundsson and Philipp, 2006; Kavanagh and Pavier, 2014). Salem granites, such as the Stinkbank pluton, are mostly concordantly emplaced into the lower parts of

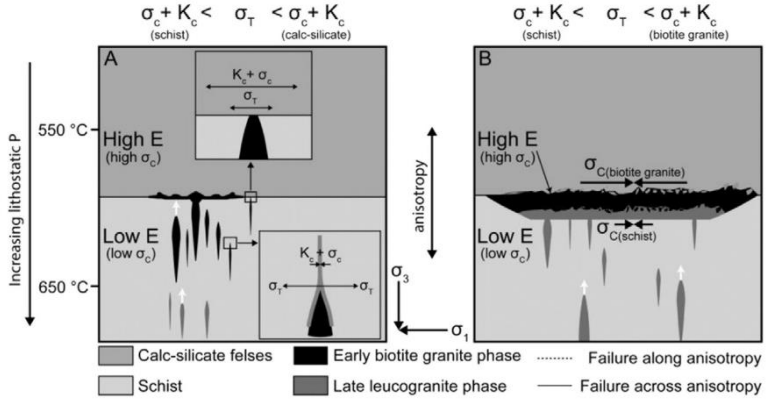

Fig. 8. Simplified schematic illustration of the role of subhorizontal rigidity anisotropies in the emplacement and assembly of the Stinkbank pluton. (A; lower inset) Magma ascent within the less rigid schists (lower Young's modulus (E)) occurs where the buoyancy-derived tensile stress ahead of a magma-filled fracture (σ_T) exceeds the sum of any fracture-normal compressive stress and the fracture toughness of the wall rocks ($\sigma_T \gg K_c + \sigma_c$). (A; upper inset) This situation is reversed in the calc-silicate felses where the layer-parallel compressive stresses are much higher and magma ascent is halted and lateral sheet propagation promoted along the interface between wall rocks of highly contrasting rigidities. (B) The solidification of early granite sheets induces similar rigidity anisotropies that act as magma traps for later intrusive phases, resulting in the formation of composite plutons. Curved-head arrows indicate fracture propagation directions; temperatures cited are a crude estimation based on the local P–T estimates of Puhan (1983).

the Kuiseb Formation, which includes up to 20 m thick meta-psammite and calc-silicate fels marker horizons. Although the dyke-to-sill transition of the earliest uppermost Stinkbank phase is not exposed, the competent calc-silicate felses are likely to have acted as stress barriers during deformation of the otherwise biotite-schist dominated metaturbiditic sequence (Fig. 8A). The vertical growth of the Stinkbank pluton by underaccretion of significantly younger granite sheets near the base of the earlier emplaced phases better illustrates the control of contrasting rigidities and stress barriers during granite emplacement (Fig. 8). The angular blocks contained within the intrusive breccias along the sheet contacts suggest that relatively earlier granites were fully crystallized prior to the emplacement of subsequent phases. Earlier granites would thus have provided rigid and, at least during the earlier phases of folding and fold amplification, suitably orientated stress barriers in the otherwise metapelitic Kuiseb Formation. A similar association of earlier, subconcordant megacrystic granites and later, structurally lower leucogranites has been described for other Salem-type granites plutons (Jacob, 1974; Miller, 2008; Anthonissen, 2009) and may reflect the regional significance of granite-induced rigidity contrasts for the assembly of macroscopically composite plutons in the Damara Belt.

The effect of horizontal shortening on the stress distribution within mechanically layered sequences is reversed if the sequence is vertical or steeply inclined. In such cases, high angle compression (σ_1 horizontal) results in layer-parallel stretch. Incompetent lithologies can accommodate layer-parallel stretch by ductile flow, and the plasticity of the rocks prevents the build-up of large differential stresses (Fig. 9A–B). At similar strain rates, stiffer layers are not able to accommodate the stretch by ductile flow and will experience an increase in differential stress compared to adjacent units, increasing the diameter of the Mohr stress circle (Fig. 9C). Where the differential stress becomes larger than the difference in tensile strength and cohesion along and across bedding and/or foliation planes (Fig. 9C), the Mohr stress circle intersects the failure envelope and stress relaxation may occur by the development of brittle extensional fractures in the presence of lithostatically pressurized fluids (Fig. 9C).

The shallow dips of the roof and sharp wall-rock contacts of the northern lobe of the Kubas granite are consistent with emplacement by fracture propagation along the plane of subhorizontal shortening. More importantly, its highly discordant contacts against the moderate to steeply-dipping Etusis Formation and intrusion largely into the AMC represent a unique setting for granite plutons in the Damara Belt. The discordant relationships against the quartzofeldspathic basement, the compositionally similar overlying metapsammites as well as the basement-cover contact itself probably arises from high competence of the wall rocks, as is indicated by the lack of pervasive Pan-African fabrics in both units. The flat-topped roof cuts sharply across steeply-dipping basement gneisses and moderate to steeply-dipping lower parts of the DSG alike, suggesting magma emplacement was controlled by subhorizontal fracturing during layer-normal compression (Fig. 9). The staircase-like roof contacts of the Kubas granite against the well-bedded Damara sequence probably results from the effect of the mechanical layering of individual formations on fracture propagation. Steeply-dipping, subconcordant contacts are predominantly developed in schist or marble units whereas shallowly-dipping, sharply discordant segments are confined to competent units, such as metapsammites and meta-arkoses of the Etusis Formation (Fig. 7). This suggests that the failure of the rocks by extensional fracturing was promoted within competent units that experienced layer-parallel stretch in response to subhorizontal compression.

Apart from modal mineralogy, the rigidity of crustal rocks depends on a number of parameters including, amongst others, grain size and textural relationships, strain rate and confining pressure, the presence and composition of a fluid phase and, most importantly, temperature (e.g., Handy et al., 1999). Local peak-metamorphic conditions in the Erongo region reached the mid- and lower amphibolite facies (T ~555–645 °C, P ~3 ± 1 kbar; Puhan, 1983; Steven, 1993; Wulff et al., 2010) and the syntectonic granites discussed here intruded before the local peak of metamorphism probably into slightly lower-grade wall rocks. These conditions are approaching the onset of feldspar plasticity (e.g. Tullis and Yund, 1992). At higher temperatures feldspar plasticity would likely

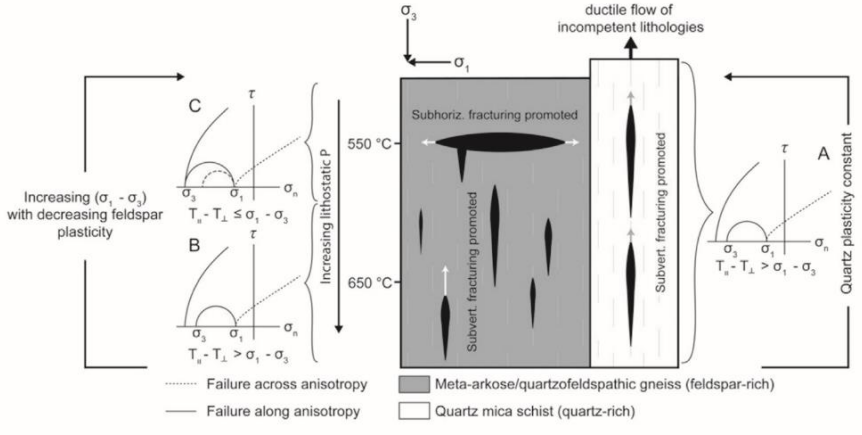

Fig. 9. Simplified schematic illustration of the role of wall-rock competence during the emplacement of the Kubas granite into a vertically-layered sequence (A, B) Anisotropy-parallel magma ascent is promoted where the differential stress ($\sigma_1 - \sigma_3$) is less than the difference between the rock tensile strength parallel and perpendicular to the anisotropy ($T_{\parallel} - T_{\perp}$). The Mohr stress circle thus intersects the anisotropy-parallel failure envelope. (C) As magmas ascend, differential stresses in the wall rocks increase with decreasing temperature. Between ~650 and 550 °C, the increase in differential stress is more pronounced in feldspar-rich than quartz-rich lithologies and ($\sigma_1 - \sigma_3$) becomes $\geq(T_{\parallel} - T_{\perp})$. The Mohr stress circle intersects the anisotropy-normal failure envelope and subhorizontal rather than subvertical fracturing is promoted. The ascending magmas are then emplaced along subhorizontal extensional fractures that accommodate layer-parallel extension at high angles to σ_3 in the competent meta-arkoses. Similar subhorizontal fracturing of the less competent quartz-rich layers is not promoted at similar levels and the quartz-rich wall-rocks instead accommodate the layer-parallel extension by ductile flow (extrusion) normal to shortening. Curved-head arrows indicate fracture propagation directions; temperatures cited are a crude estimation based on the local P–T estimates of Puhan (1983).

Erratum: the key to the failure envelopes in the Mohr diagrams illustrated in figure 9 is reversed. The dashed failure envelop represents failure parallel to the anisotropy and the solid envelop failure across the anisotropy.

reduce rigidity contrasts between quartzofeldspathic lithologies and less feldspar-rich rocks of the DSG. At the lower amphibolite-facies conditions of the Erongo region however, rigidity contrasts were probably more pronounced. This effect of temperature on the rigidity and competence of wall rocks for the emplacement of the Kubas granite is illustrated schematically in Fig. 9. At depth, magma ascent along steeply-orientated wall-rock anisotropies in both basement and cover rocks is promoted by conditions of very low differential stress (Fig. 9A–B). At lower temperatures and into the field of feldspar plasticity, rigidity contrasts between the quartzofeldspathic basement gneisses and Etusis Formation and the mixed metapelite-marble dominated succession of the upper DSG become more pronounced. Rigidity contrasts develop, differential stresses increase within the feldspar-rich rocks and the formation of subhorizontal fractures is promoted, resulting in the emplacement of the subhorizontal granite sheet into the competent basement sequence and similarly rigid overlying Etusis Formation (Fig. 9C). This illustrates the control of temperature on wall-rock competence and the dyke–sill transition in the mid-crust, as well as the effect of the lithological and mechanical heterogeneity of the wall rocks.

4.1.2. *The effect of rheological contrasts – emplacement of the Mon Repos diorite*

Stress relaxation within locally more ductile zones is thought to be important during the emplacement of magma into crystal mushes in growing plutons (Wiebe and Collins, 1998) and the underplating of mafic magmas in the lower crust (e.g. Parsons et al., 1992; Watanabe et al., 1999). The emplacement of the Mon Repos diorite along the prominent subhorizontal rheological anisotropy between the basement gneisses and the pervasively recrystallized marbles of the Karibib Formation demonstrates a more focussed role for wall-rock rheological contrasts during initial pluton emplacement. The arrest and/or deflection of buoyancy-driven magma-filled fractures along contacts between comparatively stiff strata overlain by ductile units can be related to stress dissipation and the relatively higher fracture toughness of the softer, more ductile units (e.g. Gudmundsson and Brenner, 2001). Magma-filled fractures propagate due to the magnification of the tensile stresses generated ahead of their tips (Fig. 10A; Clemens and Mawer, 1992) and may be arrested where the sum of the wall-rock fracture toughness and any fracture-normal compressive stress exceeds the tensile stress ahead of the fracture tip. Another manifestation of this phenomenon is the change in fracture shape where fractures propagate into relatively ductile layers (Sumita and Ota, 2011) within which lower yield strengths and ductile flow lead to a widening of the fracture tip aperture (Johnson et al., 2006; Kisters et al., 2009; Fig. 10B). This fracture blunting may dissipate the tensile stress ahead of the fracture tip to the point that it becomes smaller than the fracture toughness of the overlying ductile layer. As a result, the fracture-controlled ascent conduit is not able to penetrate the softer layer and the fracture becomes arrested. Lateral fracture propagation is then driven by any excess pressure in the stalled ascent conduit along the likely weakly cohesive contact between the two units, particularly within horizontally layered sequences undergoing horizontal shortening (Fig. 10C). The position of the thin, diorite sheet of the Mon Repos diorites along (1) the subhorizontal unconformity between (2) competent quartzofeldspathic basement gneisses and highly ductile overlying marble units illustrates exactly this combination of rheological contrast and suitably orientated anisotropy which would promote the development of an exceptionally thin and laterally extensive intrusive sheet.

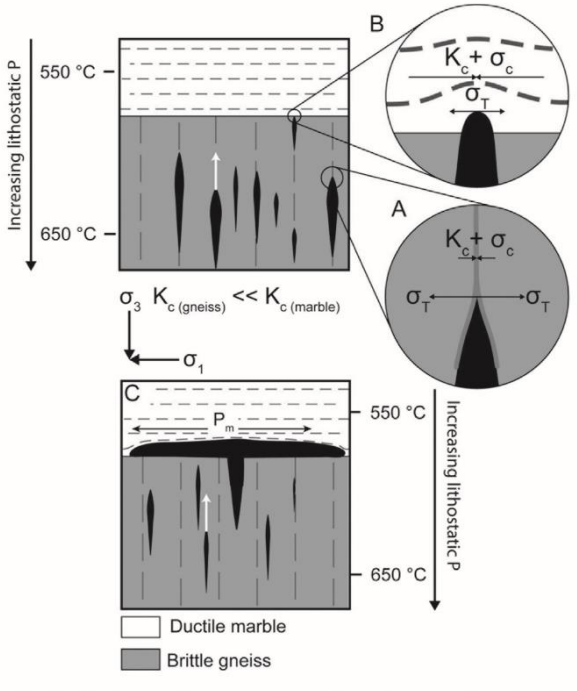

Fig. 10. Simplified schematic representation of the emplacement of the Mon Repos diorite along a subhorizontal rheological anisotropy. (A) Fracture-controlled magma ascent occurs where the buoyancy-derived tensile stress ahead of a magma-filled fracture (σ_T) exceeds the fracture toughness of the wall rocks in addition to any fracture-normal compressive stress ($\sigma_T \gg K_c + \sigma_c$). (B) Where ascending magmas cross the contact between relatively brittle gneiss and relatively ductile marble, σ_T is dissipated due to ductile flow, the fracture tip bluntens and continued ascent is inhibited ($\sigma_T < K_c + \sigma_c$). (C) Excess pressure in the conduit (P_m) is accommodated by sheet propagation along the interface, in this case favourably orientated subnormal to σ_3, promoting the development of a thin, laterally extensive sheet. Curved-head arrows indicate fracture propagation directions; temperatures cited are a crude estimation based on the local P–T estimates of Puhan (1983).

5. Implications

5.1. *The regional role of rigidity contrasts*

A larger-scale role for rigidity contrasts during the emplacement of Damaran granites is hinted at by the degree of syn-to post-emplacement deformation of the three plutons discussed here. Magmatic and solid-state fabrics and the upright F3 folding of the sheet-like Stinkbank pluton are typical for most Salem-type granites that are emplaced into the metapelitic Kuiseb Formation (Fig. 4; Miller, 2008; Kisters et al., 2012). Yet, despite their similar timing, the Kubas granite and even older Mon Repos diorite, which are emplaced immediately above and largely within the quartzofeldspathic gneisses of the AMC respectively, display no or only very weak fabric development, and their gently-dipping planar roof contacts do not appear to have been affected by D3 strains. The absence of regional fabrics and structures in the plutons probably relates to their position in relation to the competent basement gneisses of the AMC, which preserve only minimally overprinted pre-Damaran fabrics. In contrast, the pervasive D3 fabrics in the Stinkbank pluton probably result from the partitioning of strain into the incompetent schist-dominated host rocks of the Kuiseb Formation during regional shortening. The vastly different strains preserved in similarly old granites in this part of the sCZ emphasize the care that needs to be taken when intrusive ages and fabric relationships in granites are used to infer the timing of regional deformation events.

5.2. Temporal and spatial variations of emplacement levels

The significance of stress barriers (Stinkbank) or stress switches (Kubas) for the emplacement of plutons in the Erongo region is consistent with the brittle–ductile transition zone being considered a mechanically significant zone of preferred granite emplacement in the continental crust (e.g. Hogan and Gilbert, 1995; Acocella and Rossetti, 2002; Brown, 2010). Around this level, mechanical contrasts between the rocks as well as the levels of supported differential stress are sufficiently large to have a profound effect on the ascent paths of magmas, as is indicated by the models (e.g. Kavanagh et al., 2006). Many of the laterally extensive sheet-like plutons in the Damara Belt can be shown to be made up of multiple magma batches, each of which advects heat into mid- and upper crustal emplacement levels. Heat advection through the granitic magmas will result in the upward displacement of the isotherms and, in turn, the thermal weakening of the upper crust. This will move the rigidity anisotropies that this study has demonstrated to play such an important role during emplacement of the granites to progressively shallower crustal levels. As a result, granite emplacement levels themselves will progressively become shallower during the maturation of the orogen. These effects are evident in the Damara Belt. The high T, low P metamorphic conditions during local peak metamorphism in the Erongo region (T ~555–645 °C, P ~3 ± 1 kbar; Puhan, 1983; Wulff et al., 2010) suggest apparent local geothermal gradients of at least ~55–60 °C/km in the upper ten kilometres of crust. In contrast, regional peak P–T estimates (P ~5 kbar; T ~750 °C; Nex et al., 2001; Jung and Mezger, 2003; Ward et al., 2008) from the higher-grade southwestern parts of the sCZ record apparent geothermal gradients of only ~45–50 °C/km. In other words, the cumulative effect of advective heat transport through sheet-like granites is likely to have a significant effect on the temperature profile and, thus, mechanical stratification of the crust with time. This, in turn, affects the emplacement levels of later granites.

5.3. Magma chamber development

It is increasingly being recognized that the igneous bodies that later crystallize to form plutons do not necessarily evolve into active magma chambers during their growth and development (Annen et al., 2015). Volumes of liquid melt large enough to form volcanic reservoirs only accumulate during periods of exceptionally high magma flux (Annen et al., 2015). The incremental assembly of plutons by relatively small magma batches over protracted periods of time means that individual magma batches crystallize quickly and are commonly largely solidified prior to the arrival of later phases (e.g. Glazner et al., 2004). This is demonstrated by the role for apparently rigid pre-existing granite sheets during the assembly of the Stinkbank pluton and is also consistent with the low-flux suggested by the well-preserved internal sheeting of the Stinkbank granites. Furthermore, the lack of contact metamorphism around the Mon Repos, Stinkbank and Kubas plutons is indicative of only very low magma fluxes (Annen, 2011) and suggests that the plutons in this study did not evolve into magma chambers during their development.

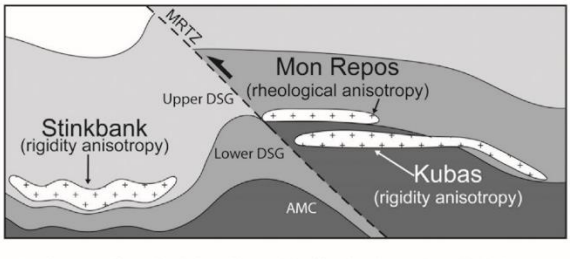

Fig. 11. The controls on the dyke–sill transition for the plutons described above vary in detail despite the close spatial and temporal association of the plutons. In each case, the level of emplacement is determined by the presence and arrangement of mechanical anisotropies that are mostly, but not necessarily, associated with lithological contacts within the mechanically heterogeneous Damara Supergroup (DSG). AMC = Abbabis Metamorphic Complex.

6. Conclusions

In this paper, we have attempted to identify the controls on the dyke–sill transition in the case of three roughly contemporaneous syntectonic granite plutons that intruded different stratigraphic levels in the Pan-African Damara Belt in Namibia. The three case histories highlight tabular and sheet-like geometries that are consistent with their emplacement during regional, subhorizontal shortening related to the high-angle convergence between the Kalahari and Congo Cratons between ca. 560 and 530 Ma. Although the actual feeder zones of the tabular granites cannot be identified with certainty, deep-crustal sources imply the presence of steep feeder networks, probably in the form of feeder dykes or hydrofractures. The transition from steep feeder to subhorizontal sheet-like pluton at the emplacement level is controlled by mechanical heterogeneities in the basement-cover succession (Fig. 11). These controls include:

- stress barriers/switches provided by relatively rigid subhorizontal horizons in the DSG or earlier emplaced solidified granite sheets and
- rheological anisotropies associated with the juxtaposition of ductile and brittle lithologies.

In these cases, the resulting plutons are largely concordant or subconcordant to the associated anisotropy, underscoring the widely held perception of granite emplacement being controlled by Damaran stratigraphy (Miller, 2008). However, the discordant nature of the Kubas granite highlights the importance of mechanical anisotropies that are not related to changes in wall-rock lithology, demonstrating discordant pluton emplacement by fracturing along an orientation determined by the prevailing regional stress field in the convergent Damara Belt. Vertical growth of the plutons following the dyke–sill transition is achieved through the underaccretion of subsequent melt batches to the base of earlier sheets that, by virtue of forming rigid layers themselves, may act as efficient magma traps for periods up to 20 Ma.

Acknowledgements

We would like to thank the owners of the farms Kubas, Tsawisis Suid, Etusis, Ubib West, Ubib East and Narubis for access to the study areas. We also gratefully acknowledge the detailed geological maps of the Stinkbank granites by Martin Vietze and of parts of the Mon Repos diorite by Chris Anthonissen. We thank Stefan Jung and Janine Kavanagh for providing constructive reviews that helped to refine the presentation and context of this manuscript. DH gratefully acknowledges financial support from the South African National Research Foundation via a grant awarded to Ian Buick (grant no.: 69858:2009).

References

Acocella, V., Rossetti, F., 2002. The role of extensional tectonics at different crustal levels on granite ascent and emplacement: an example from Tuscany (Italy).

Tectonophysics 354 (1), 71–83. http://dx.doi.org/10.1016/S0040-1951(02)00290-1.

Ameglio, L., Page, P., Jacob, R.E., 2000. 3D-geometry of the Mon-Repos granodiorite (Goas dioritic suite, Damara Belt, Namibia) inferred from gravity data. J. Afr. Earth Sci. 31 (2).

Anderson, E.M., 1951. The Dynamics of Faulting and Dyke Formation with Applications to Britain. Oliver and Boyd, Edinburgh.

Annen, C., 2011. Implications of incremental emplacement of magma bodies for magma differentiation, thermal aureole dimensions and plutonism-volcanism relationships. Tectonophysics 500 (1–4), 3–10. http://dx.doi.org/10.1016/j.tecto.2009.04.010.

Annen, C., Blundy, J.D., Leuthold, J., Sparks, R.S.J., 2015. Construction and evolution of igneous bodies: towards an integrated perspective of crustal magmatism. Lithos 230, 206–221. http://dx.doi.org/10.1016/j.lithos.2015.05.008.

Anthonissen, C.J., 2009. The Mid-crustal Architecture of a Continental Arc – a Transect through the South Central Zone of the Pan-African Damara Belt, Namibia (Unpublished MSc thesis). Stellenbosch University, Stellenbosch.

Behr, W.M., Platt, J.P., 2011. A naturally constrained stress profile through the middle crust in an extensional terrane. Earth Planet. Sci. Lett. 303 (3), 181–192. http://dx.doi.org/10.1016/j.epsl.2010.11.044.

Benn, K., Roest, W.R., Rochette, P., Evans, N.G., Pignotta, G.S., 1999. Geophysical and structural signatures of syntectonic batholith construction: the South Mountain Batholith, Meguma Terrane, Nova Scotia. Geophys. J. Int. 136 (1), 144–158. http://dx.doi.org/10.1046/j.1365-246X.1999.00700.x.

Blenkinsop, T.G., Treloar, P.J., 2001. Tabular intrusion and folding of the late Archaean Murehwa granite, Zimbabwe, during regional shortening. J. Geol. Soc. Lond. 158 (4) http://dx.doi.org/10.1144/jgs.158.4.653.

Bons, P.D., Dougherty-Page, J., Elburg, M.A., 2001. Stepwise accumulation and ascent of magmas. J. Metamorph. Geol. 19 (5), 627–633. http://dx.doi.org/10.1046/j.0263-4929.2001.00334.x.

Bons, P.D., Becker, J.K., Elburg, M.A., Urtson, K., 2009. Granite formation: stepwise accumulation of melt or connected networks? Earth Environ. Sci. Trans. R. Soc. Edinb. 100 (1–2), 105–115. http://dx.doi.org/10.1017/S175569100901603X.

Brandt, R., 1985. Preliminary report on the stratigraphy of the Damara Sequence and the geology and geochemistry of Damaran granites in an area between Walvis Bay and Karibib. Commun. Geol. Surv. Namib. 1, 31–43.

Brandt, R., 1987. A revised stratigraphy for the Abbabis Complex in the Abbabis Inlier, Namibia. S. Afr. J. Geol. 90 (3), 314–323.

Brown, M., 1994. The generation, segregation, ascent and emplacement of granite magma: the migmatite-to-crustally-derived granite connection in thickened orogens. Earth-Science Rev. 36 (1), 83–130. http://dx.doi.org/10.1016/0012-8252(94)90009-4.

Brown, M., 2010. The spatial and temporal patterning of the deep crust and implications for the process of melt extraction. Philos. Trans. Ser. A Math. Phys. Eng. Sci. 368 (1910), 11–51. http://dx.doi.org/10.1098/rsta.2009.0200.

Brown, M., Solar, G.S., 1998. Granite ascent and emplacement during contractional deformation in convergent orogens. J. Struct. Geol. 20 (9), 1365–1393. http://dx.doi.org/10.1016/S0191-8141(98)00074-1.

Burchardt, S., Tanner, D.C., Krumbholz, M., 2010. Mode of emplacement of the Slaufrudalur Pluton, Southeast Iceland inferred from three-dimensional GPS mapping and model building. Tectonophysics 480 (1), 232–240. http://dx.doi.org/10.1016/j.tecto.2009.10.010.

Clemens, J.D., Mawer, C.K., 1992. Granitic magma transport by fracture propagation. Tectonophysics 204 (3), 339–360. http://dx.doi.org/10.1016/0040-1951(92)90316-X.

Coleman, D.S., Gray, W., Glazner, A.F., 2004. Rethinking the emplacement and evolution of zoned plutons: geochronologic evidence for incremental assembly of the Tuolumne Intrusive Suite, California. Geology 32 (5), 433–436. http://dx.doi.org/10.1130/G20220.1.

Davidson, C., Schmid, S.M., Hollister, L.S., 1994. Role of melt during deformation in the deep crust. Terra Nova 6 (2), 133–142. http://dx.doi.org/10.1111/j.1365-3121.1994.tb00646.x.

De Kock, G.S., Eglington, B., Armstrong, R.A., Harmer, R.E., Walraven, F., 2000. U-Pb and Pb-Pb ages of the Naauwpoort rhyolite, Kawakeup leptite and Okongava Diorite: implications for the onset of rifting and of orogenesis in the Damara Belt, Namibia. Commun. Geol. Surv. Namib. 12, 81–88.

de Saint-Blanquat, M., Habert, G., Horsman, E., Morgan, S.S., Tikoff, B., Launeau, P., Gleizes, G., 2006. Mechanisms and duration of non-tectonically assisted magma emplacement in the upper crust: the Black Mesa pluton, Henry Mountains, Utah. Tectonophysics 428 (1), 1–31. http://dx.doi.org/10.1016/j.tecto.2006.07.014.

Diener, J.F.A., White, R.W., Hudson, T.J.M., 2014. Melt production, redistribution and accumulation in mid-crustal source rocks, with implications for crustal-scale melt transfer. Lithos 200–201, 212–225. http://dx.doi.org/10.1016/j.lithos.2014.04.021.

Dziggel, A., Wulff, K., Kolb, J., Meyer, F.M., Lahaye, Y., 2009. Significance of oscillatory and bell-shaped growth zoning in hydrothermal garnet: evidence from the Navachab gold deposit, Namibia. Chem. Geol. 262 (3), 262–276. http://dx.doi.org/10.1016/j.chemgeo.2009.01.027.

Farina, F., Dini, A., Innocenti, F., Rocchi, S., Westerman, D.S., 2010. Rapid incremental assembly of the Monte Capanne pluton (Elba Island, Tuscany) by downward stacking of magma sheets. Geol. Soc. Am. Bull. 122 (9–10), 1463–1479. http://dx.doi.org/10.1130/B30112.1.

Glazner, A.F., Bartley, J.M., Coleman, D.S., Gray, W., Taylor, R.Z., 2004. Are plutons assembled over millions of years by amalgamation from small magma chambers? GSA Today 14 (4–5), 4–12.

Gudmundsson, A., 2011. Deflection of dikes into sills at discontinuities and magma-chamber formation. Tectonophysics 500 (1), 50–64. http://dx.doi.org/10.1016/j.tecto.2009.10.015.

Gudmundsson, A., Brenner, S., 2001. How hydrofractures become arrested. Terra Nova 13 (6), 456–462. http://dx.doi.org/10.1046/j.1365-3121.2001.00380.x.

Gudmundsson, A., Philipp, S.L., 2006. How local stress fields prevent volcanic eruptions. J. Volcanol. Geotherm. Res. 158 (3), 257–268. http://dx.doi.org/10.1016/j.jvolgeores.2006.06.005.

Handy, M.R., Wissing, S.B., Streit, L.E., 1999. Frictional–viscous flow in mylonite with varied bimineralic composition and its effect on lithospheric strength. Tectonophysics 303 (1). http://dx.doi.org/10.1016/S0040-1951(98)00251-0.

Hartmann, O., Hoffer, E., Haack, U., 1983. Regional metamorphism in the Damara orogen: interaction of crustal motion and heat transfer. In: Miller, R.Mc G. (Ed.), Evolution of the Damara Orogen, vol. 11. Special Publication of the Geological Society, South Africa, pp. 233–241.

Hogan, J., Gilbert, M., 1995. The A-type Mount Scott Granite sheet: importance of crystal magma traps. J. Geophys. Res. Solid Earth (1978–2012) 100 (B8), 15779–15792. http://dx.doi.org/10.1029/94JB03258.

Hutton, D.H.W., 1992. Granite sheeted complexes: evidence for the dyking ascent mechanism. Trans. R. Soc. Edinb. Earth Sci. 83 (1–2), 377–382. http://dx.doi.org/10.1017/S0263593300008038.

Jacob, R.E., 1974. Geology and metamorphic petrology of part of the Damara Orogen along the lower Swakop River, South West Africa. Precambrian Res. Unit Bull. 17, 201.

Jacob, R.E., Moore, J.M., Armstrong, R.A., 2000. Zircon and Titanite age determination from igneous rocks in the Karibib district, Namibia: implications for Navachab vein-style gold mineralization. Commun. Geol. Surv. Namib. 12, 157–166.

Johnson, S.D., Poujol, M., Kisters, A.F.M., 2006. Constraining the timing and migration of collisional tectonics in the Damara Belt, Namibia: U-Pb zircon ages for the syntectonic Salem-type Stinkbank granite. S. Afr. J. Geol. 109 (4), 611–624. http://dx.doi.org/10.2113/gssajg.109.4.611.

Jung, S., Mezger, K., 2003. Petrology of basement-dominated terranes: I. Regional metamorphic T–t path from U–Pb monazite and Sm–Nd garnet geochronology (Central Damara orogen, Namibia). Chem. Geol. 198, 223–247. http://dx.doi.org/10.1016/S0009-2541(03)00037-8.

Jung, S., Hoernes, S., Mezger, K., 2002. Synorogenic melting of mafic lower crust: constraints from geochronology, petrology and Sr, Nd, Pb and O isotope geochemistry of quartz diorites (Damara orogen, Namibia). Contributions Mineral. Petrol. 143 (5), 551–566. http://dx.doi.org/10.1007/s00410-002-0366-5.

Kavanagh, J.L., Pavier, M.J., 2014. Rock interface strength influences fluid-filled fracture propagation pathways in the crust. J. Struct. Geol. 63, 68–75. http://dx.doi.org/10.1016/j.jsg.2014.03.001.

Kavanagh, J.L., Menand, T., Sparks, R.S.J., 2006. An experimental investigation of sill formation and propagation in layered elastic media. Earth Planet. Sci. Lett. 245 (3), 799–813. http://dx.doi.org/10.1016/j.epsl.2006.03.025.

Kisters, A.F.M., Jordaan, L.S., Neumaier, K., 2004. Thrust-related dome structures in the Karibib district and the origin of orthogonal fabric domains in the south Central Zone of the Pan-African Damara belt, Namibia. Precambrian Res. 133 (3), 283–303. http://dx.doi.org/10.1016/j.precamres.2004.05.001.

Kisters, A.F.M., Ward, R.A., Anthonissen, C.J., Vietze, M.E., 2009. Melt segregation and far-field melt transfer in the mid-crust. J. Geol. Soc. Lond. 166 (5), 905–918. http://dx.doi.org/10.1144/0016-76492009-012.

Kisters, A.F.M., Vietze, M.E., Buick, I., 2012. Deformation and age of the Stinkbank Pluton and implications for the correlation of tectonometamorphic episodes in the Pan-African Damara Belt. S. Afr. J. Geol. 115 (3), 309–326. http://dx.doi.org/10.2113/gssajg.115.3.309.

Lehtonen, M.I., Manninen, T.E.T., Schreiber, U.M., 1995. Geological Map of Namibia 1:250,000 Series, Sheet 2214. Geological Survey of Namibia, Walvis Bay.

Leuthold, J., Müntener, O., Baumgartner, L.P., Putlitz, B., Ovtcharova, M., Schaltegger, U., 2012. Time resolved construction of a bimodal laccolith (Torres del Paine, Patagonia). Earth Planet. Sci. Lett. 325–326, 85–92. http://dx.doi.org/10.1016/j.epsl.2012.01.032.

Lister, J.R., Kerr, R.C., 1991. Fluid-mechanical models of crack propagation and their application to magma transport in dykes. J. Geophys. Res. Solid Earth (1978–2012) 96 (B6), 10049–10077. http://dx.doi.org/10.1029/91JB00600.

Longridge, L., Gibson, R.L., Kinnaird, J.A., Armstrong, R.A., 2011. Constraining the timing of deformation in the southwestern Central Zone of the Damara Belt, Namibia. Geol. Soc. Lond. Spec. Publ. 357 (1), 107–135. http://dx.doi.org/10.1144/SP357.7.

Longridge, L., Kinnaird, J.A., Gibson, R.L., Armstrong, R.A., 2014. Amphibolites of the Central Zone: new SHRIMP U-Pb ages and implications for the evolution of the Damara Orogen, Namibia. S. Afr. J. Geol. 117 (1), 67–86. http://dx.doi.org/10.2113/gssajg.117.1.67.

Lucas, S.B., St-Onge, M.R., 1995. Syn-tectonic magmatism and the development of compositional layering, Ungava Orogen (northern Quebec, Canada). J. Struct. Geol. 17 (4), 475–491. http://dx.doi.org/10.1016/0191-8141(94)00076-C.

Marlow, A.G., 1983. Geology and Rb-Sr geochronology of mineralised and radioactive granites and alaskites, Namibia. In: Miller, R.McG. (Ed.), Evolution of the Damara Orogen of South West Africa/Namibia, vol. 11. Geological Society of South Africa Special Publications, Johannesburg, pp. 289–298.

Menand, T., 2011. Physical controls and depth of emplacement of igneous bodies: a review. Tectonophysics 500 (1), 11–19. http://dx.doi.org/10.1016/j.tecto.2009.10.016.

Menand, T., Daniels, K., Benghiat, P., 2010. Dyke propagation and sill formation in a compressive tectonic environment. J. Geophys. Res. Solid Earth 115 (B8). http://dx.doi.org/10.1029/2009JB006791.

Menand, T., Annen, C., de Saint Blanquat, M., 2015. Rates of magma transfer in the crust: insights into magma reservoir recharge and pluton growth. Geology 43 (3), 199–202. http://dx.doi.org/10.1130/G36224.1.

Meneghini, F., Kisters, A., Buick, I., Fagereng, Å., 2014. Fingerprints of late Neoproterozoic ridge subduction in the Pan-African Damara belt, Namibia. Geology 42 (10), 903–906. http://dx.doi.org/10.1130/G35932.1.

Milani, L., Kinnaird, J.A., Lehmann, J., Naydenov, K.V., Saalmann, K., Frei, D., Gerdes, A., 2014. Role of crustal contribution in the early stage of the Damara Orogen, Namibia: new constraints from combined U–Pb and Lu–Hf isotopes from the Goas Magmatic Complex. Gondwana Res. 28 (3) http://dx.doi.org/10.1016/j.gr.2014.08.007.

Miller, R.M., 1983. The Pan-African Damara Orogen of South West Africa/Namibia. In: Miller, R.McG. (Ed.), Evolution of the Damara Orogen of South West Africa/Namibia, vol. 11. Geological Society of South Africa Special Publication, Johannesburg, South Africa, pp. 431–515.

Miller, R.M., 2008. The Geology of Namibia. In: Neoproterozoic to Lower Paleozoic, vol. 2. Geological Survey of Namibia, Windhoek, Namibia.

Miller, C.F., Furbish, D.J., Walker, B.A., Claiborne, L.L., Koteas, G.C., Bleick, H.A., Miller, J.S., 2011. Growth of plutons by incremental emplacement of sheets in crystal-rich host: evidence from Miocene intrusions of the Colorado River region, Nevada, USA. Tectonophysics 500 (1), 65–77. http://dx.doi.org/10.1016/j.tecto.2009.07.011.

Morgan, S., Stanik, A., Horsman, E., Tikoff, B., de Saint-Blanquat, M., Habert, G., 2008. Emplacement of multiple magma sheets and wall rock deformation: Trachyte Mesa intrusion, Henry Mountains, Utah. J. Struct. Geol. 30 (4), 491512. http://dx.doi.org/10.1016/j.jsg.2008.01.005.

Nex, P., Oliver, G., Kinnaird, 2001. Spinel-bearing assemblages and PT-t evolution of the Central Zone of the Damara Orogen, Namibia. J. Afr. Earth Sci. 32 (3), 471–489. http://dx.doi.org/10.1016/S0899-5362(01)90109-5.

Oliver, G.J.H., 1994. Mid-crustal detachment and domes in the central zone of the Damaran orogen, Namibia. J. Afr. Earth Sci. 19 (4), 331–344. http://dx.doi.org/10.1016/0899-5362(94)90018-3.

Ostendorf, J., Jung, S., Berndt-Gerdes, J., Hauff, F., 2014. Syn-orogenic high-temperature crustal melting: geochronological and Nd–Sr–Pb isotope constraints from basement-derived granites (Central Damara Orogen, Namibia). Lithos 192–195, 21–38. http://dx.doi.org/10.1016/j.lithos.2014.01.007.

Parsons, T., Sleep, N.H., Thompson, G.A., 1992. Host rock rheology controls on the emplacement of tabular intrusions: implications for underplating of extending crust. Tectonics 11 (6), 1348–1356. http://dx.doi.org/10.1029/92TC01105.

Petford, N., Kerr, R.C., Lister, J.R., 1993. Dike transport of granitoid magmas. Geology 21 (9), 845–848. http://dx.doi.org/10.1130/0091-7613(1993)021<0845:DTOGM>2.3.CO;2.

Poli, L.C., Oliver, G.J.H., 2001. Constrictional deformation in the Central Zone of the Damara Orogen, Namibia. J. Afr. Earth Sci. 33 (2), 303–321. http://dx.doi.org/10.1016/S0899-5362(01)80065-8.

Puhan, D., 1983. Temperature and pressure of metamorphism in the Central Damara orogen. In: Miller, R.McG. (Ed.), Evolution of the Damara Orogen of South West Africa/Namibia, vol. 11. Geolological Society of South Africa Special Publication, pp. 219–223.

Rivalta, E., Böttinger, M., Dahm, T., 2005. Buoyancy-driven fracture ascent: experiments in layered gelatine. J. Volcanol. Geotherm. Res. 144 (1–4), 273–285. http://dx.doi.org/10.1016/j.jvolgeores.2004.11.030.

Rubin, A.M., 1995. Propagation of magma-filled cracks. Annu. Rev. Earth Planet. Sci. 23, 287–336. http://dx.doi.org/10.1146/annurev.ea.23.050195.001443.

Saumur, B.M., Cruden, A.R., 2015. On the emplacement of the Voisey's Bay intrusion (Labrador, Canada). Geol. Soc. Am. http://dx.doi.org/10.1130/B31240.1 (in press). http://gsabulletin.gsapubs.org/content/early/recent.

Smith, D.A.M., 1965. The geology around the Khan and Swakop Rivers in South West Africa. Memoirs Geol. Surv. S. Afr. 3, 113.

Stammeier, J., Jung, S., Romer, R.L., Berndt, J., Garbe-Schönberg, D., 2015. Petrology of ferroan alkali-calcic granites: synorogenic high-temperature melting of undepleted felsic lower crust (Damara orogen, Namibia). Lithos 224, 114–125. http://dx.doi.org/10.1016/j.lithos.2015.03.004.

Steven, N.M., 1993. A study of epigenetic mineralisation in the central zone of the Damara Orogen, Namibia, with special reference to gold, tungsten, tin, and rare earth elements. Memoirs Geol. Surv. Namib. 16, 166.

Sumita, I., Ota, Y., 2011. Experiments on buoyancy-driven crack around the brittle ductile transition. Earth Planet. Sci. Lett. 304 (3), 337–346. http://dx.doi.org/10.1016/j.epsl.2011.01.032.

Taisne, B., Tait, S., Jaupart, C., 2011. Conditions for the arrest of a vertical propagating dike. Bull. Volcanol. 73 (2), 191–204. http://dx.doi.org/10.1007/s00445-010-0440-1.

Tullis, J., Yund, R., 1992. The brittle-ductile transition in feldspar aggregates: an experimental study. Int. Geophys. 51, 89–117. http://dx.doi.org/10.1016/S0074-6142(08)62816-8.

Vietze, M., 2009. Geology and Emplacement Controls of the Stinkbank Granite in the South Central Zone of the Pan-African Damara Belt, Namibia (Unpublished MSc thesis). Stellenbosch University, Stellenbosch, p. 109.

Vigneresse, J.L., Clemens, J.D., 2000. Granitic magma ascent and emplacement: neither diapirism nor neutral buoyancy. Geol. Soc. Lond. Spec. Publ. 174 (1), 1–19. http://dx.doi.org/10.1144/GSL.SP.1999.174.01.01.

Vigneresse, J.-L., Tikoff, B., Améglio, L., 1999. Modification of the regional stress field by magma intrusion and formation of tabular granitic plutons. Tectonophysics 302 (3), 203–224. http://dx.doi.org/10.1016/S0040-1951(98)00285-6.

Ward, R., Stevens, G., Kisters, A.F.M., 2008. Fluid and deformation induced partial melting and melt volumes in low-temperature granulite-facies metasediments, Damara Belt, Namibia. Lithos 105 (3), 253–271. http://dx.doi.org/10.1016/j.lithos.2008.04.001.

Watanabe, T., Koyaguchi, T., Seno, T., 1999. Tectonic stress controls on ascent and emplacement of magmas. J. Volcanol. Geotherm. Res. 91 (1), 65–78. http://dx.doi.org/10.1016/S0377-0273(99)00054-2.

Westraat, J.D., Kisters, A.F.M., Poujol, M., Stevens, G., 2005. Transcurrent shearing, granite sheeting and the incremental construction of the tabular 3.1 Ga Mpuluzi batholith, Barberton granite-greenstone terrane, South Africa. J. Geol. Soc. Lond. 162 (2), 373–388. http://dx.doi.org/10.1144/0016-764904-026.

Wiebe, R.A., Collins, W.J., 1998. Depositional features and stratigraphic sections in granitic plutons: implications for the emplacement and crystallization of granitic magma. J. Struct. Geol. 20 (9), 1273–1289. http://dx.doi.org/10.1016/S0191-8141(98)00059-5.

Wulff, K., Dziggel, A., Kolb, J., Vennemann, T., Bottcher, M.E., Meyer, F.M., 2010. Origin of mineralizing fluids of the sediment-hosted Navachab Gold Mine, Namibia: constraints from stable (O, H, C, S) isotopes. Econ. Geol. 105 (2), 285–302. http://dx.doi.org/10.2113/gsecongeo.105.2.285.

Chapter 6: Synopsis, conclusion and outlook

6.1 Synopsis

Models of fracture-controlled granitic magma transport developed in response to the recognition that highly permeable fracture-controlled conduits can provide pathways along which viscous granitic magma can flow sufficiently rapidly to traverse large sections of subsolidus crust. The three case studies encompassed by dissertation document a dominant role for fracture-controlled melt/magma transport at all scales in the sCZ of the Damara Belt and highlight several new aspects that provide valuable insights into the questions outlined in the introductory chapter, which are briefly reiterated as:

- Do within- and near-source leucosome/leucogranite networks represent melt transport pathways and what controls their development and preservation?
- How are the networks related to far-field magma ascent?
- How are magmas transferred through the mid-crust without leaving behind obvious evidence?
- What controls the arrest of ascent and initiation of pluton emplacement?

This synopsis independently outlines the major contributions and main implications of each chapter and how these findings have addressed the above questions. The general conclusion that follows will present the findings and implications of this dissertation in combination by briefly sketching an outline of fracture-controlled granitic magma transport at the crustal-scale.

Chapter 3 advances our understanding of near-source melt segregation and transport by demonstrating the development of outcrop-scale self-organised melt networks independently of the pronounced wall-rock heterogeneities that are commonly assumed to control the geometries of similar networks elsewhere. Thus, the development of the transport networks is controlled by

intrinsic variations in melt pressure, which can be shown to trigger the formation of the kind of large, fracture-controlled melt geometries that are commonly called for as far-field ascent conduits. However, this internal control is superimposed by external parameters, such as local and regional stress fields and local wall-rock structures, which determine the efficiency with which the networks can be drained. Nevertheless, even in poorly-drained networks, the vein geometries record the local transport of melt in response internally-generated pressure gradients, suggesting that the interpretation of leucosome/leucogranite networks as local melt/magma transport pathways in migmatite terrains is indeed sound. More interesting than the outcrop-scale preservation of individual poorly-drained melt transport networks are the broader implications for the efficiency of crustal-scale fracture-controlled melt transport in general. For example, convergent settings are characterised by subhorizontal compression that will generally result in the development of poorly-drained subhorizontal rather than subvertical fractures during times of elevated melt production. Thus, the abundant preservation of the leucogranite networks that make the western sCZ so amenable to the study of within- and near-source melt/magma transport processes could be attributed to the high-angle of the NW-SE directed convergence and collision between the Kalahari and Congo Cratons. In contrast, in obliquely convergent settings characterised by transpression, the development of large-scale transpressive or transcurrent shear zones may act as tectonically-controlled magma conduits that lead to fairly efficient drainage of melt from the anatectic zone, resulting in the preservation of fewer within- and near-source melt transport networks.

Chapter 4 advances our understanding of the nature and genesis of far-field granite ascent conduits by documenting for the first time the large-scale accumulation and episodic vertical drainage of magma along self-propagating hydrofractures from within much smaller melt/magma transport networks in suprasolidus rocks close to the source of partial melting. The ascent of

magma within critically-large fractures that close and decouple from their source networks implies an episodicity of magma ascent and a potential spatial variability of magma sources that contribute to compositional and isotopic heterogeneities within macroscopically/cryptically composite granitoid plutons (e.g. Pressley and Brown, 1999; Clemens, 2003; Clemens et al., 2009). Moreover, source and melt/magma compositions are likely to evolve continually with the successive extraction of relatively small individual melt batches from the source region. Thus, the petrological complexities of plutons do not arise entirely from processes that take place at the emplacement level, but also record the processes that occur and evolve at each stage of melt/magma transport and ascent. Another important implication related to the episodicity of ascent is that magma chambers are almost certainly not a natural consequence of crustal partial melting and melt/magma ascent, and are only likely to arise when rates of melt production in the source are high enough to invigorate frequent ascent episodes (Annen et al., 2015).

Conclusively demonstrating a role, in reality, for fracture-controlled ascent also has fundamental implications for the ascent paths of the magmas through the crust and the eventual level at which ascent is arrested and emplacement initiated. Fracturing is significantly more efficient where propagation can take place along some pre-existing wall-rock anisotropy, implying that regions of the crust characterised by steeply-dipping anisotropies will promote the ascent of relatively smaller magma batches than those that ascend through horizontally stratified wall-rock, where larger volumes are needed for efficient ascent. This role for anisotropies has important implications in determining whether the magmas are emplaced as fractures are arrested or reach close enough to the surface to form reservoirs for volcanic eruptions.

Chapter 5 advances our understanding of the controls on the level of emplacement of tabular granitoid plutons in the mid-crust by demonstrating the effects of mechanical anisotropies in the wall rocks, even at temperatures in excess of 500 °C. Moreover, the effects of increasing

differential stress on fracture-controlled magma ascent are demonstrated by the development of stress barriers independently of lithological variation in homogeneous regions of the crust. The coupling of increasing levels of differential stress along the ascent paths in lithologically heterogeneous sections of the crust amplifies the lithologically-controlled mechanical anisotropies that are thought to represent the primary control on the level of emplacement, but this effect is also dependent on the prevailing P-T conditions that determine the rheological state of the compositionally-layered wall rocks and may account for the significant variability in pluton emplacement levels.

6.2 Conclusion

The continuum of processes outlined by the case-studies presented here sketches a coherent model of fracture-controlled macroscale melt/magma transport in the south Central Zone of the Damara Belt, highlighting that while the formation of melt/magma transport conduits is internally controlled, local and regional external factors are likely to determine the degree to which the anatectic zone was drained (Fig. 6.1). The most important external parameter is the level of differential stress sustained in the wall rocks within the anatectic source and along the path of ascent (Fig. 6.1). Stress homogenisation in ductile source regions leads to very low levels of differential stress, which promotes the formation of the self-organised fracture networks. The formation of self-propagating hydrofractures is initiated during times of anomalously high melt supply and their ascent is promoted by low-levels of differential stress along steeply-orientated crustal-scale anisotropies such as upright, tightly folded sequences, basement-cover discontinuities and, although not the case in the Damara Belt, crustal-scale shear zones. The self-propagating hydrofractures are isolated magma-filled fractures whose volume is determined by the critical ascent volume at the source and should be reflected at the emplacement site by the

volumes of the sheets that make up the commonly macroscopically sheeted plutons in the mid-crust of the Damara Belt.

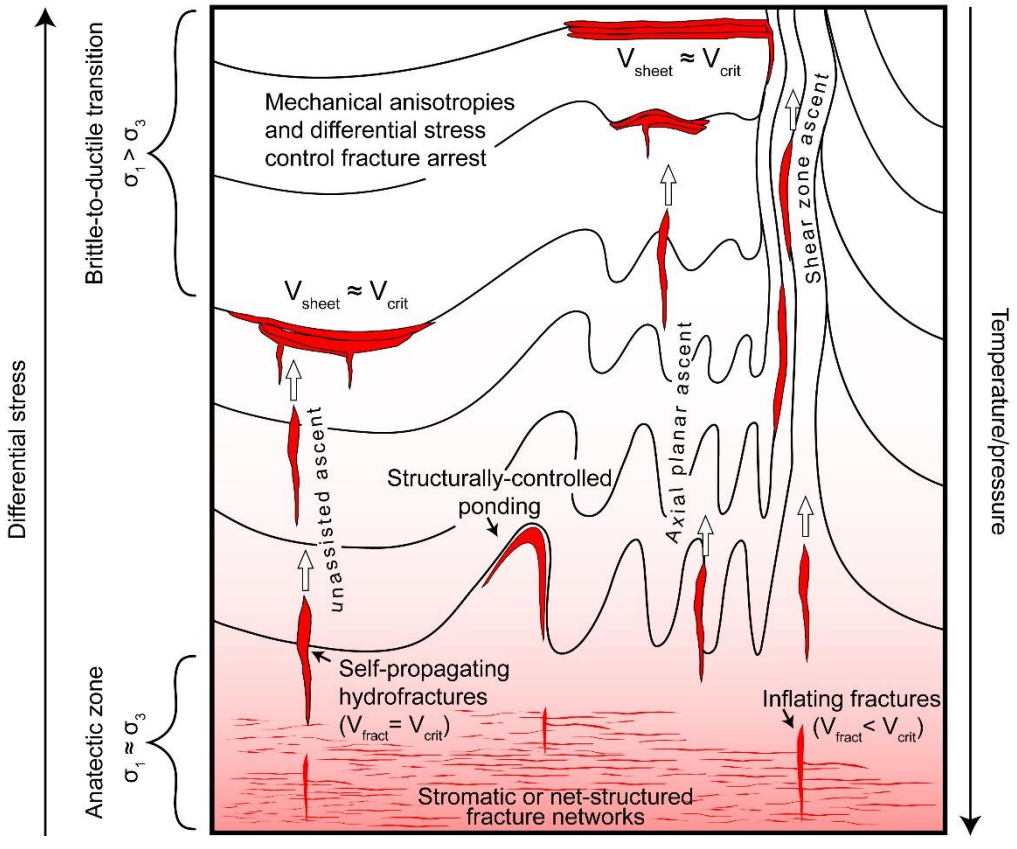

Figure 6.1: *Synoptic sketch of crustal-scale fracture-controlled melt/magma transport. Extensional fractures form and inflate within smaller-scale melt/magma networks under conditions of low-differential stress and elevated melt/magma pressure. Ascent along self-propagating hydrofractures is initiated once the fractures become critically buoyant. Fracture arrest is controlled by the mechanics of the wall rocks and may occur where (1) ascending fractures intersect ductile horizons or (2) where increasing differential stresses amplify mechanical anisotropies in the wall rocks with decreasing temperature. Areas of locally lower differential stress, such as shear zones or the axial planes of upright folds, enhance the overall efficiency of ascent, promoting ascent into higher levels in the crust.*

The actual emplacement of the plutons can also be related to differential stress, which increases as temperatures decrease during ascent towards the brittle-to-ductile transition (Fig. 6.1). Around the brittle-to-ductile transition, the differential stress reaches a maximum, and magnifies the mechanical anisotropies within the lithologically heterogeneous wall rocks of the Damara Supergroup, which in turn control the arrest of ascent. Thus, pluton emplacement in the crust broadly mimics the differential stress profile, which itself will be perturbed by the increasing temperatures with the advection of heat along with the emplacement of the magmas, leading to progressive changes in emplacement levels as the orogen matures. Pluton growth is accomplished by the repeated emplacement of the magma contained within the self-propagating hydrofractures along mechanical anisotropies introduced by the emplacement of earlier phases (Fig. 6.1). The sensitivity of the differential stress to variations in temperature and the mechanical properties of the wall rocks accounts for the occurrence of far greater volumes of intrusive than extrusive igneous rocks in convergent settings such as the Damara Belt.

6.3 Future outlook

The work presented in this dissertation mainly describes the physical processes of fracture-controlled magma transport, but the recognition of the validity of these models has significant implications for both structural and petrological aspects of granitic magmatism and highlights several outstanding questions in both research fields. The structural issues are centered around the viscosity contrasts between the magma and the wall rocks. Numerous models have improved our understanding of high strain-rate, brittle deformation in otherwise ductile rocks, but the geometries predicted by the models are not realised in reality. More accurate thermomechanical modelling of the physical properties of the near-source wall rocks (e.g. rheology, fracture toughness, elastic moduli) and the physical properties and phase behaviour of the viscous

granitic magmas are needed to better constrain near-source transport processes. Moreover, the disconnect between the rapid propagation of magma-filled fractures in subsolidus crust, where the viscosity contrasts with the wall-rocks are much higher, and the slow rates of flow of the viscous magmas should be a focus of future modelling efforts and should be considered during studies into micro seismicity in the crust beneath the brittle-to-ductile transition.

One of the key precepts of granite petrology is the linking of the geochemistry of granite plutons with phenomena that occur in the source region. This work demonstrates that the geochemical complexity of plutons, whether cryptic or otherwise, is strongly derived from the ascent and much later accretion of small magma batches at the emplacement level. Thus, extreme care should be taken in interpreting geochemical and geochronological data in plutons, and improvements in sampling techniques are needed, in particular the mapping of the broader context of sampling locations within plutons. The episodic nature of granite ascent also implies that the homogenisation of plutons presents a particular hurdle to improving our understanding of granitic magmatic systems, and research should initially be directed towards macroscopically sheeted plutons such as are common in the Damara Belt. This approach could also lead to better constraints on the volumes of individual magma batches as well as aiding in the unravelling of the degree of interaction and homogenisation of magma batches at the emplacement level.

All of the above point to the difficulty of unravelling the well-documented petrological complexities of granitic rocks and highlight the importance of interdisciplinary collaboration in the development of a more complete understanding the nature of granitic rocks.

REFERENCES

Annen, C., Blundy, J. D., Leuthold, J. & Sparks, R. S. J., 2015. Construction and evolution of igneous bodies: Towards an integrated perspective of crustal magmatism. *Lithos*, 230, 206-221.

Clemens, J. D., Helps, P. A. & Stevens, G., 2009. Chemical structure in granitic magmas–a signal from the source?. *Earth and Environmental Science Transactions of the Royal Society of Edinburgh*, 100(1-2), 159-172.

Pressley, R. A. & Brown, M., 1999. The Phillips pluton, Maine, USA: evidence of heterogeneous crustal sources and implications for granite ascent and emplacement mechanisms in convergent orogens. *Lithos*, 46(3), 335-366.

Appendix A: research outputs

Peer-reviewed articles:

Hall, D. J. & Kisters, A. F. M, 2012. ***The stabilization of self-organised leucogranite networks- Implications for melt segregation and far-field melt transfer in the continental crust***. *Earth and Planetary Science Letters*, 355, 1-12.

Hall, D. & Kisters, A., 2016. ***From steep feeders to tabular plutons–Emplacement controls of syntectonic granitoid plutons in the Damara Belt, Namibia***. *Journal of African Earth Sciences*, 113, 51-64.

Article under review:

Hall, D.J. & Kisters, A.F.M., under review by *J. Met. Geol* [assigned manuscript no: JMG-15-0086]. ***Covering their tracks – episodic accumulation and drainage of granitic magma batches in the mid-crust.***

Conference abstracts:

Hall, D.J. & Kisters, A.F.M., October 2013. Oral presentation: **Covering their tracks – collapsed magma-drainage networks in the middle crust**. *2013 GSA Annual Meeting, Denver*.

Hall, D.J. & Kisters, A.F.M., October 2013. Poster presentation: ***Roof-uplift in the mid-crust – a case study from the Damara Belt, Namibia.*** 2013 *GSA Annual Meeting, Denver*.